Software design and development of the improved OPTIMA data acquisition system

National University of Ireland, Galway

Ollscoil na hÉireann, Gaillimh

Department of Physics

Sven Duscha

Submitted to the Department of Physics

National University of Ireland, Galway

In fulfillment of the requirements for the degree Master of Science (Experimental Physics) of the

National University of Ireland, Galway

Research was conducted at the Max Planck Institute for Extraterrestrial Phyics (MPE) in Garching,

Germany.

Supervisors:	Prof. Mike Redfern	(National University of Ireland, Galway)
	Dr. Gottfried Kanbach	(MPE, Garching)
	Dipl. Phys. Alexander Stefanescu	(MPE, Garching)
Head of Department:	Prof. Thomas J. Glynn	

October 2007

Contents

Declaration

I declare that this thesis was composed by myself and that the work contained therein is my own, except where explicitly stated otherwise in the text.

Chapter 1: Introduction and motivation for this thesis

Chapter 2: Description of OPTIMA which was developed by G.Kanbach, C. Straubmeier, S. Kellner, A. Stefanescu and M. Mi¿$\frac{1}{2}$hlegger [SKS01] [Str01], [Kel02], [Ste04], [MÖ6]

Chapter 3: Description of the existing DAQ system developed by C. Straubmeier [Str01]

Chapter 4: Software development done in this thesis

Chapter 5: Scientific results

Section 5.1.1 describing data reduction with analysis tools developed by C.Straubmeier [Str01]

Sections 5.2, 5.3 and 5.4 covering the scientific results obtained in this thesis

Chapter 6: Conclusions of this thesis

Sven Duscha

Abstract

In this thesis a new computer-based software for the data acquisition (DAQ) of the **O**ptical **P**ulsar **Tim**ing **A**nalyzer (**OPTIMA**), a high time resolution photo-polarimeter, developed at the Max-Planck-Institute for Extraterrestrial Physics (MPE), is designed and implemented. The motivation for the redesign was to equip the high time resolution photometer with a modern DAQ system, suitable for OPTIMA's current and future design. Therefore the software design is kept as modular and flexible as possible to facilitate future maintenance and further development. In addition to reference implementations of the data acquisition reading software (server) and sample clients, an integrated library with application specific functions was implemented. This allows application programmers to develop future components, using a high abstraction level to access common functionality. Moreover, reduced light curves taken with the existing DAQ system at the Skinakas Observatory, during the "OPTIMA Burst" campaign in summer 2006 and 2007, are presented. The investigated objects are Cataclysmic Variable Stars, the Crab Pulsar and a Low-Mass X-ray Binary which were observed with high time resolution, and the obtained scientific results are discussed in detail.

Acknowledgements

ming problems that people with less experience in software development would not even dream about.

All the remaining people in the Gamma group who I could not mention in this short list, are thanked for their kindness and friendship.

This thesis is dedicated to my late grandparents.

Chapter 1

Introduction

Astronomy is said to be the oldest science. At the beginning it was carried out by high priests and was inseparably connected to astrology. For centuries observations of the sky were noted in some form by hand. The invention of the telescope by Dutch lens maker Hans Lippershey[1] and its use in astromomy by Galileo Galilei[2] in 1609 allowed far more detailed observations. It still required a skilled observer that could draw accurate sketches of his observations before doing any further analysis.

Notable for early times is the work of Danish astronomer Tycho Brahe[3] whose careful celestial observations were later used by German astronomer Johannes Kepler[4] to deduce the laws of planetary motions which later became known as Kepler's laws.

Irish astronomer William Parsons, 3rd Earl of Rosse[5], can be considered as one of these skillful astronomers in the 19th century. Earl of Rosse self-designed a 72-inch telescope, located at Birr, County Offaly, which went on to become known as the "Leviathan of Parsonstown" for its unprecedented size, which made it the largest telescope in the world for many decades. With this telescope he discovered the first spiral galaxy (see figure 1.1), and the Crab nebula. Two of his remarkably detailed sketches are shown in figure 1.1.

1.1 Milestones in astronomical instrumentation

Though the historical observations of astronomers are extremely valuable to modern astronomy, some inconsistencies, found for example in Messier's catalogue [Gin60], [mis07], might very well be due to inaccurate note taking. Exact and reliable data recording is the very essence of the scientific method.

---

[1] 1570 - September 1619

[2] Italian physicist, mathematician, astronomer and philosopher, 15 February, 1564 - 8 January, 1642

[3] December 14, 1546 - October 24, 1601

[4] December 27, 1571 - November 15, 1630

[5] June 17, 1800 - October 31, 1867
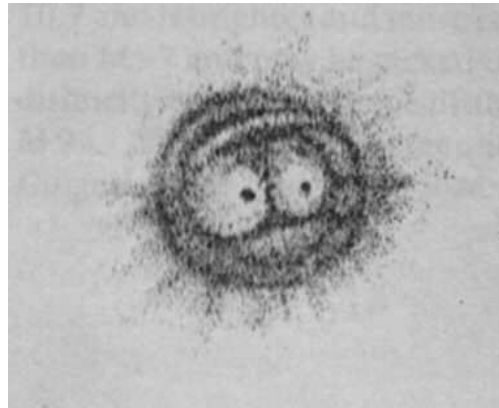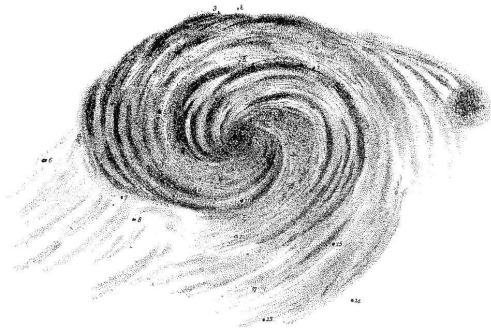
Figure 1.1: Earl of Rosse's sketches of M51 and M97 (images from [m5107] and [m9707])

Technological progress, especially in the twentieth century lead to great progress in the conduction of astronomical observations. Only with photography and the use of photographic plates that were sensitive for faint star light, astronomical observations required less artistic skills. Above all, this furthermore allowed archiving and objective comparison of data.

Moreover data acquisition soon replaced the problem of taking notes. Photographic plates were difficult to handle and required long exposure times. The development of photomultiplier tubes (PMTs) and their first use in astronomy [Kro46], made high time resolution at subseconds scale feasible. Due to their low efficiency (see chapter 2.3.3) and the lack of high spatial resolution, their use was limited to aperture photometry.

The progress in the development of semiconductor devices lead to charge coupled devices (CCDs). Their higher sensitivity and electronic read-out allowed shorter exposure times and a much faster handling of observational frames. They were much slower than PMTs, but they offered a high spatial resolution over an extended field of view.

The light gathering power of today's large aperture telescopes[6], along with much more sensitive imaging chips reduced exposure times considerably. CCD based instruments are mainly limited by the time it takes to read out the chip through "row-clocking", where the electrons collected in wells during the exposure are clocked successively to a readout column of cells. Modern chips such as those used in Ultracam [DM01] utilize multiple readout-columns, and low-noise amplifiers that can be operated at high-frequencies without introducing too much read-out noise. Time resolutions of less than a second are feasible with these devices.

On the other hand, technological progress with aperture-based instrumentation, thanks to new semiconductor devices, could alleviate the disadvantages of early PMTs. The introduction of avalanche amplified photodiodes, so-called avalanche photodiodes, to astronomical observations

---

[6]The telescopes with the currently largest primary mirrors are the South African Telescope (11 m primary mirror), the Gran Telescopio CANARIAS (10.4 m) and the two Keck telescopes (10 m mirrors).

[DDD$^+$93] provided high time resolutions, but lacked sufficient spatial resolution. More reliable and cheaper manufacturing of semiconductor devices seems to promise to provide the advantages of both worlds: The high time resolution and a sufficient field of view. Instruments using multi-anode multi-channel arrays (MAMA) such as TRIFFID [Red91] / TRIFFID-2 [OBS$^+$02] or Josephon-Superconducting Tunnel Diodes [MVP04] demonstrate that such requirements can be satisfied. The technical challenges involved in their operation and necessary further development, though, have yet prevented a wider use of these devices in astronomy.

1.2   High Time Resolution Astronomy

The ability to achieve reasonable signal-to-noise ratios at shorter exposure times gave rise to a new branch of astronomical research specialising in the investigation of fast physical processes in the Universe. High time resolution astronomy (HTRA) is concerned with physical processes that happen on a second to subsecond scale.

These processes are usually associated with compact objects, like neutron stars, black hole candidates, cataclysmic variable stars or Gamma-ray bursts (GRBs). The time-scale of a process is intrinsically related to the extension of the region it is happening in through the so-called "light time" argument. "Light time" defines the time it takes light to get from one side of a region to the other. Any fluctuation of the observed region happening on a time-scale smaller than that will be smeared out and cannot be resolved.

1.3   Observations and Data storage

OPTIMA, the **O**ptical **P**ulsar **TIM**ing **A**nalyzer[7], represents one[8] of these modern high time resolution instruments. It is a fibre-aperture based instrument using avalanche photodiodes (APDs) to achieve time resolutions down to microseconds.

The challenge with an instrument like OPTIMA lies in providing a data acquisition backend that is capable of acquiring and storing the data that is provided by the APDs with high time resolution. The problem lies not only in the amount of data transfer (OPTIMA uses up to 12 Avalanche Photodiodes in its current configuration), but in the additional problem of providing accurate absolute timing for the events registered in the APDs.

The task of the DAQ system is to detect the output pulses of the APDs, and create a corresponding time tag which is then recorded together with the channel number in which it occurred. OPTIMA is already equipped with a DAQ system that was built for the instrument's first version.

---

[7]OPTIMA was initially developed as an instrument to observe optical pulsars. Detailed information is given in chapter 2.

[8]A similar instrument is being developed at the National University of Ireland, Galway [RRS06].

That system had been designed under certain constraints and with limited requirements that had to be met to allow OPTIMA to fulfill its initial scientific purpose to observe optical pulsars. For OPTIMA's use in scientific observations in its current design (see chapter 2.6) a more modern data acquisition system was required.

The design and implementation of the improved data acquisition system software is the main topic of this thesis (see chapter 4). The new DAQ was designed to allow recording of photon events as close to the limit of the APDs' time resolution as possible, and to overcome the major short-comings of the existing DAQ system (see chapter 3.2.2). The new DAQ software was designed to be modular and to allow easy extendability. Thus, allowing easy adaption to new hardware and to new measurement situations.

Also, to carry out astronomical observations as flawlessly as possible, constant monitoring and error checking are necessary. This requires quick-look tools that present the data to the observer, while it is being recorded. This work demonstrates that a new approach on data handling can provide access to live-streamed data both for recording and analysis programs. The difficulties involved in this concurrent data access, and the approach taken to guarantee safe operation are also part of this thesis (see chapter 4).

Investigation of the properties of cataclysmic variable stars of type AM Her, the Low Mass X-ray Binary Aql X-1 and pulsar timing with the Crab pulsar as examples, show the scientific performance of the OPTIMA instrument (see chapter 5). Due to delays in the hardware development for the new data acquisition system, the observational data used in these had been recorded with the existing DAQ.

Chapter 2

OPTIMA

This chapter describes the OPTIMA instrument with which the data acquisition software designed in this thesis will be used. First an overview of the system will be given, and then its components will be described in detail. It follows a short introduction to the scientific application of the instrument and which classes of objects are good candidates for high time resolution astronomy. The chapter concludes with a description of the "OPTIMA Burst" campaign during 2006 and 2007.

+++

2.1 OPTIMA - a high speed photo-polarimeter

OPTIMA is an **O**ptical **P**ulsar[1] **TIM**ing **A**nalyser that uses a set of avalanche photodiodes to measure and time pulses in principle at nanosecond precision, though the overall timing resolution is currently limited by the DAQ hardware to $4\ \mu s$ (see chapter 3). The system was developed as part of a Ph.D. thesis from 1998-2001 [Str01], and was subsequently extended into today's existing sytem through several Master thesis projects: In 2002 the photometer was equipped with a rotating polariod polarimeter [Kel02], later in 2004 it was further modified to allow the observation of optical afterglows of GRBs [Ste04] and a newly developed parallel Wollaston polarimeter was designed in 2006 [MÖ6].

Compared to previous high-time resolution instruments using photomultiplier tubes or similar devices, quantum efficiency is improved by a factor of six integrated over the available bandwidth [KKS$^+$03]. The availability of commercial APDs from industrial semiconductor companies presented the solution of using a fully developed and tested device without the difficulties of developing a new semiconductor device. The APDs used in the OPTIMA system are from Perkin & Elmer[2] and sensitive in the range from 400 nm to 950 nm (see section 2.3.3).

---

[1]Pulsar, abbreviation for Pulsating Source of Radio, also abbreviated PSR.
[2]Perkin-Elmer SPCM-AQ [Las97]
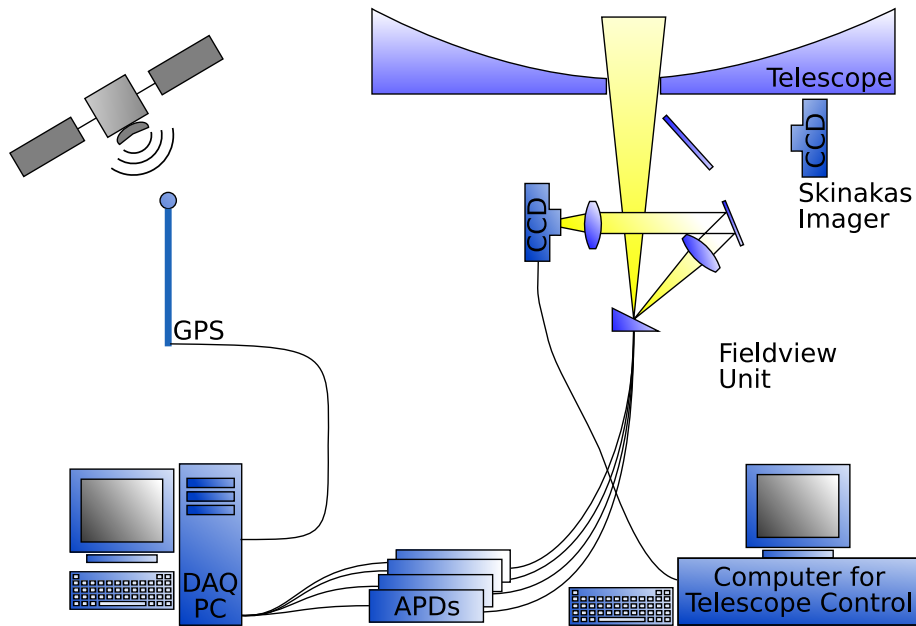
Figure 2.1: OPTIMA Burst configuration

The high precision timing accuracy is achieved by using a GPS[3]-disciplined clock. The GPS time signal is used as a highly stable reference signal, driving an oven-stabilized oscillator providing a high-precision short-time timing signal [Str01]. The combination of a long-term stable reference, together with the short-time stable oscillator is used to tag photons being registered in the APDs with a precise absolute time stamp.

This makes OPTIMA an absolute-timing single-photon-detector system. Observations of highly variable sources need not to be constrained by a choice of exposure time, as it is in the case of CCD observations. During later data analysis photons can be collected to arbitrary bin sizes[4] choosing the optimum compromise of time resolution and signal-to-noise ratio (see chapter 5.1).

2.2 Overview

OPTIMA has been designed as a modular hardware system from the beginning [Str01], [KKS+03], as such allowing to be easily transported and used at different telescopes worldwide. For operation at different telescopes the optical configuration of the focal view (see section 2.3.1) must be adjusted to the telescope's focal ratio[5] and GAM[6]. Hence, OPTIMA had been designed in such a way as

---

[3]Global Positioning System (GPS), a satellite based navigation system using high-precision atomic clocks. The positional signals are derived from the atomic clock times on the satellites and can be used as a high-precision time reference.

[4]bin: interval size in histogram building of a data distribution

[5]focal ratio: f-Number f/#, where N=f/D relating a lenses/pupils aperture, D, to its focal length, f. The focal ratio is a measure for the "speed" of the lens. Typically noted in the form e.g. f/8

[6]Guider Acquisition Module (GAM): optical unit at the telescope distributing light to different instruments

to allow the whole system to be disassembled into small parts that can be easily transported and the instrument can be used at various telescope sites whose GAM allows the installation of guest instruments. In the course of its development, OPTIMA had been extended from the purpose of a "pulsar timing" photometer to a photo-polarimeter with a rotating polaroid filter [Kel02] and in its improved version with a double-Wollaston prism [MÖ6] (see section 2.4.2). Also, a four-colour spectrometer mode that can be easily put into operation without much change in the configuration had been realized.

2.3 Components

OPTIMA consists of five main components (see figure 2.1) that guarantee its performance as an optical photo-polarimeter. Following the path of light from the telescope the components work as follows:

The GAM permits OPTIMA to be mounted as guest instrument along-side the Skinakas imager[7] and the telescope's light beam reaches an inclined plane mirror at the focus (see figure 2.1). This mirror reflects the incoming light onto a lens optics where a CCD[8] images the area of the sky the telescope is pointed to. The position of the optical fibres in the field of view can be determined with respect to neighbouring stars. The mirror is inclined at 20 degrees in the focal plane of the telescope, such that the focal plane intersects the mirror's surface along a line, where the fibre bundle, background and spectrometer fibres and the polarimeter aperture are positioned. Thus, the infalling light from the telescope can be correctly focused at the fibres' positions and the fibres pick up the light of objects of interest. The difficulties linked to observations of celestial sources via fibre optics will be described in detail in section 2.3.2. The photons collected in the fibre aperture get recorded in the APDs semiconductor sensor on the other end of the fibre. Through the avalanche amplification effect (see section 2.3.3) a single incoming photon triggers an electronic circuit delivering a TTL[9] pulse that is registered in the inputs of the DAQ computer. The software on the DAQ computer records the signal on the input lines and generates a high-precision time stamp from the GPS-disciplined clock (see section 2.3.4). Target acquisition, CCD camera control and sending commands to the TCS[10] are done by the additional OPTIMA control computer.

The following sections will describe all these components of the OPTIMA system in detail:

- Focal plane mirror and CCD camera (section 2.3.1)

- Fibres (section 2.3.2)

---

[7] CH360 CCD camera using a Photometrics Thomson chip with 1024×1024 19 μm pixels

[8] Apogee AP-6 CCD camera

[9] Transistor-Transistor Logic, where 0 V is logical false and 5 V logical true.

[10] TCS = telescope control system, allows external control of telescopes via a serial device connection
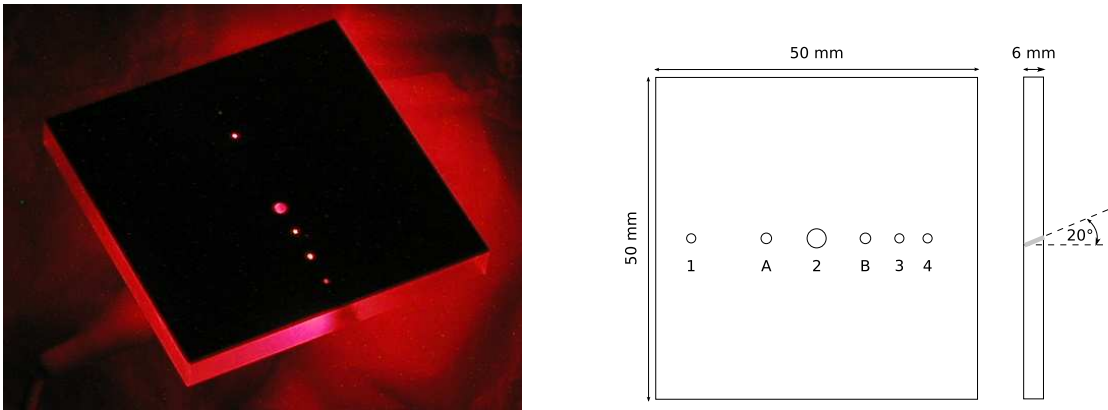
Figure 2.2: Focal plane mirror with holes for fibres, spectrometer and Wollaston polarimeter

- Avalanche photodiodes (section 2.3.3)

- Data Acquistion System (section 2.3.4)

- Telescope Control Computer (section 2.3.5)

2.3.1 Focal plane mirror and CCD camera

The light gathered by the telescope's primary mirror is reflected by the secondary mirror into the Cassegrain focus and the GAM mounting permits the observatory's standard instrumentation or guest instruments such as OPTIMA to be used on site. OPTIMA's GAM mounting is fitted to the telescope such that the aligned fibre apertures and polarimeter aperture lie in the focal plane of the telescope, i.e. the intersection of the 20 degree mirror with the focal plane covers them. The holes in the mirror are at a 20 degree angle, too, so that all the apertures are parallel to the incoming light beam and the efficiency of light entry into the fibres and the polarimeter aperture is maximized.

The reflected image of the mirror is focused through a second set of optical lenses onto the CCD chip of an astronomical CCD camera. The camera is an Apogee AP6 astronomical camera with a resolution of 1024×1024 pixels. The pixel size is $24.4\ \mu m$, resulting in a chip size of $25 \times 25\ \mathrm{mm}^2$. The field of view is typically a few arc minutes[11]. This is particularly important for the task of identifying an unknown source in the frame and to command the telescope control unit to position it on the optical fibre (see section 2.6).

The primary task is to image the telescope's field of view to allow orientation and get exact astrometry. Additionally the camera is used to monitor seeing conditions and to perform photometry on neighbouring stars. This photometry can be done with a cadence of ~ 10 s and provides data on seeing and transparency (see chapter 5.1).

---

[11]At the 1.3 m Skinakas f/7.64 telescope the CCD view covers a field of view of roughly unit$17' \times 17'$, but due to comatic abberation and vignetting $10'-12'$ are useable in OPTIMA.

8
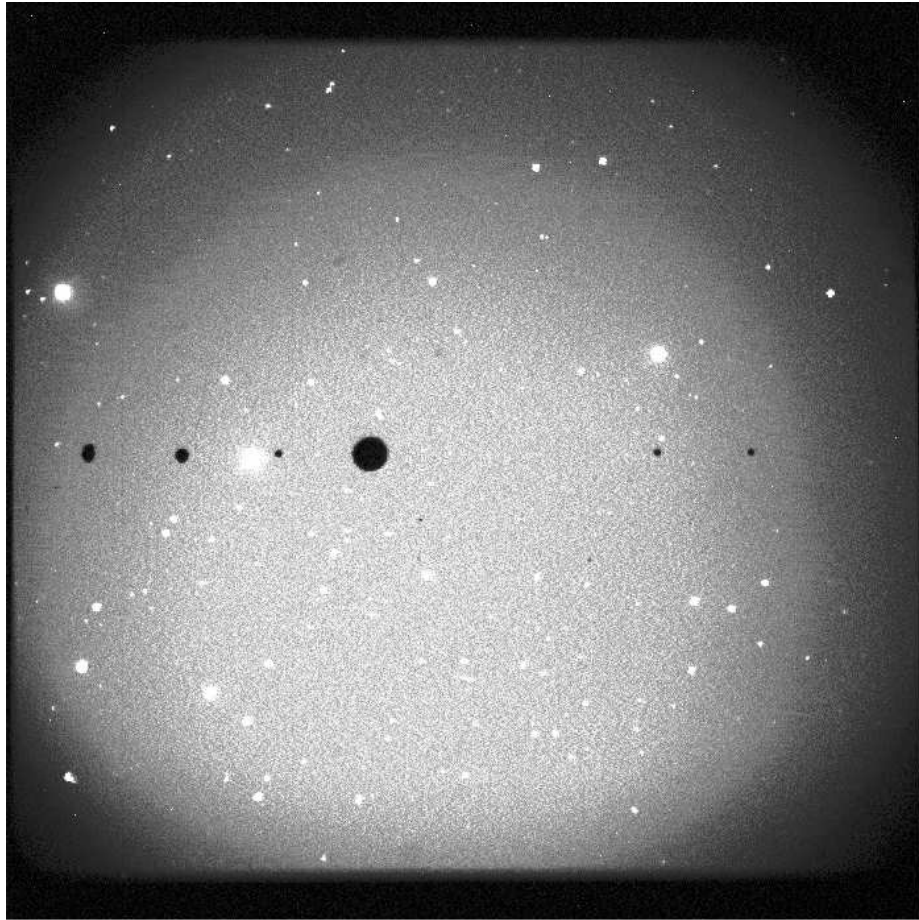
Figure 2.3: HU Aquarii positioned on central fibre, vignetting of field of view due to CCD lens optics, the image is turned by $180°$ w.r.t. figure 2.2

The CCD camera used in OPTIMA uses thermoelectric cooling and can be read out in 1 second. The camera is connected to the OPTIMA control computer via a PCI card in the docking station of the laptop computer. Its fast readout of about 1 second is important for the quick field of view acquistion required by the search for GRB afterglow candidates, where a series of frames is taken to identify the fading afterglow candidate (see section 2.6).

The telescope's f-ratio of 7.64 must be converted to f/3.5 for the camera with focal reducing optics to fit the image to the CCD chip's dimensions of the Apogee AP6 camera. This conversion is done by a focal-reducer consisting of two ZEISS aerial photography large-format lenses. This commercially available lens optics was preferred to a custom built solution. The result is a vignetting effect at about half way from the centre to the edge of the CCD image, as seen in figure 2.3. Also image distortions towards the edge of the image can be seen.

The CCD frame is used for controlling the telescope. Objects of interest are usually in the central field of the image, where the fibre apertures are located, thus the image vignetting is irrelevant in

this usage case. Left and right of the centre of the mirror there are two holes with light emitting diodes (A and B)[12]. These can be switched on and by knowing the exact postion of these light sources on the mirror the fibre aperture positions can be determined in the CCD image. Although the mechanics of the OPTIMA optics are rigid, slight shifts of the mirror/camera position of the order of a few μm have been observed. This is enough to affect the exact positioning of sources on the fibres. Hence, after considerably large movements of the telescope (a few tens degrees) it is advisable to do a calibration measurement against the LEDs, to obtain the exact aperture positions in the CCD frame. The calibration measurement and calculation is done automatically, but must be triggered by the operator before starting an observation in the new field.

2.3.2 Fibres

The goal in OPTIMA's development was to build an instrument capable of high time resolution photometry and polarimetry from standard components. The structure of the chosen single-APD-modules does not allow easy placement in the telescope focus. The solution was to build OPTIMA as a fibre-fed instrument where optical fibres pick up the light in the focal plane and then lead the light to the APD modules which can be placed conveniently outside the focus. In order to use a fibre-fed instrument two requirements must be met. A star of a size of a few arc seconds must be accurately placed on the aperture of the fibre, and the point spread function (PSF)[13] of target stars must fit the aperture size.

The positioning of the target star is done by using the CCD field view unit on the OPTIMA control computer and sending precise positioning commands via TCS to the telescope. This was implemented using a microcontroller unit connected to the OPTIMA control computer via a serial connection [Ste04], and tested during several observational runs at the Skinakas observatory in Crete in years 2004 to 2007. Before the implementation of the controller unit the positioning had to be done manually by checking the image on the CCD and entering TCS commands manually [Ste04].

OPTIMA's single-photon counting apertures are determined by the diameter of the optical fibres. As mentioned in section 2.3.1 these have a diameter of $300 \ \mu$m in the focal plane of the telescope. This diameter was chosen to be about twice to thrice the typical "seeing"[14] diameter of stars in the image. The value depends of course on the f-ratio of the telescope, and the fibres must be chosen so that their diameters match the typical profile of stars at a particular telescope. Measurements carried out by Boumis et al. [BSM$^+$01] showed that seeing conditions of less than 1 arc second can be achieved at Skinakas observatory (see figure 2.5). Observations with OPTIMA in recent years showed, that these ideal conditions are rather rare and an average seeing of 2 to 2.5 arc seconds is

---

[12]Light emitting diodes (LEDs) are semiconductor p-n junctions which emit incoherent light in a narrow spectrum.

[13]The point spread function defines the response of an imaging system to the light of a point source.

[14]"Seeing" denotes the effect of the Earth's atmosphere due to turbulences that causes stars to be imaged as disks with a finite diameter; the term is also used to denote the full width half maxima of the disk's Gaussian profile

Figure 2.4: OPTIMA at the Skinakas 1.3 m telescope, Crete, Greece
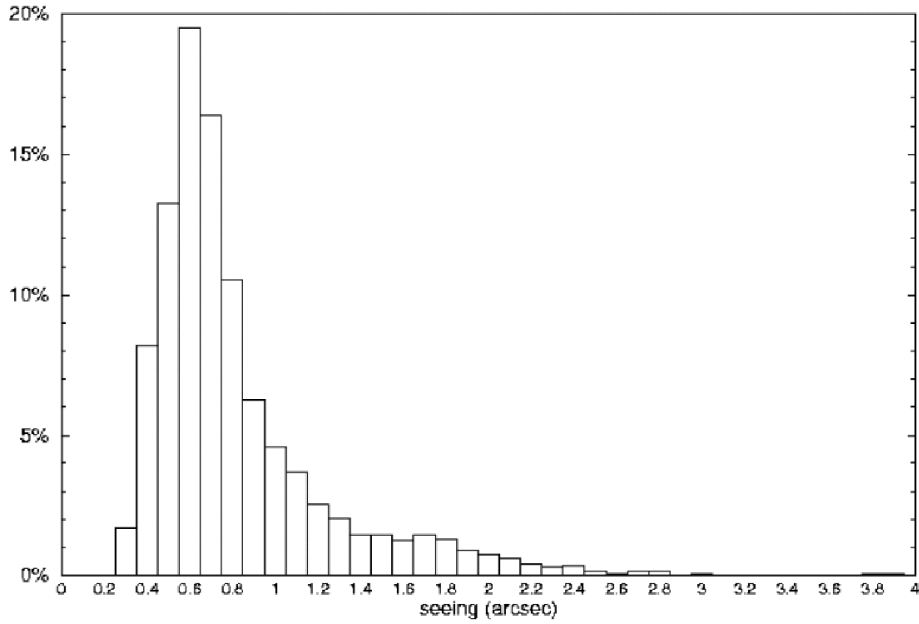
Figure 2.5: Histogram of seeing distribution at Skinakas observatory for spring 2001 [BSM$^+$01]

more usual.

The relationship between a star's FWHM diameter in the image and its object angle is given by

$$d = f \cdot \tan \alpha, \tag{2.1}$$

where α is the object angle, f the focal length and d the size of the object's image in the focal plane.

The Skinakas 1.29 m telesope's focal length is 9.857 m and taking 2 arc seconds as a typical FWHM seeing value for a star, leads to a diameter of $\sim 48~\mu$m in the image on the focal plane mirror. In order to capture most of the light of the target star, the fibre aperture should be about at least twice that diameter. A larger diameter would make the background contribution large and would also risk light from nearby stars entering the aperture. So choosing an appropriate fibre diameter does not only depend on the f-ratio of the telescope, but also on seeing conditions. On the other hand, a fibre diameter that was chosen too small would increase the contribution due to noise, if large parts of the star's seeing disk would not enter the aperture, when the star inevitably moves due to seeing conditions. The airy disc changes due to random fluctuations in the seeing conditions on a small time scale. When parts of the star extend beyond the rim of the fibre and light is lost, an increase in noise in the signal is caused.

Due to the fact that the APDs' active area has a diameter of 100 μm the fibres are tapered from 300 μm diameter at the side where the light enters the fibre in the focal plane to 100 μm on the APDs' side. The tapered fibres contribute further to the light loss, in addition to losses due to the coupling of light into the fibre at the aperture and losses caused at the interface of fibre and semiconductor in the APD.

12

Figure 2.6: Hexagonal bundle fibre, fibres illuminated from the backend

The light losses are not the same for all fibres, since each fibre has its own transmission and coupling characteristic. All fibres have the same aperture diameter and hence cover the same area in the focal plane. Although, due to the afore mentioned differing light to fibre coupling, different transmission efficiencies and interface coupling to the APDs, the resulting photon counts from the APDs may differ. Therefore in order to perform correct photon counting this has to be corrected for in data analysis (see chapter 5.1).

The fibre holes in the mirror can be seen in figure 2.2. At the far left there is a $345\ \mu$m aperture where light enters a parallel Wollaston prism (1). This is the "OPTIMA Burst" polarimeter for simultanous measurement of the Stokes parameters I,Q and U (see section 2.4.2).

In the centre of the mirror there is a 1.7 mm hole ((2) in figure 2.2), housing a hexagonal fibre bundle of 7 optical fibres (see figure 2.6). The centre fibre of the bundle is used to acquire the target star's light while the neighbouring fibres measure the background contribution of the surrounding sky background. This is particularly important for observations of extended sources, e.g. the Crab pulsar in the Crab nebula [Str01], to differentiate the contribution of the diffuse nebula emission from the sky background. Each fibre has a $300\ \mu$m diameter and the hexagonal packaging guarantees that the bundle fibres cover the target source's surroundings as densely as possible. For protection, in addition to each fibre's individual cladding, the bundle is packed in a thin metal tube. The whole metal tube is then placed in the central hole in the mirror.

About 1cm to the left there is another $300\ \mu$m hole for a fibre allowing coarse spectrometry ((3) in figure 2.2). The light picked up by the fibre is spread into its spectrum by a dispersion prism (see figure 2.14). At the exit side of the prism up to four optical fibres can be placed at positions of interest in the continuous spectrum to do simple 4-colour-spectroscopy. Since the current data

Figure 2.7: Avalanche photodiode by Perkin-Elmer

acquistion system can only record 8 channels simultaneously and the number of available APDs is limited, the spectrometer is not mounted in OPTIMA's standard configuration. It is easily possible to mount the spectrometer and to switch four photon counters to the spectrometer's output channels (see section 2.4.3).

On the outer right is the $300\ \mu$m hole for the background fibre (4). This fibre collects sky background light, so that the contribution of photons from the sky can be substracted from the target fibre counts. If by chance a star is located on the background fibre the surrounding bundle fibres can be used as background reference.

2.3.3 Avalanche photodiodes

Avalanche photodiodes versus photomultiplier tubes

The first single-photon counting instruments were photomultiplier tubes (PMTs), invented by Russian physicist Leonid Aleksandrovitch Kubetsky[15] in 1930 [Lub06]. PMTs are ubiquitiously used in any area that relies on detecting faint photon sources from nuclear physics to medicine.

PMTs have some disadvantages that made their use in astronomy difficult, whereas modern semiconductor devices such as avalanche photodiodes can excel. The greatest advantage of avalanche photodiodes over PTMs is their higher quantum efficiency[16]. PMTs have typically quantum efficiencies of 20–25 percent. Integrated over the spectral area APDs have about six times the QE of standard PMTs. The reason for the low QE of standard PMTs lies in the fact that the active volume, where interaction of photons with the cathode material occurs, is small. The electron must leave

---

[15]Although the issue about the inventor of the photomultiplier tube (PMT) is somewhat controversial.

[16]Quantum efficiency (QE) is probability of detection of an incident photons
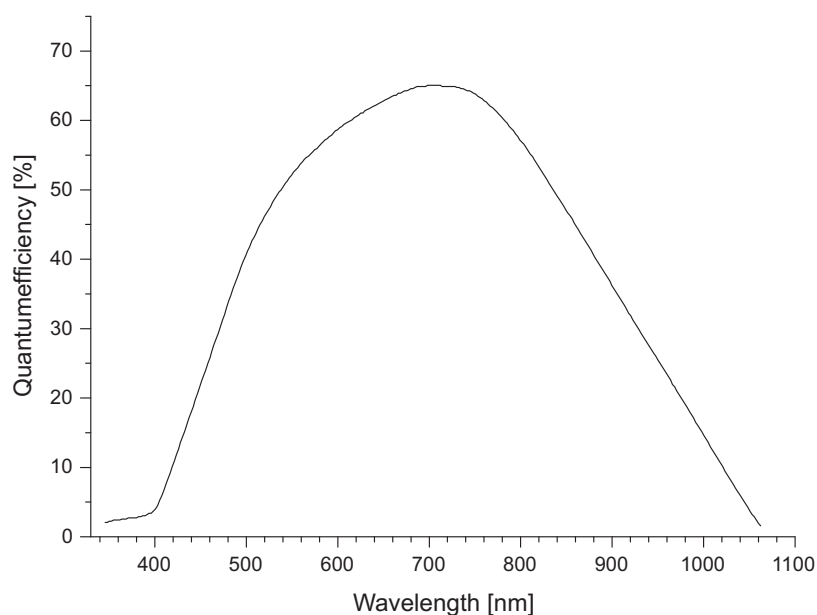
Figure 2.8: Quantum efficiency of Perkin & Elmer APDs [Per07]

the material, hence, the cathode can only be a very thin layer where the photon enters on one side and the electron leaves on the other. Avalanche photodiodes also cover a broader spectral range than typical PMTs, which are typically sensitive in the UV region to red, 200 nm to 600 nm, while Si-APDs cover all of the visible region to IR, 400 nm to 950 nm. Figure 2.8 clearly shows the high quantum efficiency of the Perkin-Elmer APD which is up to 64 percent and stays at more than 50 percent over a wide range of their spectral sensitivity.

In addition APD modules are smaller and more rugged than PMT glass tubes, and independent of magnetic influences. PMT also continuously draw current through the voltage divider circuit, which converts to resistive heat.

Physics of avalanche photodiodes

In the 1980s further development of improved p-n semiconductor photodiodes led to so-called avalanche photodiodes. These are silicon-based p-n junction diodes that are operated at a high reverse-bias voltage[17]. For the greatest amplification of factors up to 10^8 certain APDs are operated above their breakdown voltage, the so-called Geiger mode.

The dectection of a photon with an APD can be imagined as follows. Figure 2.9 shows a sectional drawing of the semiconductor structure of an APD. Incident photons pass through an antireflective coating and create an electron-hole pair in the depletion region. The hole is accelerated towards the anode where there is a negative bias voltage, while the electron moves towards the

---

[17]The reverse break-down voltage for Silicon is typically 1000V depending on doping and thickness of layers, some APDs operate at up to 1500V reverse voltage.
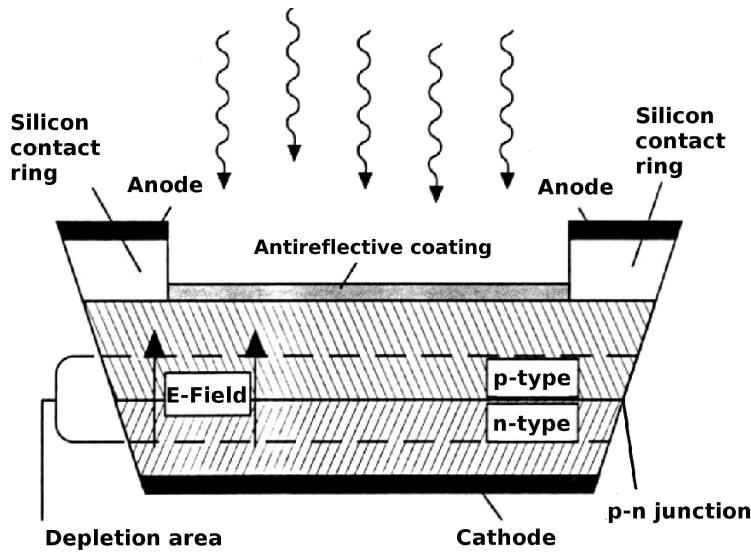
Figure 2.9: Schematic of an avalanche photodiode (adapted from [Str01])

postively biased cathode.

In the depletion region around the p-n junction, the electron is accelerated by the strong electric field, generated by the high reverse bias voltage. On collision with the valence electrons in the silicon it creates secondary electron-hole pairs, which are separated, accelerated, and can in turn generate further electron-hole pairs. This exponential amplification effect behaves like an "avalanche", thus, giving this type of p-n photodiodes their name.

In contrast to conventional p-n photodiodes where the diode current can only reach a detectable minimum value, if a sufficient number of photons hits the silicon at the same time, the internal signal amplification of APDs allows detection of single photons [DDD+93].

Noise sources in avalanche photodiodes

As any other electronic semiconductor device, APDs suffer from different noise sources. Because OPTIMA operates the APDs in Geiger mode, which means that interaction of single photons with the silicon lead to an avalanche current in the APD, the internal noise contributions in the avalanche process are of no concern. The avalanche current arriving at the cathode is registered in the read-out electronics and generates an output pulse. Hence, the energy of the photon and therefore the number of created electron-hole-pairs in the silicon is not relevant in this mode of operation. Regardless of the number of created electrons and holes in the avalanche process the detection is only registered as one count. Therefore APD-internal noise contributions due to excess noise[18], which depends on

---

[18]Excess noise is the noise contribution due to the stochastic nature of the avalanche mulitplication of electrons.

the multiplication factor M[19], are not relevant in Geiger mode.

OPTIMA registers the detection counts in the DAQ computer (see section 4). The important noise contribution here is the number of "dark counts" in the APD, even if no photon entered the detector. These are caused by electron-hole-pairs that are created through thermal excitation in the semiconductor. The location for these lies near the boundary region of the p+ and the depletion layer, where the dopings of the two different regions cause impurities in the crystal. These impurities depend on the quality of the epitaxial manufacturing process of the APD, and selection of detectors exhibiting low dark counts, i.e. having a lower number of impurities, provides detectors with low dark count rates. The creation process is also governed by Poisson statistics and is exponentially dependent on temperature. Through cooling of the detector the amount of dark noise can be significantly reduced by about one magnitude per 8-10 degrees of cooling.

Characteristics of APDs used in OPTIMA

OPTIMA uses commercially available avanlanche photodiodes (APDs) modules by Perkin & Elmer[20] (see figure 2.7) to detect incoming photons. The dark noise of an individual APD is unique, the manufacturer only guarantees an upper limit for the devices. The APDs used in OPTIMA have dark count rates of roughly 50 counts per second [Per07][21]. The "FC-15"-class APDs from Perkin & Elmer are selected individual devices that have been tested to exhibit the guaranteed low dark rate.

The Perkin & Elmer APDs are sensitive over a range from 400 nm to 950 nm [Per07], covering the visual part of the spectrum to the near infrared (see figure 2.8).

APD Signal readout

The APDs used in OPTIMA have a response time of 300 ps to a photon hitting the detector area [Per07]. Both this time and the transit time of ~ 7 ns through the 2 m long fibre are negligible compared to the other uncertainties of the timing of the DAQ.

On detection of a photon, the APD electronics creates a TTL pulse of length of 8 to 40 ns, followed by a dead-time of $40 - 50$ ns, where the electronics of the APD module actively quenches the avalanche process in the detector.

A peculiarity of APDs is that within 40 ns after the photon absorption in the bulk region self-illumination through photons generated within the bulk region is possible. These photons have a broad spectral distribution (mainly in the IR) and can be reflected back onto sensitive regions triggering another avalanche. This happens on a time scale of 35 ns [Per07]. In case of the OPTIMA system the read-out times of the TTL pulses are 4 μs in the currently used DAQ (see chapter 3), so

---

[19]Each avalanche process constitutes a stochastic process, so M is not the same for each detection, and the resultant number of created electrons can differ.

[20]Perkin & Elmer SPCM-AQR-15-FC type avalanche photodiodes

[21]SPCM-AQR-15-FC are cooled by two stage Peltier elements for temperature-stabilized operation.

that this is of no concern. Depending on the reaction time of the input lines of the improved DAQ hardware, self-illumination must be taken into account.

The Perkin & Elmer APDs are specified for a maximum guaranteed count rate of 2 million counts per second, because of heat-up of the detector element at these high count rates [Per07].

In recent years great progress has been made in the development of two-dimensional single-photon counting detectors using multi-anode micro-channel arrays (MAMA) [MBSK03], e.g. on the TRIFFID camera [Red91] or as compact solid-state detectors [MVP04]. Due to the advantages of 2-dimensional single-photon arrays, these will be more prevalent with optical observations in the future.

2.3.4 Data Acquisition System

As with any other astronomical instrumentation OPTIMA requires a reliable form of data storage. Especially OPTIMA's ability to record the arrival time for every single photon detected puts a high requirement onto the DAQ system. It must be both accurate in terms of timing and must be able to sustain high data rates.

OPTIMA's DAQ had been developed in tight connection with the rest of the instrument as part of a Ph.D. thesis project [Str01]. The DAQ system performs two tasks:

- time tagging the registered photons with the GPS time signal

- writing photon events to permanent storage

The details of the DAQ system, its principle of operation and shortcomings are described in detail in chapter 3. The development of an improved DAQ system for OPTIMA, which is the topic of this thesis, is laid out in detail in chapter 4.

2.3.5 Optima Control Computer

A peculiarity about fibre-fed systems like OPTIMA is the difficulty associated with target acquisition. In observations with CCDs a pointing accuracy within an arc minute is adequate to acquire the target of interest in the field of view. Positioning an individual star on an optical fibre only slightly larger than the diameter of the star's image in the focal plane is far more difficult. The mechanical construction of the telescope's drive does allow positioning within the limits of sub-arcseconds, but most telescope control software does not offer such a degree of accuracy.

For that purpose OPTIMA uses direct access to the TCS to send slewing and off-set commands to the telescope drive. This is done via a microcontroller device that interfaces the OPTIMA control computer with the serial input of the TCS.

In the case of the Skinakas telescope control system, the microcontroller imitates the signals generated by the keypad of the "hand paddle" to off-set the telscope. The hand paddle control of

course allows only relative positioning. Using information from the field view unit CCD camera (see also section 2.3.1) relative positional information about the fibre bundles' location can be calculated.

The OPTIMA CCD camera images the current field of view of the telescope via the focal mirror (see section 2.3.1). Figure 2.10 shows a screenshot of the OPTIMA control software. It offers control panels for CCD readout, while the acquired image is displayed in DS9[22]. The OPTIMA control software was developed as part of a Master's thesis [Ste04] with the aim to improve the OPTIMA photometer/polarimeter into a quick-response system to allow prompt observation of Gamma-ray burst optical afterglows (see section 2.6).

Furthermore the OPTIMA control computer uses the open source astronomical software Xephem [xep07] to provide an easy method for target acquistion of astronomical sources of interest. UNIX scripts and Xephem's built in telescope serial device support allow to select a target in the catalog or the "sky view" to which the telescope slews on request.

Apart from these control tasks, the OPTIMA control computer offers quick look photometry of other sources in the CCD image via IRAF[23]. Also, semi-automated focus adjustment is done through the control application. A script steps through different focus positions and measures the FWHM diameter of a selected star in the image. A fitting algorithm computes a parabolic fit to the data and the user verifies the correctness of the fit. That way the best focal point for OPTIMA, depending on temperature, can be found at the beginning of every observational night.

In the previous system the manufacturer supplied CCD software was only used for read-out. The position of the stars with respect to the fibres were checked by eye only. The rewritten software allows to use pixel information in the image to automatically generate suitable TCS commands such that a star chosen in the CCD frame is easily positioned on one of OPTIMA's optical fibres. Especially with respect to early observations of GRB afterglows, it is essential that the target acquisition process could be accelerated in such a way (see section 2.6) [Ste04].

2.4   Operational Modes

OPTIMA was intended as a high-speed photometer for observations of faint, strongly variable sources. The principle of picking up light with optical fibres at the focal plane of the telescope allows (relative) photometry[24]. Differential photometry requires the comparison with a standard source. Due to the difficulties involved in aperture-fibre instruments (see section 2.3.2), a moveable fibre must be placed on a suitable standard star in the field of the science target. OPTIMA's current configuration is not equipped with such.

OPTIMA's "white-light"[25] photometry allows to observe an object's luminosity in the overall

---

[22]DS9 is a commonly used FITS viewer with image examination functions [JM03].

[23]IRAF = Image Reduction and Analysis Facility [ira06] developed by the NOAO.

[24]OPTIMA can do relative photometry on objects with respect to photon counts the APDs register (see section 2.4.1).

[25]OPTIMA has a mount for a filter wheel, which was used to do filtered observations a couple of times, the usual
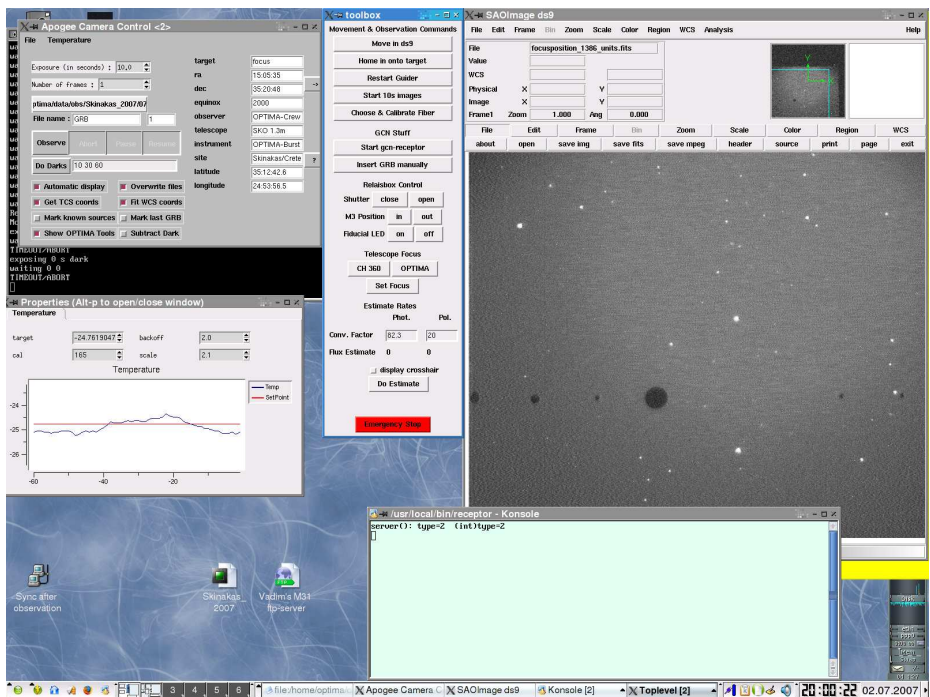
Figure 2.10: OPTIMA control software: left: CCD camera control, middle: TCS control and shutter/focusing adjustment, right: ds9 field view image, with fibre holes in the mirror, bottom: logging window of GCN receptor [Ste04]

Telescope site		Year campaign was carried out
La Silla 2.2m	Chile	1999, 2000
Mt. Stromlo	Australia	2000
Cananea	Mexiko	2001
Skinakas	Crete	2001, 2002, 2003, 2004, 2005, 2006, 2007
Calar Alto	Spain	2002
NOT	Canary Island	2003
Sutherland	South Africa	2004

Table 2.1: OPTMA Observational campaigns

spectral range of the APDs used, but it is not possible to distinguish between higher or lower brightness in parts of the spectrum, e.g. the "red", "blue" or "green" contributions to the object's overall brightness. Comparison to observations done by other astronomical instruments that usually use filter systems, must be done by converting the filtered observational data.

OPTIMA has been used successfully at different telescopes in the last seven years (see table 2.4), yielding unprecedented results in high-time resolution astronomical observations [KSSB01] and [MBSK03].

2.4.1 Photometer

The photometer mode is the most often used mode for observations with OPTIMA. In this mode the light from the telescope optics falls directly onto the fibres in the focal plane and photons are registered by the APDs at the other end of each fibre.

In this mode the hexagonal fibre bundle along with the background fibre is used, thus, eight channels are recorded by the DAQ simultaneously. As mentioned in section 2.3.2 the hexagonal arrangement of the fibre bundle allows observation of the source and its surrounding background simultaneously.

Due to the fact that both transmission efficiencies and APD detector responses differ, the counting output of each channel must be calibrated. This is done by measuring a diffuse light source[26] and calibrating against one of the fibres as reference. Instead of using the diffuse light source[27] calibration can be done against the target fibre, while all fibres are measuring sky background under the

---

operation is in white light though.

[26]OPTIMA-Burst is equipped with a switchable diffuse light source, called AROLIS=Artificial OPTIMA Light Source, to do this calibration measurement.

[27]This would correspond to a dome flat.
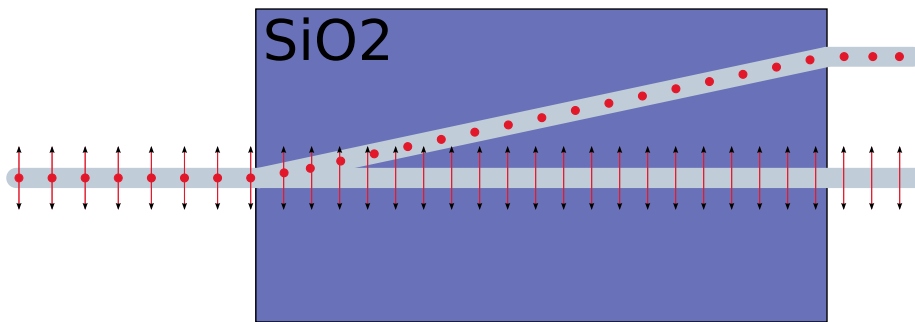
Figure 2.11: Birefringence in a Quartz crystal acts as a polarizing beamsplitter

assumption that the dark sky is uniform over a region of ~ 0.5 arc min[28] (see chapter 5 for details).

The resulting photon counts in all channels are a relative measure of the light flux from the target. Alternating observations of target star and a reference star can be used to perform non-simultaneous differential photometry with photometric standard stars.

2.4.2 Parallel Wollaston polarimeter

In 2002 OPTIMA was equipped with a rotating polaroid filter polarimeter to do polarimetric observations of astronomical objects [Kel02]. Polarization measurement with a rotating polaroid filter is subject to the following constraints:

- one polarization component can be determined at a time

- only slowly varying (or periodic) objects can be studied

- polaroid filters typically transmit ca. 64 percent of parallel polarized light

- transmittance is dependent on the wavelength

The problems linked to polarimetry with polaroid filters led to the decision to build a more sophisticated polarimetric extension of OPTIMA utilizing a parallel Wollaston prism, based on birefringing crystals, to allow measurement of the full set of linear Stoke's parameters in each time bin [MÖ6].

In birefringing crystals an incident light beam encounters two configurations of crystal lattice. Depending on the orientation of its $\vec{E}$ field vector, the interaction with the electrons in the crystal lattice is different. Thus, different polarization directions experience different refractive indices, when passing through the birefringing crystal. Passing through the material the light beam is split into its two polarized vector components (see figure 2.11).

---

[28] This corresponds to a sky flat in CCD astronomy terms.

Figure 2.12: Parallel Wollaston SiO_2 prism with darkened glass plate inbetween both prisms
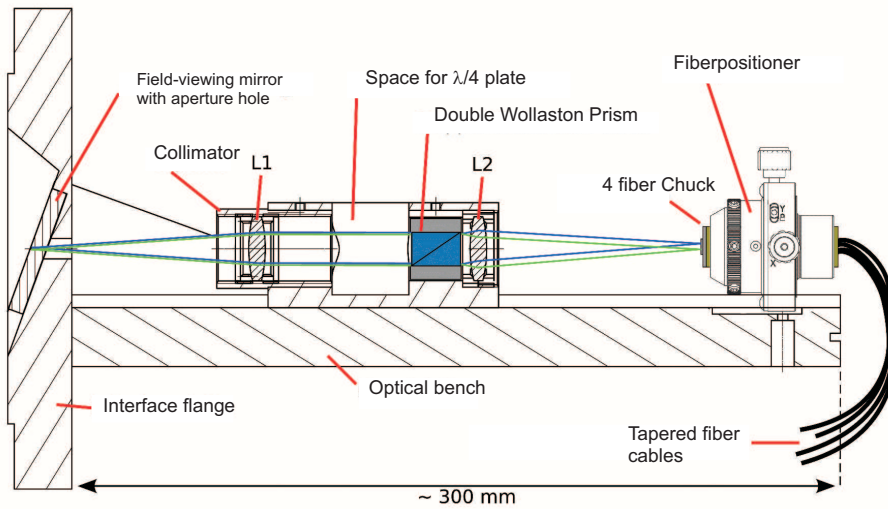
Figure 2.13: Schematic cross-section of the OPTIMA parallel Wollaston polarimeter [MÖ6]

The quartz in the Wollaston prism manufactured by the B. Halle company in Berlin, acts as a polarizing beam splitter, since both orthogonally components pass through. The ordinary and extraordinary ray differ by approximately $1°$.

Since two polarization vectors perpendicular to each other are not sufficient to yield an unambigious solution to the polarization angle of the incident light beam, the OPTIMA prism polarimeter consists of two Wollaston prisms whose birefringence axes are rotated by $45°$ to each other. The two prisms are laminated together, with a dark glass plate between them to avoid stray light influence from one prism to the other.

For polarization measurements it is important not to have any $45°$ mirror in the light path, since that introduces an additional polarization component. In order to avoid this difficulty the "OPTIMA Burst" configuration for the polarimeter was altered in a way to put the polarimeter directly under

the focal plane mirror, such that no additional mirror is necessary. The light from the telescope's secondary mirror falls directely into the 345 mum polarimeter aperture in OPTIMA's focal plane mirror (see figure 2.2).

Figure 2.13 shows the optical path in a cross-section schematic of OPTIMA's parallel Wollaston prism. The f/8[29] light beam passing through the aperture is collimated into a parallel beam by a collimating lens L1, such that the two halves of the parallel Wollaston prism are illuminated evenly. The light exits the parallel Wollaston prism in four different directions, with each pair seperated by about $1°$ in each prism. These beams are imaged by lens L2 onto four optical fibres with a diameter of $400 \, \mu m$ mounted in an adjustable chuck. These correspond to the polarization angles $0°$, $45°$, $90°$ and $135°$, where the individual brightnesses allow the mathematical reconstruction of the polarization angle and degree of polarization of the incident light beam. The construction details and mathematical treatment of polarization are treated in [MÖ6].

The new parallel Wollaston prism in "OPTIMA Burst" has several advantages over the old rotating polaroid filter version. It measures the three linear Stokes parameters I, Q and U simultaneously, thus the time resolution for polarization measurements is now only limited by the DAQ. The light loss in the optical lens system and the SiO_2 itself is negligible and fainter sources can be observed.

The only disadvantage lies in the fact that only the target, one spot of the surrounding background or a reference star can be placed on the polarimeter aperture at a time, where the rotating polaroid filter polarized all the light in the field of view which allowed measuring the degree of background polarization simultaneously. This was particularly important in measuring the polarization of the optical pulses of the Crab pulsar [KSKS05].

Currently the OPTIMA polarimeter is restricted to the measurement of linearly polarized sources, but the mechanical mounting has space for a $\lambda/4$ plate that will be able to be moved into the light beam in front of the Wollaston prisms to allow measurements of circular polarization on request.

2.4.3 Spectrometer

Another optional component of OPTIMA is a simple 4-colour spectrometer. Through an optical fibre pickup in the focal plane mirror (see section 2.3.1, (3) in figure 2.2) light of a target star can be fed into a prism.

A 60-degree dispersion prism spreads a spectrum from 500 nm to 900 nm over 1.1 mm at its exit side. Four fibers of $320\mu m$ diameter mounted on a three-axis micrometer stage can be adjusted to pick up four "colours" out of that spectrum simultaneously. Due to low optical quality of the prism used and the small fill-factor of the pickup fibers the spectrometer has an overall efficiency of 5–10 percent [KSD[+]06]. It was primarily intended to extend OPTIMA's photometric measurements to observations of variations in different "colours" of rather bright sources (e.g. Cygnus X-1).

---

[29]f/8 is the focal ratio of the Skinakas 1.3 m telescope where the OPTIMA Burst polarimeter has been used to date.
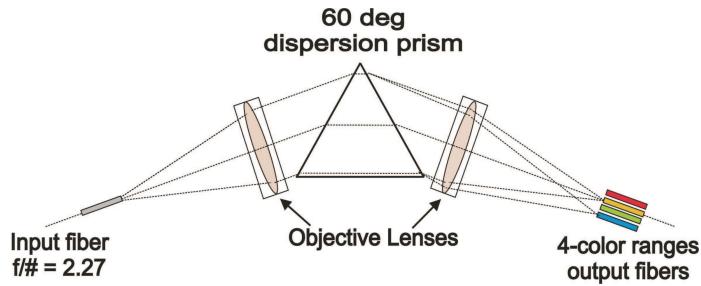
Figure 2.14: Schematic of the prism spectrograph for 4-colour-photometry [KSD+06]

This should give information about timing correlations in different spectral bands and about colour variations during outbursts.

2.5 Scientific goals

In order to observe physical processes in the universe that happen on small scales, high time resolution is essential. Amongst this class of objects are pulsars, cataclysmic variables [KKS+03], black hole candidates [KSSB01], Gamma-Ray Bursts and other objects. The "light time" links the smallest observable structures to their time variation. A source that varies on a timescale of Δt is thus expected to be of size $\Delta x \sim c \cdot \Delta t$. In the case of smaller or extending objects, e.g. a GRB fireball, the early phases of these objects are thus perfect candidates for observations with high time resolution instruments such as OPTIMA. At later stages, where time resolution is not the most important parameter anymore other instruments, e.g. CCD based cameras, are more suitable. With the improvement of OPTIMA over the last years, it became a particularly useful tool to study the whole range of the aforementioned variable objects.

The following section will describe a few of these compact objects that have been studied with OPTIMA in more detail.

2.5.1 Pulsars

Pulsars are neutron stars that show pulsations in their emission characteristics. Neutron stars were only objects theoretically predicted to be the final result of stars exploding in a supernova, resulting from equation of state calculations by Baade and Zwicky in 1934 [BZ34]. The discovery of radio pulsars [HBP+68], and later the detection of their optical pulsar emission [CDT69] provided observational data for the theoretical interpretation of these objects.

Neutron stars are compact stellar objects with radii of ca. $10 - 15$ km. They have masses between 0.2 and 2.0 solar masses, depending on the mass of the progenitor's core that collapsed in their creation. The one to two solar masses of the progenitor's core collapse until electron degeneration is overcome. The increasing density forces electrons into the nuclei of the core and electrons
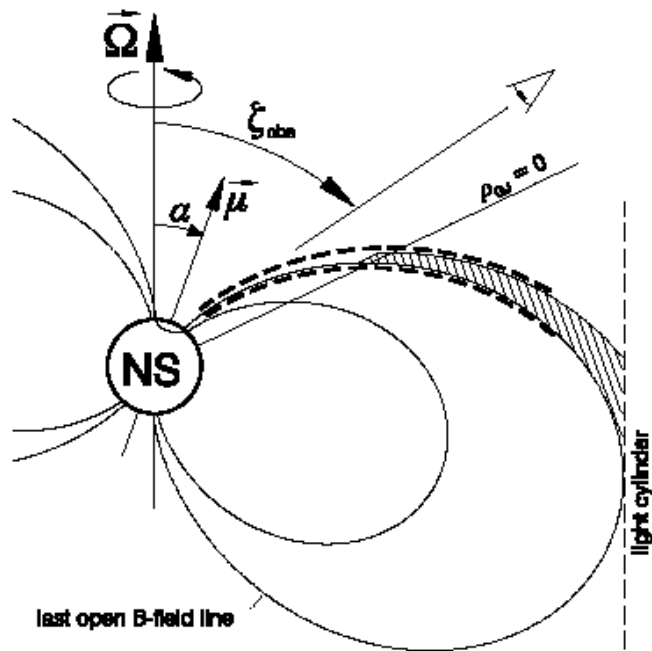
Figure 2.15: Canonical model of a neutron star [DR03]

and protons combine to neutrons. Thus, a neutron star consists of neutrons or neutron-rich nuclei, depending on the depth from its surface. The resulting object is a very dense star with 1–2 solar masses of neutron matter in a volume of $10 - 15$ km. The resulting densities are up to 10^{15} kgcm^{-3} in the core, which is thought to be of solid neutrons.

The energy source of pulsars lies in their rotational energy. The energy radiated must come from a reduction of their rotational frequency [Gol68]. Their emission is mainly governed by the interaction of charged particles ejected from their surface with the strong magnetic field extending into the surroundings of the neutron star. The details of these processes will be explained in the following section.

Magnetic fields of Pulsars

Neutron stars possess a strong magnetic field. In the collapse of the progenitor star, the conservation of magnetic flux leads to an increase in the magnetic field strength from some 100 G in a main sequence star to 10^{12} G in the compact neutron star. The magnetic field governs many of the observed properties of pulsars. The period increase of the Crab pulsar was first measured by Richards and Comella in 1969 [RC69] and Franco Pacini had already shown that the observed slowdown in the period of pulsars implies a high magnetic field [Pac68]. The following effects are depicted in figure 2.15:

Outside the neutron star the strong magnetic field dominates the forces on charged particles. It

is strong enough to eject surface electrons from the polar caps of the neutron star [GJ69], which leads to high-energy particle generated synchrotron radition like it is observed for example in the Crab pulsar. The dipole's misalignment with the rotational axis causes a "lighthouse" beam pattern that can be observed at the rotation frequency.

The rotating magnetic field also induces an electric field which extends out to a region limited by the "light cylinder". This is at a distance $r_c = c/\Omega$ from the neutron star, where a co-rotating (angular velocity Ω) extension of the neutron star would have a radial velocity equal to the speed of light, c. Within the light cylinder a high-energy plasma of ionised particles exists. These are confined to a magnetosphere that co-rotates with the neutron star. The magnetosphere is the source for the observed beam of radiation emanating from the poles of the neutron star.

Also the neutron star's interior interacts with the magnetic field. The neutron fluid contains a small number of free protons and electrons that are strongly coupled with the magnetic field. Since the magnetic field is bound to the particles in the solid core, the observed rotational frequency of the electromagnetic beam is the same as the core's rotational period. The upper layers of the neutron fluid that can penetrate the crust are not as strongly coupled to the magnetic field and can rotate at a different rate. The coupling can change suddenly, leading to a step in the rotation rate. This is sometimes observed as a so-called "glitch" in the pulsar's light curve [LG98].

Emission characteristics of pulsars

Pulsars usually emit energy across the whole range of the electromagnetic spectrum. Energy output has been observed in all wavelengths from radio to UHE γ.

There is highly variable and highly polarized **radio emission** that emanates from a height of a few stellar radii above the magnetic poles. The high intensities of the radio emission cannot be caused by thermal emission or by incoherent synchrotron emission processes. The magnetic pole origin is supported by the observed pattern of linear polarization that swings by an angle up to $180°$ in an integrated pulse. There is usually also a circularly polarized component observed close to the centre of a pulse.

Optical emission is only observed from young pulsars or rejunivated pulsars in binary systems. It originates from a different region than the radio emission, closer to the light cylinder. The continuous spectrum is caused by charged particles, mostly electrons and positrons, which are confined to travel along the magnetic field lines. These charged particles travelling at relativistic speeds along magnetic field lines emit synchrotron radiation.

The observed emission cannot yet be fully reconciled with theoretical models of pulsars. The "outer gap model" [RY95], [TSHC06] and the "polar cap model" [DH82] reproduce the intensity light curve in good agreement with observations of the Crab pulsar. Yet, they cannot completely explain the polarization characteristics. Newer models such as the "striped wind model" [KSG02]

and the "two pole caustic model" [DR03] seem to give qualitative explanations for the polarization characteristics.

The striped wind model assumes the emission region to be within the toroidally wound magnetic field lines at distances of ca. 10 to 100 light cylinder radii. The two pole caustic model assumes the emission region lies just outside the closed field lines, where open magnetic field lines occur, and the observer can see alternately the two poles. The main pulse and inter pulse are then caused by the caustic superposition of photons emitting at different heights above the neutron star.

Search for optical pulsars

OPTIMA was intended to provide an instrument for the search for optical pulsars. Most pulsars were initially discovered in the radio. The first identified optical pulsar was PSR B0531+21, the Crab pulsar, in 1969 [CDT69], shortly after the initial discovery of radio pulsars. Only a small number of pulsars have been found that show optical pulsation. Many optical pulsars are older pulsars that have been rejuvenated by spin-up processes of a binary partner [LG98]. The difficulties in searching for pulsars lie both in the sensitivity and time resolution of suitable instruments to search for optical emission of pulsars.

Most known pulsars are weak light sources, mostly having visual magnitudes dimmer than 22^m, with the exception of the Crab pulsar that has a visual magnitude averaged over the period of 16.6^m.

The search for optical pulsars starts with looking at pulsars that show pulsations in the radio- or gamma-regime. The question is then whether these also show optical variation at the typical rotational period of the pulsar. Only a small fraction of the total energy is emitted in the optical region. This requires long integration times with ground based instruments or highly sensitive detectors, like avalanche photodiodes, to be used to detect faint pulses emitted by the pulsar. Another problem lies in the fact that due to their rapid rotation, a consequence of the progenitor star's contraction and the conservation of angular moment, the pulsation period of optical pulsars is very short. Slower pulsars have periods of about one second. There is also a number of fast, young pulsars of periods of less than a second and a small population of pulsars with milisecond periods (see figure 2.16).

Thus, instruments such as OPTIMA that provide high time resolution with a good signal to noise level are required to search for pulsars. Up to the time of writing, only a few sources that show optical pulsations have been confirmed [SG02]: PSR B0531+21 (Crab pulsar) [CDT69], PSR B0833-45 (Vela) [WPM$^+$77], PSR B0540-69 [MP85], B0656+14 [SRG$^+$97] and J0633+1746 (Geminga) [SGH$^+$98]

High time resolution of the Crab light curve

OPTIMA's performance was first demonstrated with measurements of the Crab light curve in 1999 at the Calar Alto observatory in Spain. An unfolded light curve (see figure 5.2) clearly reveals a

28
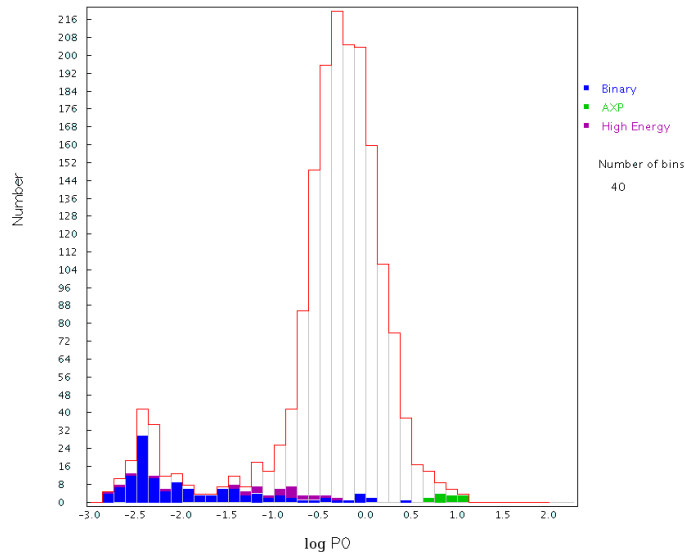
Figure 2.16: Distribution of the periods of $\sim$ 2000 known pulsars as of 25th September 2007, generated from the Australia Telescope National Facility Pulsar Catalogue site [atn07], [MHTH05].

train of main pulses and inter pulses [SKS01].

Through folding a better signal to noise ratio for the light curve can be obtained (see section 5.1.1). The resulting light curve (see figure 2.17) of the main pulse and inter pulse showed full agreement with measurements done with the high-speed photometer aboard Hubble.

The high time resolution of OPTIMA, currently 4 μs, enables the search for example for changes in the light curve. These are thought to be related to the magnetic field generated in the core of neutron stars (see section above) or due to precession, for example in the relativistic pulsar B1913+16 [Kra98].

Polarization measurement of the Crab pulsar

As mentioned above radio emission from pulsars is highly polarized. Optical emission shows far less polarization, but current models predict polarized emission from certain regions (see section above), although these models cannot yet be brought into full agreement with observational data.

Observations with OPTIMA's rotating polarimeter in 2001 performed at the Calar Alto observatory[30] supplied high time resolution polarization measurments of the Crab pulsar and its surrounding nebula (see figure 2.18).

The light curves show that the Crab pulsar emits highly polarized optical emission, particularly in the bridge and the "off-pulse" phase. Also the polarization properties of the main pulse and the inter pulse are very similar. Comparison with the radio curve shows that the minimal optical polarization degree is at the phases of maximum radio emission. A bump in the polarization degree

---

[30]OPTIMA was used at 3.5 m telescope at the Calar Alto observatory on the Sierra de los Filabres, Spain.
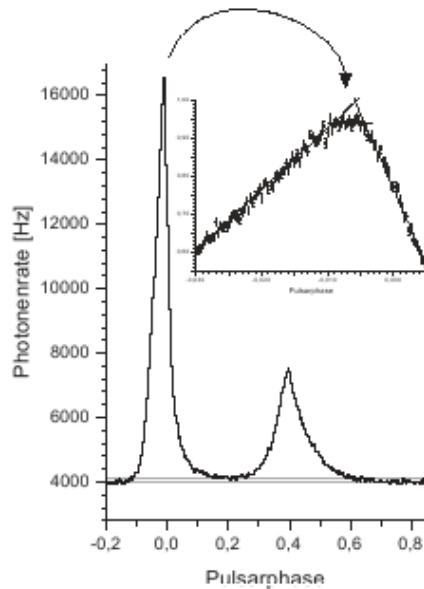
Figure 2.17: Optical light curve of the Crab pulsar at 112 μs resolution

can be seen on the rising flank of the main pulse and there is an indication for such a bump in the inter pulse, too [SKS07].

2.5.2 Cataclysmic Variables

Cataclysmic variable stars (CVs) are binary systems, containing a white dwarf of typically 0.3 to 1.3 solar masses as the primary and a red dwarf or a late main sequence star as the secondary. These revolve around each other in close orbit, usually at distances of only a few hundred thousand kilometers. At this small separation the larger secondary star fills or even overfills its Roche lobe. The Roche lobe determines the region, where material of a star is entirely bound to it. If the star overflows its Roche lobe, the material that passes the Lagrangian point L1 between the two stars experiences a net force in the direction of the white dwarf and depending on its kinematics, might eventually be drawn towards it.

This stream of material from the secondary to the primary leads to a series of effects. In contrast to "normal" stars that vary only on small scales and small timescales, CVs show changes in magnitude, outburst and flares on small time-scales of hours, minutes or even seconds in their light curves.

Although the secondary star with a radius of about 0.15 $R_{\odot}$ is much larger than the white dwarf with a radius of a few 1000 kilometers, it is by far cooler, temperatures are ca. 2900 K and 60000 K respectively. Thus the overall brightness of the white dwarf outshines its companion. In an eclipsing
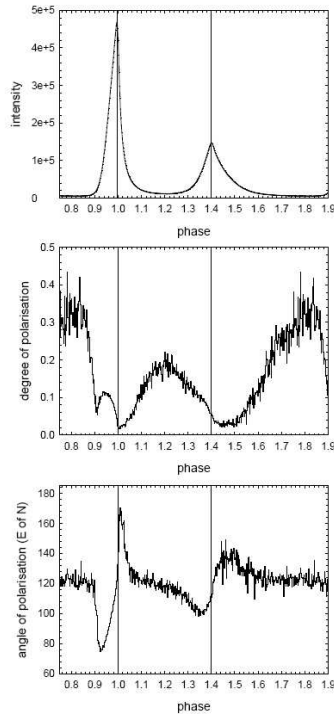
Figure 2.18: High resolution optical polarimetry of the Crab pulsar [SKS07]

binary the orbital plane is entirely or nearly lying parallel to the line of sight of the observer[31], and the two stars are eclipsing each other at the orbital period. When the secondary eclipses the much hotter and brighter white dwarf, this can be seen as a deep eclipse in the lightcurve.

Types of CV

Despite their similar nature, cataclysmic variable stars are classified into different types, depending on the properties of their light curves, which are influenced by the following effects:

The hot white dwarf in CV systems is often surrounded by an accretion disk of material accreted from its companion star. Dynamical processes in the disk, caused by the interaction of gravitation, viscosity and differential rotation within the disk, lead to distinct features that can be observed in their light curves. The light curve is a superposition of all the effects causing emission in the CV system: The hot primary, the cooler secondary star, emission from the extended accretion disk, the accretion stream from the secondary to the primary and the accretion spot where the accretion stream hits the disk (or the white dwarf's pole in the case of magnetic CVs).

The naming scheme of CVs is based on the principal representant of a class of physical behaviour which often was only later discovered to be not a variation of another type[32], but to constitute its own type. Amongst others are Novalike CVs, AM Her, AM CVn and SU UMa CVs.

---

[31]Inclination angle, i, close to $90°$

[32]Classification according to AAVSO.

31

Novalike CVs are the prototype of a Cataclysmic Variable where the material flowing from a late type main sequence star onto a white dwarf eventually builds up to such high densities that nuclear reactions start again on the white dwarf, leading to a massive output of energy that can be observed as a brightening of several magnitude decaying over the time of a few weeks. AM Her type CVs are systems where the white dwarf has a strong magnetic field which prevents material flowing from the mass-donating star to form an accretion disk. Instead the material is funneled along the magnetic field lines and impacts at the poles of the primary.

OPTIMA has been used in observations of several CVs in the past years [SKS01] and [Str01]. During the "OPTIMA Burst" campaigns in 2006 and 2007 (see section 2.6) observations of the AM Her type CV HU Aqr were carried out, and their analysis is presented in this thesis (see chapter 5 section 5.2).

2.5.3 X-ray binaries

X-ray binaries are binary systems with strong emission in the X-ray region, indicating that non-thermal processes are the source of the high energy emission. X-ray binaries are classified into Low Mass X-ray Binaries (LMXB) and High Mass X-ray Binaries (HMXB), depending on the type of companion star. The primary is either a neutron star (see section 2.5.1) or a black hole. LMXB have a low-mass, late-type star as companion with a luminosity much lower than that emitted in X-rays. Typical orbital periods are of the order of a few hours or days. Observations of an object of this kind, Aquila X-1, are presented in chapter 5.

In HMXB the secondary is an early-type giant or a supergiant. Due to the higher mass of the companion Kepler's laws dictate that the orbital periods of HMXB must be longer than those of LMXB. The periods can be a few days to hundreds of days. Correlated observations of optical and X-ray emission in a multiwavelength campaign performed with OPTIMA and XTE to investigate the nature of the black hole candidate XTE1118+480 were published in [KSSB01].

The X-ray sources in LMXBs and HMXBs are often surrounded by thick accretion disks. The processes of material accreting onto the disk dominate the X-ray emission and by far outshine the luminosity of the primary and secondary.

X-ray pulsars are a slightly different class of object. These are accreting neutron stars in binary systems that do not show pulses like those of the high-energy young pulsars. The source of this X-ray emission is non-thermal and thought to originate from matter that falls from the secondary onto the compact object. The strong magnetic field funnels the matter along the magnetic field lines and close to the magnetic poles high-density shock-waves cause the observed X-ray radiation. Examples of X-ray pulsars are Hercules X-1, Centaurus X-3 and the Small Magellanic Cloud X-1.

2.6 "OPTIMA Burst" campgain

In 2004 OPTIMA underwent a major redesign to make the instrument suitable as rapid-response instrument for the observation of Gamma-Ray Burst afterglows [Ste04]. The scientific aim of the "OPTIMA Burst" campaign was to observe the GRB afterglow from as early as three minutes after the initial trigger.

The University of Crete (UOC) operates a 1.3 m telescope on Skinakas mountain, near Iraklion on the island of Crete. Close cooperation between the Max Planck Institute for Extraterrestrial Physics and UOC presented the opportunity of OPTIMA being used as a guest instrument for three months periods in 2006 and 2007. In both years two long-term standby observational campaigns at the Skinakas observatory were carried out.

The Skinakas observatory is located ca. 30 km from the city of Iraklio, which deteriorates light conditions on the Eastern horizon, but the seeing conditions at a height of 1800 m in the Ida region are amongst the best in Europe [BSM$^+$01].

The telescope itself is a Ritchey-Chrétien design, which is a design to minimize optical aberrations. The primary mirror has a diameter of 1290mm and the system has a focal length of 9857 mm. This results in the previously mentioned f-ratio of f/D = 7.64. The telescope has an equatorial mount by DFM Engineering and its comparably small size allows it to slew quickly. The mounting slews at a maximum speed of $2.5°s^{-1}$, so it can reach any point on the sky within about 100 s [Ste04], which makes it suitable for rapid response observations of Gamma-ray burst afterglows in the optical.

During the "OPTIMA Burst" campaigns in 2006 and 2007, several events triggered OPTIMA observations. For example OPTIMA observed a X-ray transient object, which showed a gamma ray outburst and triggered a GRB message, "GRB070610", distributed to the GCN[33] [SSK$^+$07]. The Skinakas observatory granted OPTIMA considerable amounts of observational time, so that secondary science targets could be observed. Some of the observations taken and the results obtained are presented in chapter 5.

---

[33]NASA's Gamma-ray Burst Coordinates Network distributes so-called notices about the position of Gamma-ray bursts which are detected by space-based instruments [gcn07].

Chapter 3

Existing Data Acquisition System

Although the OPTIMA system has undergone various hardware improvements since its first version in 1998, the concept and implementation of the data acquisition (DAQ) system has remained unchanged. It was implemented as part of a Ph.D. thesis [Str01] during OPTIMA's initial development. Its principle of operation, implementation along with its shortcomings and disadvantages will be described on the following pages, and chapter 4 is dedicated to the new improved DAQ system, which was developed as part of this thesis.

3.1 Hardware

As described in chapter 2 avalanche photodiodes (APDs) are used to register incoming photons that pass through the telescope and fibres. These generate a short TTL pulse for every incoming photon.

The challenge for the DAQ is to first register these pulses and then associate them with an absolute time tag. Systems that perform single photon counting with relative timing, with respect to a trigger, are commercially available and widely used in other areas of science. Absolute timing is not well covered by commercial systems. Thus, in order to achieve the desired time resolution on the order of microseconds a digital DAQ system, using a GPS-disciplined oscillator as an absolute time reference, was developed in house [Str01].

3.1.1 Digital input

A digital I/O card[1] is used to input the signals of photon events to the DAQ computer. The card used offers up to 16 channels that can be configured as input or output, where the current system uses them only as input ports. Although the DAQ card has no integrated logic for processing of data, it has a buffer for 2048 samples of input states of all channels. As will be described in detail in the next section, this allows it to be used in a hardware-controlled mode.

---

[1]National Instruments PCI-DIO-32HS

3.1.2 Timing and clocking

The GPS card generates an absolute UTC from the signal of several[2] satellites[3]. The GPS was intended to provide positional information at virtually all points on the globe to high accuracy. This goal is achieved through 24 satellites in orbits of about $20,000$ km altitude that carry atomic clocks on board. The orbital trajectories of the satellites are known and using the time signal on board of the satellite as reference, transmission times of a signal from the satellite can be timed. Each signal transmission timing basically restricts the position of the receiver in question to a circle on the geoid. It can easily be seen that by receiving and timing the signal of four different satellites simultaneously, the receiver's position in three-dimensional space can be determined[4]. The accuracy of this measurement depends on the ability of high-precise relative timing and the knowledge of satellite trajectories (these are stored in the GPS receiver and updated with information from the satellites themselves). Although due to the military importance of the system, the publicly available accuracy is deteriorated to a final accuracy of approximately 3 m.

As a side-effect of the working principle of the GPS, the atomic clocks on board of the satellites can also be used to compute a high-precision time reference at the receiver's position. This information is used in OPTIMA to acquire a reliable, precise absolute time signal. Due to jitter in the GPS time signal, it is not possible to use it directly as a high-speed timing reference. It does provide a highly stable long-term time reference which can be used to discipline an oven-stabilized oscillator which in turn provides a short-term stable high-speed timing.

The GPS card has such an internal oscillator. An oven-stabilized quartz oscillator provides a clock with a very stable frequency, though the desired frequency can have a slight offset over longer times (minutes or hours). This creates a noticable inaccuracy. The oscillator is referenced to an averaged measurement of many GPS pulse per second (PPS) signals, thus, avoiding the GPS inherent jitter. The combined time signal is then used to compensate the oscillator's internal drift on regular intervals. Combining the short-term stability of the oscillator with the long-term stability of the GPS PPS signal, a clocking error of less than 5 out of 10^8 oscillator cycles can be achieved. Since the oscillator is adjusted with the GPS-generator correction on the order of 1000 seconds, it is guaranteed that the time signal used in OPTIMA never looses a complete clock cycle [Str01]. The GPS card's internal oscillator can be tuned to frequencies of up to 10MHz.

A stable time reference through the GPS-disciplined oscillator enables absolute time tagging of photon events. A related problem is that the input states of the digital I/O card must be tagged with that absolute time on read-out.

The I/O card's input states can only be read through polling on regular intervals. On a non-realtime operating system this cannot be guaranteed. The solution taken in [Str01] is to do as

---

[2]At least 4 (see chapter 2)

[3]The Datum bc627AT GPS card provides a time signal with an accuracy of 2 μs.

[4]To solve a system with four unknowns, (at least) four equations are needed to acquire a solution.

much of the time tagging as possible in hardware. The National Instrument's card can be externally triggered on one of its input channels. By feeding the oscillator clock output signal generated on the GPS card into one of the I/O ports of the DAQ card, regular triggering on the exact oscillator interval timing can be achieved. On every clock trigger the input states of the 16 I/O ports are sampled and written to the DAQ card's internal buffer. The buffer only holds up to 2048 samples and the card does not possess any logic to sort out input channels which state was zero, i.e. no photon event was registered. That means that the triggered reading of input states to the interal buffer is an intermediate storage.

Depending on the polling frequency the GPS card's oscillator is set to, this internal buffer only holds up to a few miliseconds of data. Although the computer does not have to guarantee real-time processing on the clock interval anymore, that means that the DAQ computer must read out the card's buffer regularly before a buffer overrun occurs. The system currently used[5] in OPTIMA showed in laboratory tests to support a clock frequency of up to 250 kHz.

The OS must copy the internal buffer to the computer's RAM at least every 8ms[6]. The solution adopted in [Str01] is to allow the DAQ application to acquire almost all processing time of the Windows98 operating system. Although Windows98 already supports pre-emptive multitasking[7], this is achieved by quitting all unnecessary running programs, and increasing the priority setting of the DAQ application.

Should an overrun of the DAQ card's internal buffer occur before it is being read out, this is flagged by the DAQ software and the user notified. The last good data samples are saved to hard disk and the observation stopped. Since reading the DAQ buffer on regular intervals is so critical, this means that the DAQ PC should not be used for any other tasks than reading out the DAQ and saving the data.

Input signal shaping

Because the TTL pulse generated by the APD itself only has a pulse width of 9 ns that occurs at an arbitrary time within the clock interval of $4\,\mu$s, it would only be registered if it is coincident with the trigger pulse. The DAQ card is triggered on the 250 kHz oscillator signal and hence the APD signals on the card's I/O line must be stretched to a length of $1/250\,$kHz $= 4\,\mu$s, so that a TTL pulse is not missed during the interval (see figure 3.2). This is done by pulse shapers that extend the 9 ns TTL pulse to the clock interval length. If an incoming photon is registered by the APD within the clock interval, that input level will be raised, the $4\,\mu$s pulse will coincide with the clock trigger and be registered as a detected photon.

---

[5]A 700 MHz Pentium-III PC.

[6]2048 samples/250 kHz = 8.192 ms of measurement time

[7]Pre-emptive multitasking is a multitasking method scheduled by the Operating System, which divides time slices between all running processes.

Figure 3.1: Electronics rack that peforms signal shaping of APD output pulses

The difficulties of this method to register the photons within fixed interval lengths with external triggering will be explained in the following section 3.2 on the DAQ software system.

3.2 Software

This section deals with how the hardware clock is implemented in detail with the software reading the internal buffer, creating correct time tags and saving the recorded data. A custom designed software then tags the registered pulses with a time stamp, running on a standard PC with Windows98.

The choice for this solution instead of a real-time operating system were mainly due to cost efficiency and easier development [Str01]. Also, the easier replacability of standard PC components played an important role for the OPTIMA system.

3.2.1 DAQ timing

Figure 3.2 shows how the GPS PPS, oscillator clock signal and DAQ software perform the measurement of the input states of the digital I/O card. If the DAQ software is set to record data (3), the measurement ist started on the next GPS PPS signal (2). From then on, at each 250 kHz oscillator pulse (1) the input states of the data I/O card (5) are sampled in its internal buffer. The DAQ card possesses no internal logic, so it can only dump the the 2 Byte input word to its buffer. The buffer can take 2048 samples, which corresponds to a measurement time of ca. 8ms. This poses the limit
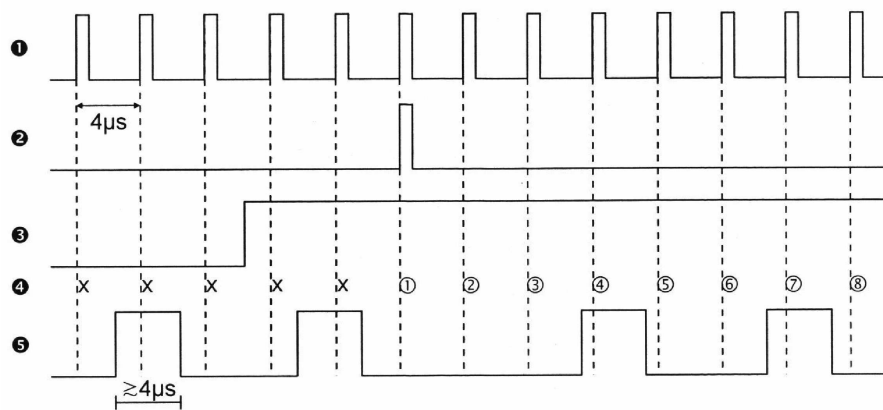
Figure 3.2: DAQ read-out timing [Str01] (1) Clocking (250kHz) (2) GPS Pulse per second (3) Start setting of control software (4) Index number of clock interval (5) Signals of APD detector

for the DAQ system to regularly empty the internal buffer of the I/O card to the computer's RAM. It is a far lesser constraint than the $4~\mu$s reaction time, if the polling had to be done entirely in software, but still means that the CPU of the DAQ PC should not have to perform any other tasks than pushing data.

3.2.2 Difficulties with DAQ polling

Triggering on a fixed pulse length causes two difficulties in the data acquisition process:

- The pulse length of input signals must correspond to the DAQ clock frequency

- If more than one photon arrives in one interval they are detected as a single event

Pulse length

First, the pulse length created by the shaping electronics must match the clock interval length very accurately to create a possibility close to one to detect an incoming photon. If it is too short, a photon might not be registered, because the input pulse might not coincide with the clock trigger. On the other hand, a pulse length that is too long, can coincide with two clock triggers and hence one photon would be registered as two events. The NIM electronics allows precise shaping of the pulse, so that these two requirements can be met and the probability to register a photon that arrives in the APD is practically one (see figure 3.2).

Secondly due to the fact that one event already raises the input level of this channel and the pulse length is stretched to the clock interval length, a second photon arriving in the same interval at the APD is not detected.

39

Pile-up of photons

With observations of brighter sources, the inability to detect two photons in the same clock interval leads to a pile-up effect. The higher the intensity of the observed target, the higher the probability that more than one photon arrives in one clock interval.

The probability of the number of photons per clock interval for the given intensity of a target is governed by Poisson statistics. Thus, the probability, p_k, of falsely detecting only one photon, even though k=0, 1, 2,...N photons were incident in one clock interval, can be calculated from the Poisson distribution formula:

$$p_k = \frac{\lambda^k}{k!} \cdot e^{-k}, (k = 0, 1, ...) \tag{3.1}$$

where

λ : expectation value of photons per clock interval

k : actual number of photons per clock interval

p_k : probability of k photons per clock interval

and a constant average number of photons per time interval $\lambda = \Delta T \cdot I$ is assumed, with ΔT being the length of the clock interval and I the average photon counts per second.

The dependence of the probability to detect only one photon on the actual number of incident photons is shown on the graph in figure 3.3. If an error of 1 percent is deemed acceptable, the Poisson formula can be used to solve for the count rate, λ, where that limit is met:

$$0.01 \geq \sum_{i=2}^{\infty} \frac{\lambda^k}{k!} \cdot e^{-\lambda} \tag{3.2}$$

Instead of evaluating an infinite sum, the property of probability $P(\bar{A}) = 1 - P(A)$ can be used for an easier calculation of the probability of having two more photons in one interval, in the following way

$$p_{k \geq 2} = 1 - p_0 - p_1 \tag{3.3}$$

using the Poisson formula and 1 percent confidence value from above leads to an equation in lambda

$$0.01 \geq= 1 - e^{-\lambda} - \lambda \cdot e^{-\lambda} \tag{3.4}$$

Through rearranging it transforms into an expression for $1 + \lambda$

$$e^{-(1+\lambda)} \cdot (1 + \lambda) \geq \frac{0.99}{e} \tag{3.5}$$

Substituting $x = (1 + \lambda)$ and applying the natural logarithm to both sides of the equation, gives an equation in x:

$$\ln x - x \geq -1 + \ln 0.99 \tag{3.6}$$
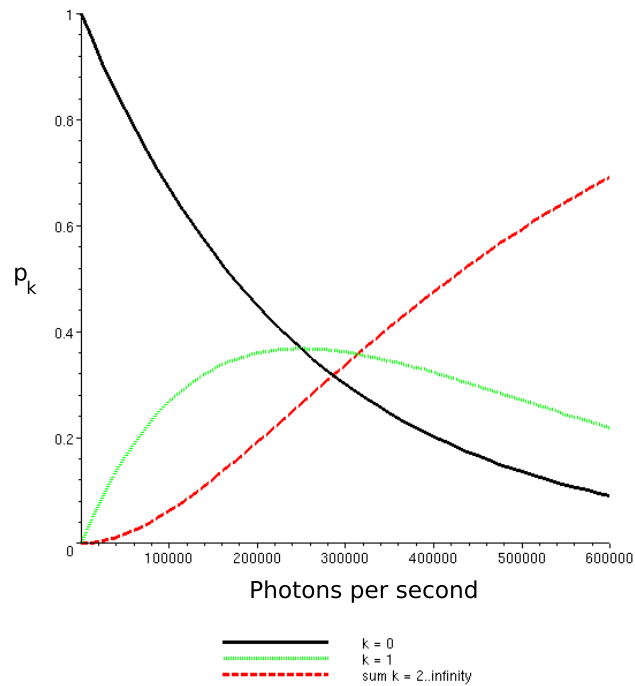
Figure 3.3: Photon pile-up due to finite polling interval of $4~\mu$s

Solving for x and resubstituting back to λ, it can be shown that at a photon intensity of more than 37,138 counts per second the confidence level of 1 percent is not met anymore.

Such high count rates are not to be expected in observations of pulsars even with telescopes with large apertures[8]. Furthermore, it is possible to apply correction factors, using the known clock frequency and Poisson statistics, to determine the detected number to the recorded number of photons to get an estimate of the most probable actual number of incident photons at high count rates [Str01].

Internal buffer overrun

The most critical failure of the DAQ process occurs, when the internal buffer of the DAQ card is not emptied on time by the DAQ computer and a buffer overrun leads to a loss of data. The DAQ control software can check whether this occurs. In case of a buffer overrun the running measurement is stopped, the previous data that was still unaffected is saved and the user notified.

---

[8]The brightest optical pulsar, the Crab pulsar, has only a theoretical count rate of 15,000 counts per second at the 3.5 m Calar Alto telescope [Str01].

3.2.3 Event processing

When the DAQ control software reads the DAQ card's internal buffer, it uses DMA[9] transfer to write the samples directly to system RAM. The great advantage of using DMA lies in the fact that it is the fastest method of transferring information within the computer system, as opposed to copying data using the CPU.

In the post-processing step, the cycle number (4 Bytes) and the channel number (1 Byte) are saved for all channels containing a photon. Along with the known start time of the observation, the index number of each measurement cycle allows to compute the corresponding event time for each photon in the later data analysis.

3.2.4 Application software

DAQ recording

The necessity to empty the D-I/O buffer on regular intervals, and the fact that the system cannot provide both fast memory transfer to RAM and to the hard disk at the same time, does not allow to save the data immediately to hard disk. When the RAM[10] is filled, the measurement cycles are stopped and the content of the RAM is written off to hard disk. With typical transfer rates of PC hard disks, this takes a few seconds, during which no photon data is recorded. Once writing to disk has finished, the measurement cycles are started again on the next PPS.

For every event the software records the corresponding index of the measurement cycle number (4 Byte) along with the channel number (1 Byte). That means the maximum index number is $2^{32} = 4,294,967,296$, and the length of a continuous observation at a $4~\mu$s cycle interval is limited to ca. 17180 seconds, which is 4.8 hours. In practice the maximum RAM buffer sets a much lower limit of ca. 10 minutes.

Ratemeter and System status

In addition to storing the data the DAQ application shows numerical ratemeters for all channels, allowing at least some quick-look of photon rates currently occuring in each channel. Furthermore, there is a system check application that assures that the GPS card receives enough satellite signals to generate a GPS pulse-per-second signal and that the GPS card's internal oscillator has achieved its equilibrium state. This usually takes roughly 10 minutes after startup of the system and the DAQ can only be started if a correct hardware-clock is assured.

---

[9]DMA = Direct Memory Access allows system components to access system memory indepedently of the CPU.

[10]Its size can be set up to 250 MB. This corresponds to a total of $250 \cdot 1024 \cdot 1024 Byte/5 Byte = 52428800$ events.
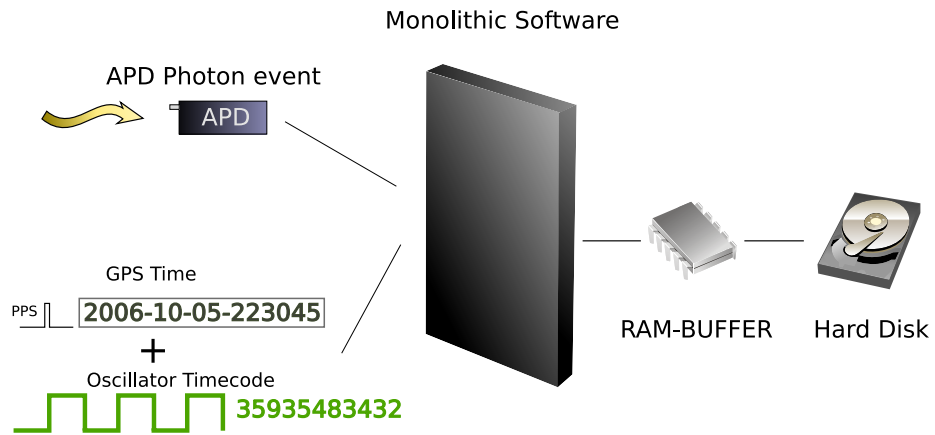
Figure 3.4: The existing DAQ application is a monolithic application that performs only recording and rate monitoring

3.2.5 Disadvantages of the current software

Considering restrictions in terms of project time and available resources the development of the current software was the best compromise. The detailed reasoning for the decisions taken are given in [Str01]. In addition to the already mentioned disadvantage of its monolithic design, there are three further shortcomings of the current DAQ software.

Monolithic software

The software is written in a monolithic way, meaning all functionality is put into only one application. GPS status, DAQ recording, ratemeter and even analysis packages are compiled into one application. Although the user can choose which functionality should be used for the problem at hand, e.g. display photon rates in the ratemeter, start DAQ recording, it makes extending the program's functionality difficult.

A change in one part of the application can easily lead to affect other parts of the software, since the whole package is interdependent and has to be recompiled as a whole. Due to the critical time tagging of photon events, a change in handling the data at one point, might affect the overall performance of the program in an unforeseen way.

Direct Memory Access and RAM buffer

The performance requirement to empty the internal buffer of the DAQ card in short time demands the use of DMA (see section 3.2.1). In order to do this at the time of development of the OPTIMA DAQ software, this was most easily achieved by circumventing memory protection. Windows98 is the last operating system of the MS-Windows family that still allows applications to access memory

without memory protection.

Thus, porting the software to more modern versions of Windows was difficult and had not been done in the past years.

Due to the fact that both transfer to memory and CPU performance for event processing meant bottlenecks in the current software, it is not possible to save the data to hard disk at the same time it is stored in RAM buffer. If the software was writing data off to hard disk, the pure memory transfer rates would allow so, but the real-time time tagging of photon events within $8\,\mathrm{ms}$ means that the necessary CPU time could not be dedicated to the hard disk transfer. Therefore event data is intermediately stored in the RAM buffer and only if that has been filled up, it is written in one go to hard disk, during which the current observation is interrupted.

The intermediate storage of data in RAM means that a software crash leads to loss of data that is in the current RAM buffer, instead of having most of it already in long-term storage on disk. Also, interruptions of several seconds due to emptying the RAM buffer and writing off the data to hard disk, creates gaps in the recorded light curves.

Pile-up effect

The pile-up effect of falsely recording only one photon event, while two, three or more photons were detected in the APD is a major disadvantage of the fixed clock interval. Using the probability derived from the Poisson distribution this can be corrected for to a certain degree [Str01].

Because this is a statistical correction, this method has its limits. With increasing count rates the errors increase. At count rates below 37,000 counts the error is less than 1 percent (see section 3.2.2). Count rates of $\sim 100,000$ photons per second are the current limit of the DAQ software, where non-linearities dominate [Str01], and at 250,000 cps the system experiences saturation, where the hardware can not handle the amount of data. Observations of bright standard stars or other bright sources at telescopes with large apertures become difficult with OPTIMA's current DAQ system, if high photon rates lead to non-linearities in the count rates.

No online analysis

In every astronomical observation it is convenient to have a quick-look analysis of the object that is observed. Not as much as to deduce scientific results from it, but to make sure that the desired object for observation is in the field and to rule out major instrumental misadjustments. Astronomical data reduction is usually a lengthy process and observing time at telescopes is precious. Realising that hours of valuable observing time have been lost due to some technical difficulty that had been overseen is extremely inconvenient.

OPTIMA's current DAQ only offers a numeric ratemeter (see figure 3.5) that displays a rough estimate of the counts occuring in the channels being recorded. It requires both experience with

OPTIMA observations and good knowledge of the object that is being observed to deduce from the numbers alone what is currently going on.
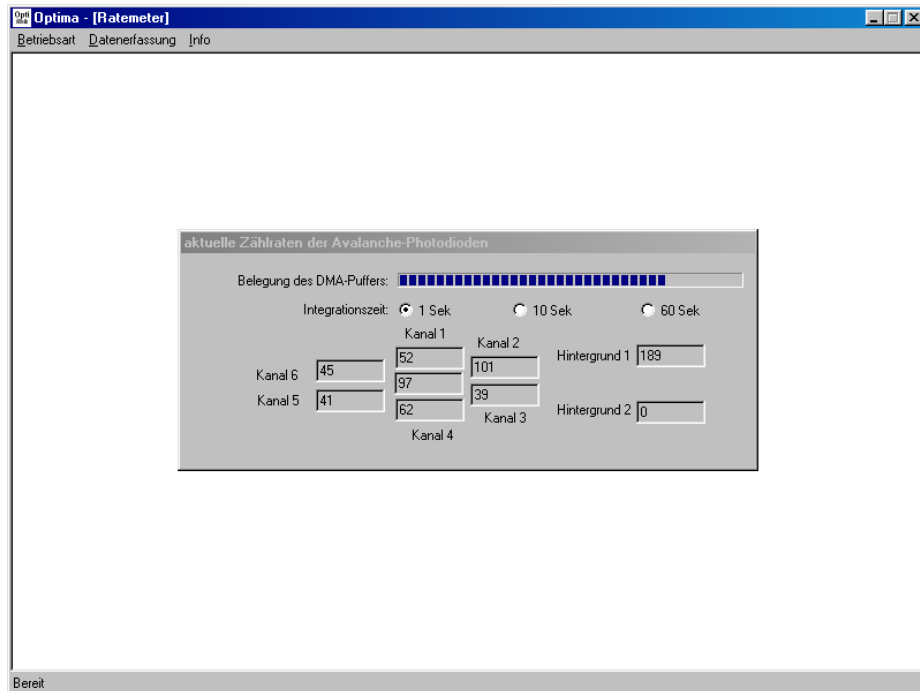
Figure 3.5: DAQ numerical ratemeter for 8 recorded channels

More sophisticated ways of quick-analysis tools such as a graphical plot of the photon rates in the channels, or an autocorrelation analysis of several channels would allow to get deeper insight of the quality of data, while it is being recorded.

The current DAQ system has been designed in a way that its sole feature is writing data to the RAM and then flushing it to the hard disk. Available computer systems at the time were just capable to ensure the real-time UTC time tagging of photon events, but did not leave much processing power for any other operations on the data. It was not advisable to jeopardise data integrity on behalf of online analysis functionality. Thus, the implementation did not provide any interface to access the data in the RAM to perform analysis routines on it.

The new DAQ software designed in this thesis offers a different approach that allows access to the entire event data stream, so that small applications can provide quick-look analysis of the observed data, without affecting the DAQ recording process.

Chapter 4

New Data Acquisition System

This chapter covers the design and implementation of the new DAQ software for OPTIMA, which is the main topic of this thesis. The existing DAQ made an adaption of the system to further development difficult. The idea for an entire redesign of the OPTIMA DAQ system and its key features are laid out in this chapter. In addition, reference implementations that were done in this thesis project are given as examples that show the performance of the new system.

4.1   Desire for a new data acquisition system

The shortcomings of the original OPTIMA DAQ had been taken into account when the instrument was designed and considered not to be of major concern for the original purpose of the instrument: high-time resolution observations of optical pulsars. In these observations the achievable time-resolution of 4 microseconds was sufficiently high to obtain the desired results. Furthermore, a limitation to 250MB of samples (corresponding to roughly 5.4×10^7 events) was uncritical, since pulsar light curves were later obtained through folding. Thus, short interruptions in the light curves could be easily overcome.

After testing and using the original OPTIMA system, the conceptual design had undergone further improvements (see chapter 2): The greatest improvement was the use of new fibre apertures allowing 4-colour spectrometry, and the addition of a polarimeter. OPTIMA has been used for observations of other highly variable sources, e.g. Cataclysmic Variable Stars and in 2005 to 2006 and it had been redesigned to allow observations of Gamma-ray burst (GRB) afterglows in the optical.

With these new applications the requirements on the DAQ system have increased. Observations of CVs whose periods are in the range of minutes to hours[1] benefit from light curves uninterrupted

---

[1]There exist extreme cases with periods of several minutes, e.g. RXS J0806.3+1527 [IPC$^+$99], [BR01].

by DAQ drops. It is understood that it is rather undesirable to introduce unnecessary instrumental errors in the data recorded.

Also, as described in chapter 2, the hardware components of OPTIMA are capable of much higher time resolution. The maximum detectable photon flux is determined by the APDs, which have a count rate limit of 10^7 counts per second. In practice heating of APDs at high rates sets an upper limit to the count rate at around 2×10^6. It is therefore very inconvenient to have an even stricter limit on possible count rates due to DAQ limitations. Especially with observations at larger telescopes high photon count rates can easily exceed this limit.

Hence, there has been the idea to redesign the OPTIMA DAQ system to have a more modern data acquisition system for the instrument.

4.2   Hardware

As described in chapter 3.1 the most severe disadvantage of the existing DAQ system is the fact that the GPS time tagging is done in software. Every multi-tasking operating system allocates processing time to all running processes via time slices. Thus, creating the impression of multiple processes running simultaneously, while a (single) processor can only execute one process at a given time. Time slices allocation is done by the operating system's (OS) process scheduler and can be adjusted to a certain degree by setting kernel parameters or giving certain processes a higher priority to favour their execution over other processes.

This causes problems with any attempt to perform accurate timing in software only. The avalanche photodiode photon detectors output a TTL pulse on arrival of a photon, the arrival time of which has to be recorded. In order to do this it must be related to the absolute timing signal of the GPS time. This is implemented using a GPS-disciplined clock[2] to drive an oscillator. The fundamental difficulty involved in this is to guarantee that a read-out is performed by the OS on time. Losing a poll interval of the DAQ card does not only cause the possible loss of photon events, but also corrupts the timing counter and results in false photon arrival times and thus invalidating the remainder of this second's interval. In the existing DAQ system a stress test was performed in the laboratory [Str01] showing that the computer used as DAQ PC was capable of performing reliably a 250 kHz oscillator clocking. A newer PC with a faster CPU, harddisk and I/O performance might stretch this limit a bit further, but it must be emphasized that improvement of the hardware used does not alleviate the principal difficulty of having no guarantee of near real-time polling of the DAQ card.

The solution to this lies in doing the time tagging not in software, but solely in hardware. This can be done with an accordingly configured **F**ield **P**rogrammable **G**ate **A**rray (FPGA). Modern FPGAs are available with integrated developer kits, such that much work of designing peripheral

---

[2]Datum bc627AT GPS card

circuits to drive the FPGA chip does not have to be done by the application hardware designer. The chips can be driven at high clocking rates of up to 600 MHz, and therefore reach processing speeds formerly only achieved by general purpose CPUs. Hence, there is sufficient performance available to perform the time tagging in the dedicated FPGA, relieving the DAQ computer of this critical task. The remaining difficulty of building a satisfactory DAQ system lies in providing guaranteed throughput from the external hardware to the DAQ computer and sufficiently quick data storage. This is far easier tackable with modern computer hardware than it is to guarantee execution times.

4.2.1 GPS Timebase and FPGA time tagging

The new DAQ system also uses a GPS-disciplined clock to generate event time tags for photon events. The principle of operation of generating a GPS-disciplined high precise timebase was already explained in chapter 3 in the case of the existing DAQ. For the new system an external Trimble GPS receiver was chosen to provide a fully external hardware system, together with the planned external USB-based FPGA hardware.

As outlined in the previous section 4.2 the use of a FPGA combines both the advantages of simple development and application specific operation. Several companies provide ready-made development boards that do not only include an FPGA, but also the necessary peripheral circuits. In case of the new OPTIMA DAQ hardware a FPGA module from Cesys was chosen[3].

Via a serial interface the board can initialise the GPS receiver, get system status and satellite information. This information, encoded with the Trimble standard interface protocol (TSIP)[4], is decoded in the FPGA and sent on request to the OPTIMA control computer via USB as status information packets.

4.2.2 USB connection

USB2.0 constitutes an interface, practically universally found in all modern computer systems, capable of providing the high transfer rates required for the desired event rates of OPTIMA. USB2.0 allows a net transfer rate of 480Mbit/sec. In practical applications transfer rates of 40-50MB/s are achievable, depending on the host's USB chipset. With 64 bit constituing one event in a channel this results in a maximum net rate of about 5 million events per seconds. The advantage of using internal FIFOs and sending mingled packages via the USB interfaces lies in the fact, that this limit is only the net limit of events having occured in all channels. In the usual case the main part of the data will come from a high event rate object fibre, while a second channel only observes the sky background. So there is no event rate limit per channel, like it has been imposed upon all channels with the old DAQ system through the clock rate of 250 kHz.

---

[3]Featuring a Xilinx Virtex-II XC2V1000-5 gate array.

[4]This is the proprietary communication protocol used in the Trimble GPS receiver.

The USB interface is provided by a pluggable USB interface module[5] that is connected to the FPGA peripheral hardware. The Cypress module features a microcontroller[6] handling USB data transfer independently through FIFO buffer. USB enumeration (registering the device with the USB host controller) and negotiating of data transfer rate (high-speed or full-speed) are done by routines in the microcontroller and do not have to be implemented by the board designer. If the FIFO buffers are filled via an external logic, i.e. by the FPGA chip residing on the ODASSE board, USB2.0 "full-speed" transfer rates can be achieved via the USB interface on the PC-connector side.

4.3   Software

The OPTIMA DAQ system was a tightly integrated development of hardware and software, when it was first implemented by Christian Straubmeier [Str01]. With the use of a new DAQ hardware, the existing DAQ programs could not be used anymore without redesign. The original software had been developed for Windows98, partly due to preference of Windows over other operating systems, but also due to the fact that the implementation of using the memory as a raw buffer and regular polling of the National Instruments I/O card required an operating system that allowed such direct access to the hardware. In modern versions of Windows, e.g. 2000, XP etc., and Linux a hardware abstraction layer[7] prevents user space applications from direct access to the hardware.

Due to the advantages of its stability and extensive documentation along with the open source tool chain, it was decided to use Linux as operating system for the ODASSE DAQ software.

4.3.1   Requirements

The new software should of course avoid the limitations of the existing DAQ. The critical timing problem about tagging the photon events is taken care of by the improved hardware design. Also, querying and receiving of status information from the FPGA will be done in hardware.

Thus, the main task of the software is reading data packets from USB, decoding the data stream into event data and status information and presenting both to the user in a useful manner. The current OPTIMA DAQ software consists of a single, monolithic application (see chapter 3.2), whose main task lies in verifying the GPS system status and recording data to hard disk. The only additional functionality is a ratemeter. Online-analysis or quick inspection of the data recorded was possible at all with the old DAQ. When conducting an observation of a variable object, it would be extremely useful to have an online-plot to check if the behaviour of the light-curve resembles the object's expected behaviour.

---

[5]Cypress EZ-USB Cy7c68013a-218 EZ-USB Fx2-LP

[6]Cypress EZ-USB FX2, a specialised microcontroller with a 8051 core handles the USB transfer

[7]An abstraction layer is implemented in the OS between the physical hardware and the user software.

In fact the monolithic design of the old DAQ software was the main obstacle to implement any improvements, since interferences with the actual data acquisition could not be excluded when major parts of the software were altered. The monolithic software approach in the current software also proved to make the software hard to maintain and the new DAQ software should fulfill the following requirements:

- Sufficient speed for up to 5 millions events per second

- Reliability

- No gaps in data records

- Easy maintenance

- Extended online-analysis tools

- Expandability

4.3.2 Design

Server and clients

Instead of putting all functions into one piece of software, the new design should strictly distinguish between the hardware related handling of event signals and the necessary handling of the subsequent event data. The idea of having one application with the sole purpose of reading event data from the DAQ hardware, makes all further event handling DAQ independent once the events have been received from the connected device. That means an analysis application can be run both with an USB-based DAQ device or any other DAQ stream device without any change to its code or data handling. Since the DAQ software "serves" the events to the analysis programs, the term "server" was introduced for the DAQ device handler and all applications accessing the data are called "clients".

Hence, by serving the data in shared memory, it can be accessed by a virtually arbitrary number of clients, e.g. providing "quick look" analysis with a plotting client (see section 4.3.5) while data is recorded by a dedicated hard disk writing client (see section 4.3.5).

Interprocess communication (IPC)

The complete separation of DAQ data reading and further handling required a method of data exchange between server and clients. The essential ability to handle large streams of online event data (up to 5 million events per second) requires an efficient method of data exchange between the server and the client applications.
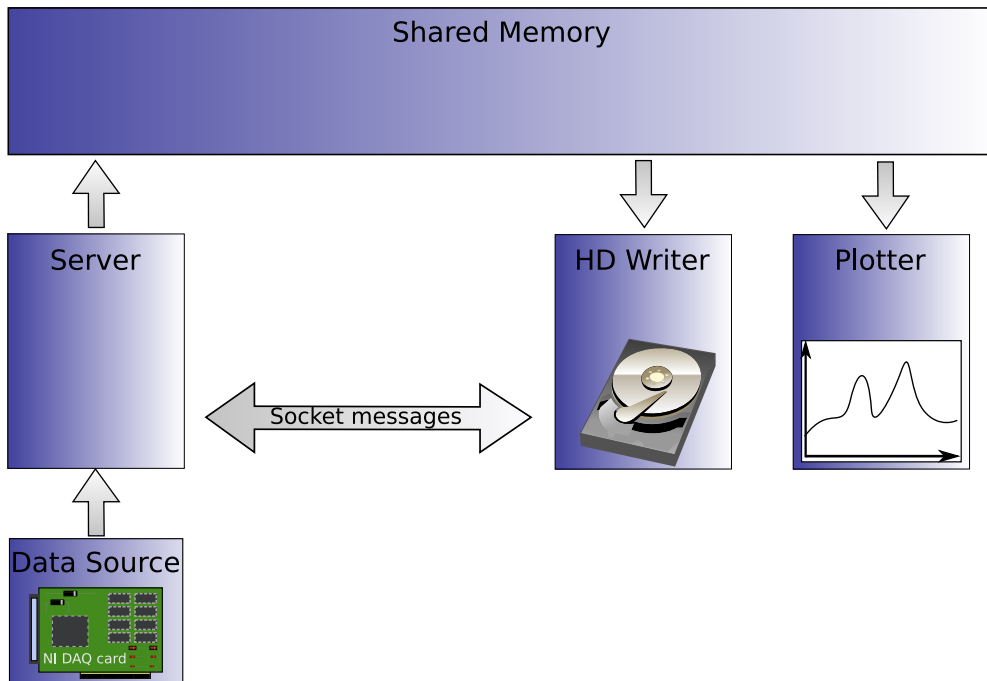
Figure 4.1: Shared memory allows several clients independent access to the data "served" by the DAQ application

Data exchange via memory provides the fastest way of interprocess communication between different processes/applications. All modern operating systems use memory protection to prevent applications from accessing memory sections dedicated to other programs. Hence, an attempt to write to memory cells that are not allocated for the calling program result in a segmentation fault. In order to still make use of the fast memory transfer rates as a method of inter process communication (IPC), the concept of so-called *shared memory* allows different processes to attach to the same memory segment and treat it like conventionally allocated memory of their own, though it is the programmer's responsibility to implement adequate mechanisms to organize concurrent access from different processes.

In order to exchange data that does not constitute event data, another method of communication between server and its clients was implemented. This sort of communication consists mostly of commands to control the server settings and start/stop of data acquistion, or messages the server had to communicate to clients.

Passing of message strings between the server and its clients is implemented through *local sockets* (also called "UNIX sockets") that provide a point-to-point communication between applications. Thus, allowing clients to send control commands to the server and the server to notify individual clients about specific events. Similar to TCP/IP sockets in WWW communication a client connects to a listening socket on the server and a point-to-point communication socket between the server

and client is established. Both client and server can send and receive data over this socket. In order to provide human-readability of these socket messages, an ASCII text based protocol was chosen to be implemented. The greatest disadvantage of slower parsing speed is of minor importance, since all time critical transfer is done via shared memory. On the other hand, sending and receiving clear-text command strings allows for quick external control of the server without a dedicated binary command generator.

Framework library

All data access functions are part of the software library to allow clients to retrieve photon events from the server via shared memory, and socket communication functions for common commands and event notifications. The complexity of concurrent data access in shared memory is hidden from the application programmer and data retrieval from the the server is virtually as easy as access to local data.

Writing an extension to the system in terms of providing a new analysis module comprises a certain number of function calls to establish a connection with the DAQ server and retrieve current settings. After these initial steps photon events can be read from shared memory via access functions provided by the library assuring thread-safe and concurrency safe access to online streamed photon events. Thus, the programmer of the new application can concentrate fully on the analysis of the data.

Creation of new functionality for the OPTIMA DAQ system, e.g. a hard disk writing application that writes event data in FITS format [WG79], can be added without touching the server application. The framework provides a fixed application programmers interface (API) (see API documentation [Dus07]), so that new applications can use the framework's functionality transparently without touching the difficulties with internals of data handling. By using API functions and linking the library object file to the client or server application the program can make use of the shared memory data handling.

4.3.3 Implementation

After the desired requirements of the new DAQ system, described in the previous section, had been laid out in the initial software design process, several considerations regarding their implementation had to be taken into account:

- implementation in a high-level programming language

- representation of OPTIMA data

- thread-safety of data exchange via shared memory

- additional communication between server and clients

Programming language

The framework should be a self-consistent library against which other applications can be linked, so that these can use ODASSE's functions to access online streamed data from the DAQ. The ODASSE library offers a range of C functions to read and write DAQ data from and to shared memory, and additional communications and administration functions (see ODASSE API [Dus07]).

It was decided to use C as a suitable high-level programming language to implement the above mentioned criteria into a framework library. Glibc compatability is generally obeyed, so that any application designed to run on GNU/Linux could use the framework's functionality.

Events

Internally, photon events are represented as *unsigned long long integer* numbers. The allowed range of the 64 bit unsigned long long integers[8] is sufficiently large to provide up to nanoseconds precision for typical observation lengths. The absolute time tag of an event is given with respect to UNIX time in nanoseconds since 00:00:00 UTC January 1 1970. Though reading and writing of 64 bit data types has to be done in two steps of reading two 32-bit words on today's still commonly used 32-bit CPUs, 32-bit integers would not provide both the necessary range of covering absolute timing and the desired accuracy down to at least microseconds. On 64-bit computer systems reading and writing of 64 bit unsigned long long integers can be executed in one processor execution. So, using a 64-bit CPU system as a DAQ system would provide a significant advantage for the production system.

Events have been defined throughout the library as a new type *event_t*. So, by redefining it to a different type and recompiling/linking of the framework, the library's functionality can be used for any other type of data. These have neither to be of the type currently used, nor consider an event time tag[9].

Events are individual items and treated as such on reading from and writing to the ringbuffer. Storage in the ringbuffer is determined by the size in bytes of each *event_t*, while the library's internal functions just step on by pointer incrementation/decrementation. All functions handling *event_t* data types therefore handle the appropriate number of memory cells, as long as *event_t* is correctly defined in the includes. This is important for the proper operation of the ringbuffer mechanism and the coordinated reading and writing as well, because all channel memory access is internally handled on a raw pointer basis.

By using a type definition these difficulties occur only once on compilation time and are then transparent in the usage of the library. A change of the *event_t* data requires a recompilation of

---

[8]$2^{64} - 1 \approx 1.84 \times 10^{19}$

[9]Though the intention of the library was to be used with OPTIMA event time tags, and library functions have been designed upon that precondition, the online data-streaming is not restricted to this kind of data.

clients, but no change in the data access code is needed. The programmer must be aware of the exact type of data that is sent to/received from the ringbuffer. A hard disk writing client, for example, can be readily adapted to a new data type by simple recompilation/linking, if its only writing off the data to hard disk. An analysis client on the other hand must be aware of the data format it is doing computation on.

Data transfer

The data transfer of events to and from shared memory is critical for two reasons. First, it must be fast enough to provide the desired event rates (up to 5 millions events per second). Secondly, access through multiple clients poses the difficulty of thread-safe writing and reading of data.

Data integrity through locking

This situation is similar to the producer/consumer problem, occuring in many multithreading scenarios. In the classical implementation the concurrent access of data is solved through locking. Locking involves the introduction of a "lock" to each data segment. This is a special kind of variable, usually a semaphore or a mutex[10]. These are both atomic variables[11] that serve as a lock that must be checked before access to a data segment is attempted.

In the case of **mutex locking**, the mutex is acquired by a process or thread that wants to have exclusive access to the data. Acquiring the mutex means "locking" it, any attempt by another process B to lock a mutex that is already locked by process A fails. Process B wanting to get access to the variable has to wait and try again to lock the mutex some time later. This creates two problems: There is a polling situation, because process B has no method of knowing when the mutex will be released by process A. Secondly, there is no queueing of access requests, i.e. a third process C can acquire the mutex before process B, if it is faster in accessing it after release by process A. This problem is illustrated in diagram 4.2.

Locking through **semaphores** provides a method of queueing requests. A semaphore is basically a special form of an atomic integer variable. It can be set to any value on initiliazation, but after that it can only be incremented or decremented by different processes. It is not necessarily the process or thread that tries to acquire the semaphore that gets executed. So semaphores provide fairer access to shared resources.

Yet, these and other locking methods suffer from two principal problems. If any of the processes handling the locks does not behave nicely, this can lead to deadlocks. If the programmer forgets to release the lock in one possible execution path, no other process ever again gets the chance to access the resource. Careful attention must be paid to the correct release of locks.

---

[10]Mutex is an abbrevation for mutual exclusive access.

[11]An atomic variable is a variable that is small enough to be read or written by the processor in one instruction.
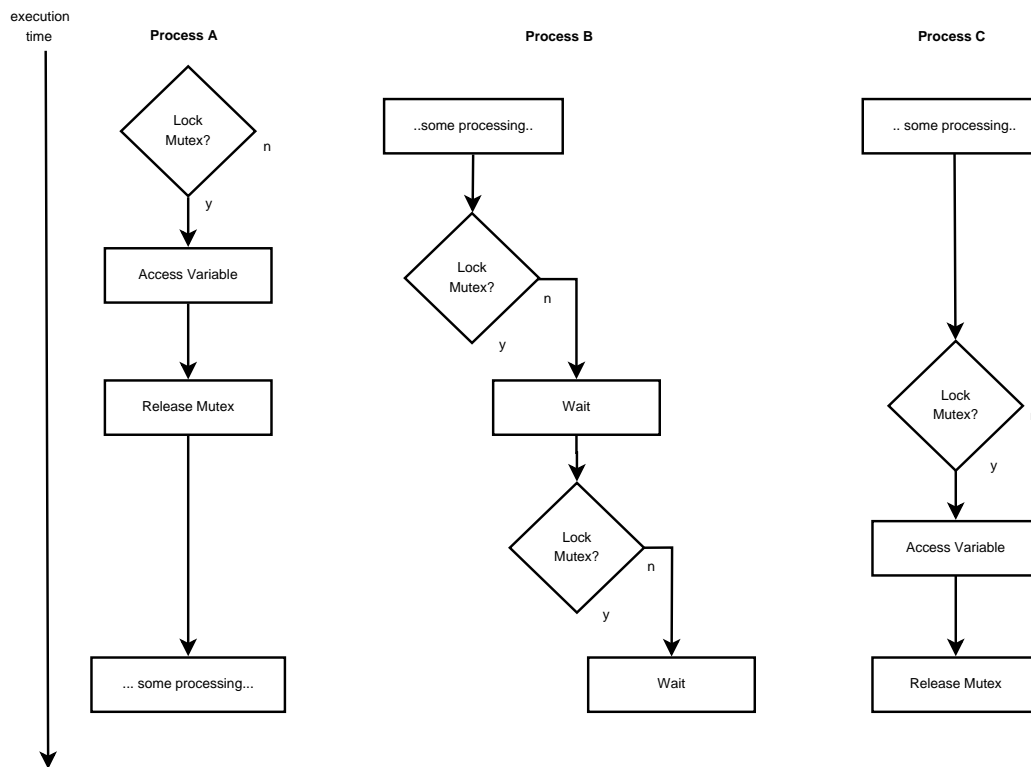
Figure 4.2: Mutex locking does not guarantee fair access to variables for multiple processes

A dead lock can also happen, when the processes crashes or hangs while being in possession of the lock. In case of an astronomical data acquisition system which is meant to record observations, a restart of the system means inadvertly loss of valuable observational data that might not be recovered in a later observation.

Even if the processes behave nicely and do not crash, the approach to lock resources that are accessed frequently experiences two problems. These are known in computer science as the "first readers-writers problem" and the "second readers-writers problem":

The first readers-writers problem states that the locking should not prevent two readers from accessing the data, since reading from the same variable is uncritical. Only when the writer is currently writing at that position, access must be denied to readers.

The second readers-writers problem describes the problem that in most applications the writer should be given preference over the reading processes. In mutual exclusive locks a reader locks the resource for reading and at the same time prevents the writer from writing to it. This situation is undesirable as any new data from the writer should be given preference and thus the writer should get the lock first, write to the resource and only after that the reader should get access to it. This is known as "writers-preference".

These two problems occur exactly in the situation of the OPTIMA data acquisition:

The conceptual design of the new DAQ planned to have more than one reading process in a

typical DAQ execution. For almost all observations one of the client process would be a hard disk writing client, writing data for permanent storage off to hard disk - or some other permanent storage media. Any other running client, such as a plotting client or a quick-look analysis client, requires concurrent access to the DAQ stream. The number of clients running simultaneously is only limited by the available processing power of the DAQ computer system. Thus, the situation of multiple readers is quite typical and clients, "readers" in the above scenario, unnecessarily locking each other should be avoided.

During observations the APDs constantly deliver photon events. In order not to lose any events the DAQ server process, the "writer" in the above scenario, must be given absolute preference over any reading client. A slow reading process must not block the writer, keeping it from delivering the event data. A further complication occurs if a reading client crashes while being in possession of an exclusive lock, stopping the writer entirely and terminating the whole DAQ handling. Thus, an exclusive locking mechanism for readers should be avoided in the DAQ implementation.

Managed concurrent access to data

The solution taken for the new OPTIMA DAQ system is to use a method of "managed" concurrent access for readers. The situation in case of the DAQ system is a bit simpler than the most general case, for there is only one writer. The DAQ server reading event data from the hardware is the only process writing data to shared resources.

Therefore it is an appropriate approach to use the server to manage data access for clients. The server knows to which part of the ringbuffer it is writing at the moment. A client trying to read from the ringbuffer at first has no knowledge of the server's writing activity, nor of the actual position the server is writing to. Therefore the server must indicate to the client where the current writing position is and thus give the client the ability to read from an allowed section of the ringbuffer.

The server writes its last writing position to a shared variable in the channel header. A reader wanting to read from that particular channel uses this as an indicator to not read past that position. The handling of this data access management is hidden from the application programmer through the library framework by providing special *write request* and *read request* functions:

A DAQ server application uses a *write request* to reserve a section of variable size to write to the channel's ringbuffer. The framework then returns the start and end point of the section to write to to the server. The server then writes individual events to individual ringbuffer cells, until the segment provided by the library has been filled up. Since the current writing segment is blocked exclusively for the server and readers are prevented to access it, the size of the segment must be carefully chosen.

Depending on the current data rate a large segment might not be filled in an appropriate time, thus, leading clients trying to access events to starve. Similarly a small segment size would lead

Channel Ringbuffer coordinated reading and writing
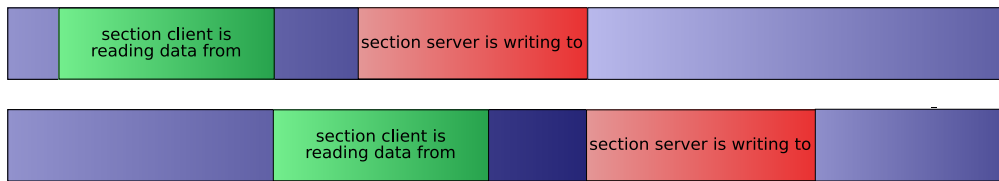
Figure 4.3: Blockwise writing by the server to the ringbuffer. Clients read from sections that contain events that the server has already written entirely to the ringbuffer.

to an unnecessarily large number of *write requests*, if the channel experiences a high event rate. Therefore the library adaptively adjusts the provided segment sizes according to the data rates, regulating segment sizes that are blocked by the server for writing.

Management of reading from the channel is done for clients by the library, too. A client that wants to read events from a particular channel lances a *read request*, and the library returns a segment of the channel that is safe to read. Effective reading is the client's responsibility, it can ask for a segment of arbitrary size, but is not guaranteed to actually get the requested size. If the requested size reached an area the server reserved for writing, it is given an accordingly smaller size. Also, the wrap-around situation at the end of the ringbuffer can cause the client to be given a smaller segment size, if the requested size exceeded the ringbuffer. For correct seamless reading the client must provide the library with the last position it read data from, the library then assures to return an adjacent segment that is safe for reading.

As only the current writing segment of the server is exclusively blocked, multiple clients requesting to read from the channel do not interfer with each other. They are each provided with a reading segment of appropriate size. If the requested size can be provided they are granted it, if not, they are granted an accordingly smaller segment.

In figure 4.3 the coordinated writing and reading process is illustrated. The ringbuffer is filled by the DAQ server from left to right, so this direction in the figure corresponds to increasing event times (indicated by the darker colour gradient in the figure). Writing and reading is done blockwise, where the server writes individual events to a section of the ringbuffer. Starting from left, these sections step adjacently through the ringbuffer, filling it with events that were read from the DAQ. After writing up to the right end of the ringbuffer a "wrap-around" occurs. Writing starts on the left side again, and previous events are overwritten by the server.

Hence, a client must be reading fast enough before old events are overwritten by the server. A large ringbuffer size can avoid difficulties at peak count rates of events, but a client that takes too long to complete its *read requests* still will eventually be "overtaken" by the server writing events to the ringbuffer. In order to detect these cases where a client would read corrupt data, the managed

Channel Ringbuffer and Consistency Map
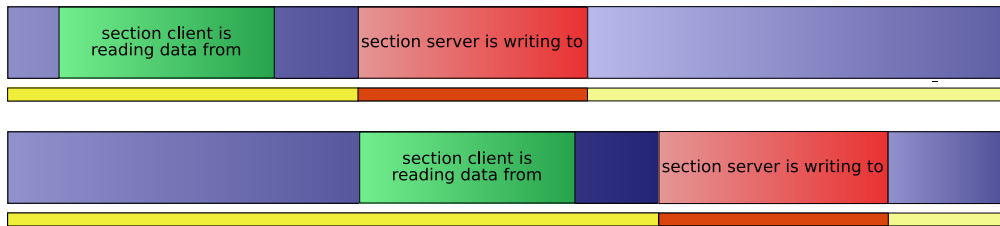
Figure 4.4: The corresponding map to each channel entry assures data integrity for clients reading from the channel.

data access must also provide some form of data integrity check.

Data integrity check

Allowing concurrent access to the data stream in a ringbuffer introduces several possible situations where a client could read corrupt data:

- The server enters a segment a client is currently reading

- The server writes one full ringbuffer while a client is reading and overtakes the client entirely

Though the event data itself provides one criterion for consistency, namely that event times must be increasing monotonously, this is not sufficient to check for all inconsistencies that can be encountered. Comparison of event times would recognize the first data inconsistency: If the server wrote into a segment a client is currently reading from the event time at the start of the client's segment would be greater than the one at the end. This is a clear indication for an inconsistency.

An example where this fails is if the server overtook the client entirely, before the client finished its reading process. The start and end event times of the client's reading segment are still monotonously increasing, and since event rates from observed sources might be totally arbitrary no sure deduction is possible from the difference in event times alone.

In order to cover all possible scenarios of data corruption, an additional checking variable was introduced. This is a mapping value for each ringbuffer cell, consisting of a single integer value. Initialized to zero, for a segment the server reserved for writing the server increments this number by one for each cell of the segment (see figure 4.4).

Thus, in the area the server reserved for writing, the map value has an uneven value, i.e. the least significant bit equals 1. Once the server has written events to the entire reserved segment, it increments the corresponding map values again by one. That means, regions valid for reading by clients, have a corresponding even map value, i.e. lowest order bit 0. The marking of valid and invalid regions could be achieved with a one bit value only, but the case of the server overtaking

the client, while the client reads from a segment, needs some form of knowledge how many times a cell has been written by the server. This needs not to be in terms of an absolute count, but must be sufficient for a worst case slowly reading client to recognize if the server has overtaken one or more times. Therefore the mapping value is an indicator if the server has done a writing operation to a segment, while a client has requested it for reading. This is best illustrated in an example (see figure 4.5):

Figure 4.5: Map values assure data consistency for reading clients.

In the top part of the figure the **regular reading** case for a client is illustrated. The region the server reserved for writing is mapped with an uneven value, 3. The region left of this has already been written to and is ready to read for clients, having an even map value, 4, associated to it. The rightmost region has only been first written to in the previous run, indicated by a map value of 2. At the time of the issueing of the read request the region returned to the client has a map value of 4 (indented map values in the figure 4.5). In the regular reading case, the server has only written in regions right of the requested reading segment, that means after reading the events the client can verify reading of valid events through the fact that all map values still have the same, even, value of 4.

The middle part shows how the server catches up with a slowly reading client and the **server writes into a segment the client intended to read**. A part of the client's reading segment has then an uneven map value, 3, associated to it. On checking the map values the client can see the inconsistency between the left and the right map value, and reject the data it read.

The bottom part illustrates the case where a client started to read a section that was flagged as valid with an even map value of 4. While reading the section, the server has done some fast writing of many events, e.g. in case of a burst or flare in the source, not only writing to a great part of the ringbuffer entirely, but also having wrapped around and having **overtook the reading client**. The

client started reading the section, when the corresponding map values were 4, but with the server having written to the section again, these are now 6. From this argument follows that it is necessary to not only check the map values when trying to access the segment to read from, but also to check them after the reading has taken place and compare it to the value when the read was requested.

Write requests and read requests

The previous paragraphs illustrated possible scenarios that lead to data corruption. The mechanism of consistency checks is hidden as far as possible from the application programmer. In order to do this as seamlessly as possible, the library provides data stream access functions both for the server application and for clients. These are called **write requests** and **read requests** accordingly.

For the server the situation is quite easy. As described in the first readers-writers problem, it is given absolute preference for writing. That means, on a **write request** issued by the server the library provides it with a writable segment. Because a writing segment is only allowed to be read if it has been entirely written, the server must execute a *committing* function. This function increments the previously uneven map values of the writing segment by one, updates the current marker of the last writing position in the channel header and further meta information. Thus, writing through the server is a two-step process to assure that clients will not encounter an incompletely written segment of event data.

On calling a *write request*, the library returns an adjacent segment of the ringbuffer. Two possible difficulties can occur which lead to ineffective writing procedures. If the server reserves an extremely large segment, this would block a large part of the ringbuffer preventing all readers reading from that section, though in essence the server writes at a given time only to a certain position of it.

Thus the framework initiates a "premature" commit on the writing segment after an adjustable timer, so that clients can read updated events regularly. If a timer resulted in a premature commit of a previous write request the return size of write requests is decreased. Similarly, if a writing segment was committed before the timer elapsed, the default return size is increased to provide a more efficient writing process to the ringbuffer.

So, depending on the last data rate in the channel a *write request* was issued for, the library returns a buffer object to the server, containing pointers to the start and end of the writable segment.

Access to the shared ressource of the channel ringbuffer is given to the server through direct pointer access. This allows writing to the ringbuffer to be handled just like writing to any memory ressource that was local to the server. Also, direct pointer access provides the fastest access method, as opposed to handling writing of individual events through function calls. In the case of high event rates the server still can use existing functions of the glibc library to execute bulk writes, e.g. through the *memcpy()* function, since these can transparently use the pointers to shared memory.

Thus both efficient and non-starving writing conditions can be guaranteed, without the server application programmer having to worry about ideal writing segment sizes.

In a similar way, a client requesting to read event data from the ringbuffer must execute a two-step process. A client must request a region it can read from, and after reading check for consistency of the data it read:

- issue a read request for a segment of the ringbuffer

- check consistency of data read from the segment

Through a *read request* the client asks the library for a readable segment of the ringbuffer. For seamless reading of events from the ringbuffer the client must provide the library with the information up to what position it read data the last time, because the library does not keep track of the reading positions of all clients. The client application programmer calls the *read request* function with the last reading position performed, and a desired segment size. A hard disk writing client for example tries to acquire large chunks of data from the ringbuffer that can be immediately written off to hard disk, while an analysis client performs better handling smaller portions of event data.

The library tries to fulfill the client's requested segment size as far as possible. If the client approaches the server's writing section, it will be provided with a segment up to the position of the last committed writing action. At the end of the ringbuffer, the segment is only provided to the last position of the ringbuffer. On the next call the next read request starts at the beginning of the ringbuffer again. An implementation that wraps around at the end of the ringbuffer would avoid this, but the performance cost of the required function calls at every single event were deemed too much of a trade-off.

The object returned by a *read request* contains the start pointer and end pointer of the readable segment, and the corresponding map values at these positions. As described above the map values at the time of the request must be compared to the map values after all events have been read from the section to ckeck for data consistency.

In summary, both *write requests* and *read requests*, provide the application programmer with a method to safely access shared memory ressources. This done in a performant way through direct pointer access to memory, and in an efficient way handled by the ODASSE library to minimise the overhead through the requests.

Committing and map checking

Due to the segment-by-segment reservation of writing regions in the ringbuffer, the server must release a blocked region after it finished writing to it. In the ODASSE framework this is called *committing* a region and implemented in a *commit* function. This function sets the corresponding
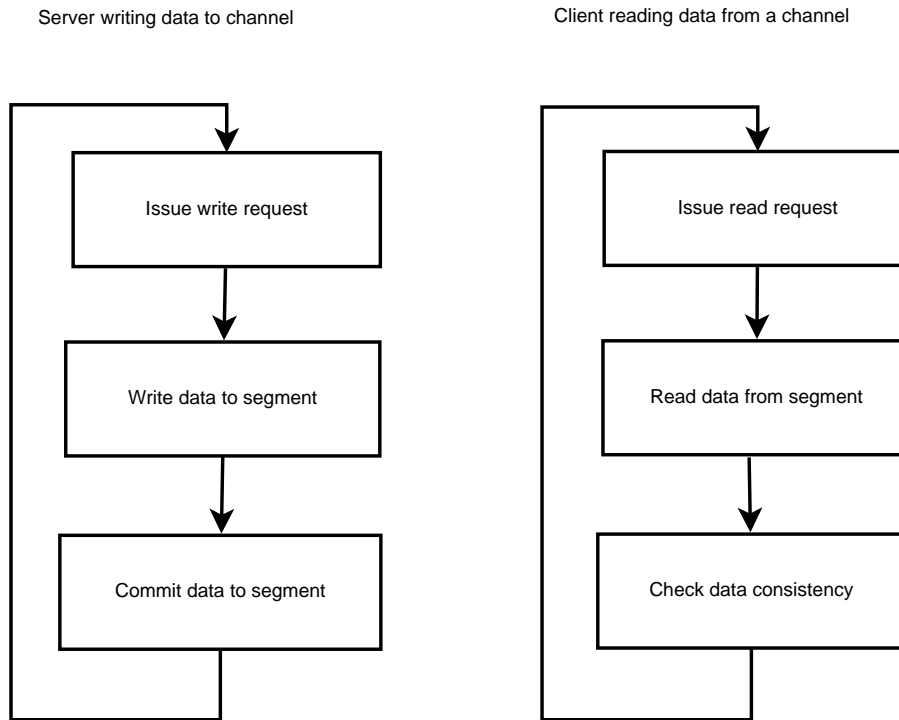
Figure 4.6: Loops for writing data to and reading data from the DAQ event stream

map values of the written segment to even values and moves the position of the last writing action marker to the end position of this segment. The *commit* function must be called by the server after writing events to the last pointer position in the reserved segment.

Also, due to the risk of the server writing to a segment that a client had reserved for reading, the client must do the data consistency check after it read the reserved segment. This is done by calling a *check map* function, that compares the map values at the time of issueing the read request with those after it has finished. The *check map* function compares the map value returned in the buffer object at the time of the read request with those currently at the start and end position. The *read request* is only valid, if the map values are all even, and all have the same value. Only in this case the server has not written into that particular segment during the time the client read from it. Because writing and reading moves monotonously from left to right over the ringbuffer, it is sufficient to check only the map values at the beginning and the end of the segment. It is not necessary to check all map values of the tested read segment. If the map values disagree, the data from that *read request* is considered to be corrupt and an error is returned. The client can react to this accordingly. As already briefly mentioned, in the case of a client recording the DAQ stream, corrupt data segments are a serious error. An analysis client might just reject the data and continue with a new *read request* for new data.

In practice, writing to data channels is a constant series of getting a segment through a *write requests*, receiving data from the DAQ, filling up the buffer and then committing it through the

commit function. These actions constitute the main tasks in the DAQ server loop.

In the same way, any client trying to work on the DAQ data, will do this through issueing a *read request*, reading events from the segment it received, checking its consistency with *check map*, and finally doing some form of action on the data. After finishing handling the data, it will issue its next *read request*. These two data writing and reading loops are shown in figure 4.6

Section 4.3.4 and 4.3.5 will illustrate the data handling with examples of reference implementations of server and client applications respectively.

Settings

For all necessary information concerning the status of the DAQ system, an additional shared memory area exists. This contains information regarding the current setup of the DAQ, e.g. available channels. Furthermore, it contains information about the channels, e.g. their DAQ identification numbers (0-15) or names given for easier identification. In representation of streamed data in online analysis clients, the corresponding channels can then be referred to as "background" or "pol 45" instead of only their non-descriptive ID number.

State variables in the settings also indicate if the DAQ process is currently running and streaming data or if it is still in configuration mode. Clients connecting to the server first attach to the settings shared memory and can then read the current server configuration. This allows them to present the available options to the user, and also to attach to available channels, since not all channels are necessarily offered for streaming by the server.

Settings are only allowed to be altered at configuration time, but not at DAQ running time.

Communication

Shared memory is very effective for the exchange of great amounts of data. The previous section showed that access to it from multiple processes has to be managed to be reliable and safe. For effortless cooperation of multiple clients with the server additional communication is necessary. In order to do this another method of communication between server and clients was implemented.

UNIX sockets provide a good method of point-to-point communication. While event data exchange concerns all clients trying to read from the DAQ stream, there are situations where only individual clients require communication with the server. Possible situations are:

- a client asking to change the server configuration

- broadcast message of the server to inform clients about a change in configuration

- notifications about new events (see section below)

UNIX sockets are also called local sockets and are similar to TCP/IP sockets which are widely used in internet communication. In establishing a point-to-point connection the server provides a

so-called listening socket that waits for clients to connect on this socket. While internet sockets are associated with a domain and a TCP port, local sockets are linked to a file in the UNIX file structure. Through knowing this connection point a client tries to establish a connection, the server recognizes this attempt and assigns a file descriptor which is used for the point-to-point communication with this individual client. For remote control the server also offers a socket connection via a TCP/IP port through which clients on remote machines can connect to the server (see section 4.3.5). This allows control from distant machines in the network, e.g. the OPTIMA control computer (see chapter 2 section 2.3.5).

Multiple clients establish their connection over the same listening socket, but get their individual file descriptor after successful connection. Thus, the server must keep a list of connected clients to address all of them individually. The file descriptor is a sufficient ID for each client.

Message sending and receiving is easily done through writing to and reading from the file descriptors. Instead of using glibc functions *write* and *read*, the framework library provides *send message* and *receive message* functions. These functions provide auxiliary functions that allow the server to handle multiple messages.

The communication protocol used over the sockets is an ASCII plain text message system. The server parses the messages for key words and performs the corresponding actions. The library possesses an *extension* mechanism via a keyword in messages that are not implemented in the standard framework protocol to allow server implementations to provide extendend functionality. The on-going communication between server and client are mainly handling of notification requests (see paragraph below), and external control of the server. The server needs not to be exclusively controlled through a graphical user interface. Semi-automated operation or processing of external information can be a possible control mechanism, and the socket communication allows easier automation of doing this.

The other direction of communication from the server to the clients occurs in the case of so-called *broadcast messages*. These are messages informing all connected clients about particular events or critical conditions, e.g the server starts/stops the DAQ or the server is exiting. The clients can receive these messages on their socket file descriptors, because the point-to-point connection through sockets allows two-way communication. On reception of a broadcast message clients should react accordingly. Currently implemented broadcast messages clients can expect are given in [Dus07].

All communication between server and clients is done in an own communication thread. The spawning and handling of this thread is encapsulated in the framework. For a server application it is sufficient to initiate communication via the corresponding library function *init communication* to handle the entire communication with its clients, without affecting the DAQ thread.

Another important aspect of necessary communication between server and clients is the sending and reception of *notification requests* and *notifications*. The purpose of these is to avoid polling

65
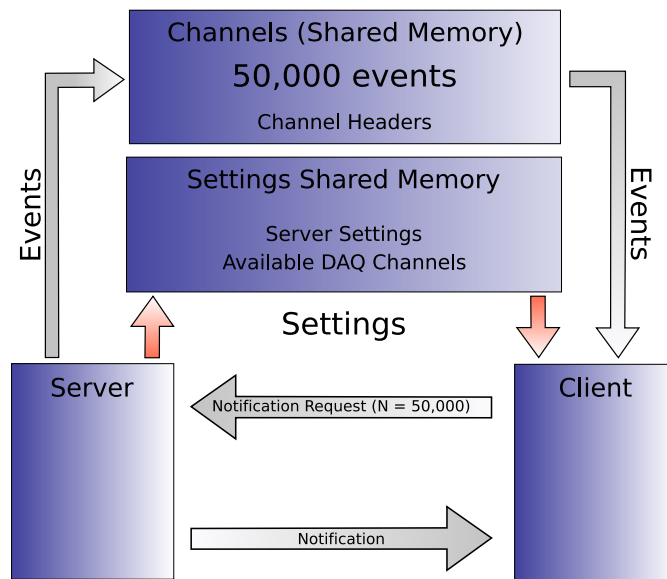
Figure 4.7: Notification requests avoid unnecessary polling from clients

situations in the data transfer between server and clients and their implementation is explained in the next section.

Notifications

In regular operational situations with a constant event rate generated in the DAQ hardware, the above described mechanism of managed data access provides seamless operation. Deadlocks are avoided, and clients do not starve because of guaranteed event updates through timer-triggered *commits*.

For clients there exists a risk of performing ineffective reading from channels. In most cases the request of data segments of constant size provides a reasonable method of reading the data from a particular channel. In case of a channel with a low data rate, e.g. a channel observing the sky background, a client might experience *read requests* that get rejected too often due to the fact there is no new event data available. A client executing its reading loop (see diagram 4.6), having finished handling the data it received in the last read, constantly lances a *read request*, in the attempt to acquire new data. This creates unnecessary load on the DAQ system. A method of notifying clients about new available data solves this situation.

Instead of constantly polling on a channel for new data through *read requests*, the client can ask the server to inform it as soon as there are new events available. On reception of a rejected *read request*, the client sends a *notification request* to the server to be informed about new events in this channel. Thus, when the server received new events for that channel from the DAQ and committed these to the channel, hence, making them available for reading through clients, it sends a *notification* to the client. The client waits for the notification, and creates no unncessary load on the system in

66

the meantime.

In order to allow clients easier handling of data, the *notification request* contains the number of new events the client wants to wait for. Even though the server might have received a small number of new events, and has committed these to the channel, the particular client prefers to handle greater amounts of data at one time. Thus, in the *notification request* an analysis client can ask only to be notified about the availability of e.g. 50,000 new events. This example is illustrated in diagram 4.7. Only after the client received the notification from the server, it executes a *read request* to read 50,000 events from the channel in shared memory.

Multiple clients can each be in multiple stages of waiting for new events. Each connected client might be connected to more than one data channel at the same time and there is a possibility that there are low event rates in several channels. This means that the server has to handle multiple outstanding *notification requests*. It has to notify clients at the time their requests for new event data can be satisfied. Like a waiter in a restaurant, the client must keep an internal list of outstanding notification requests. Since the fulfilling of a request depends on the number of new events in a particular channel, each channel has a corresponding notification list. The notification time is computed by adding the requested number of events to the total number of events in that channel at the time the notification was received. These lists contain the clients' IDs alongside the number of total events the client needs to be notified at. For in-order-execution of the requests, these lists are kept sorted by increasing number of new events to wait for. After each *commit* to that channel, the server compares the number of new events it made available for reading with the values asked for in the corresponding notifications list. If the number of events exceeds the number asked for by the first client in the list, the request is removed from the list and a *notification* about the newly available events is sent to the client. The handling of notifications is illustrated in figures 4.8(a) and 4.8(b) for the client and the server respectively.

4.3.4 DAQ Servers

The modular concept of the ODASSE framework in principle separates the task of acquiring the data from the DAQ hardware entirely from the rest of the DAQ process. The hardware-dependent routines are encapsulated in the server application. This means that any client application using the ODASSE library's data access functions can connect to any server, indepedently of the DAQ hardware the server runs on. This makes adaption of the DAQ system to new hardware easy. Writing a new server application is sufficient, all existing clients for hard disk recording, online-analysis can still be used. Due to the fixed data exchange through framework functions, these clients can be used without any recompilation with different DAQ server applications.

The only condition is that the server must provide event data to be streamed to clients. Thus, the server must create correct event times for photon events using a suitable timebase. In case of the

Client

Read request

Data available?

n → Wait for notification

y → Read events

Wait for notification → Server processing event data and handling client's notification

Server processing event data and handling client's notification → Receive notification

Receive notification → Read events
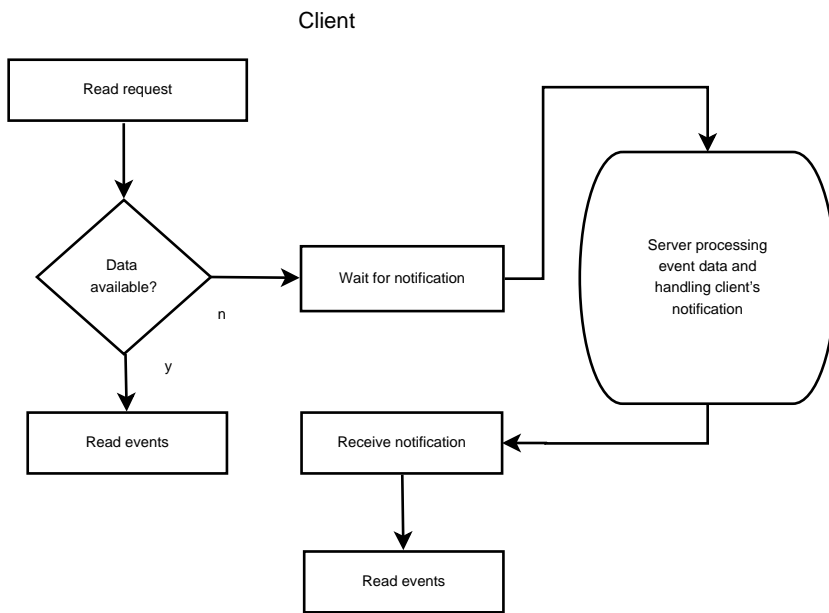
(a) notification request sent to server by a client

Server

Communication Thread

Add notification request to list

Client waiting for notification

DAQ Thread

Read data from DAQ

Commit data to channel

Compare to notification requests list

Send notification to client

Remove notification request from list
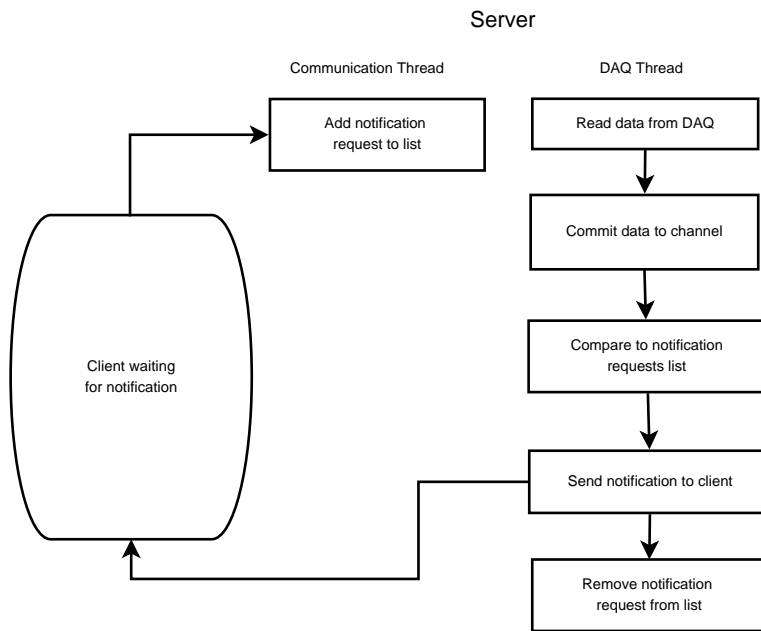
(b) notification handling by the server

Figure 4.8: Notification handling by client and server
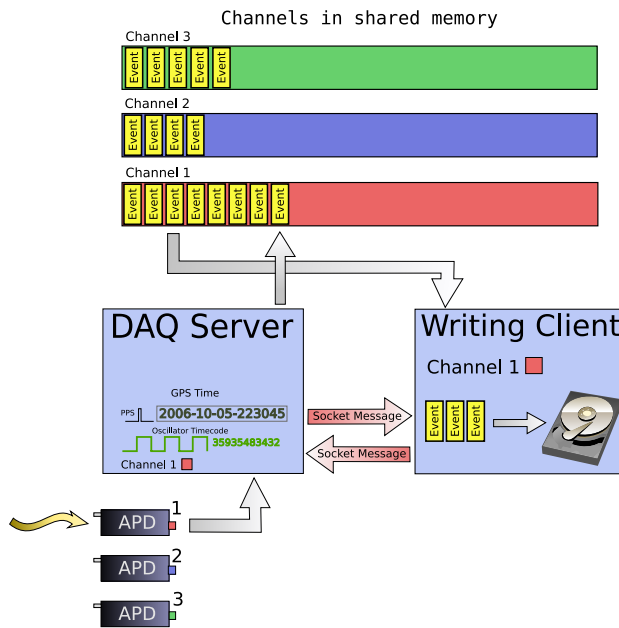
Figure 4.9: Exchange of events via shared memory

OPTIMA system this is a GPS-based time (see figure 4.9).

Raw file replay server

As proof of concept for the ODASSE framework a DAQ server was implemented that streams archived OPTIMA raw files. OPTIMA raw files recorded by the existing DAQ system provide real event data that was recorded in astronomical observations and can be used to test the library's event handling.

OPTIMA raw files are preceeded by a header, giving information on the start time of the DAQ acquisition, the DAQ oscillator frequency used in the recording, and the channels recorded. The files contain event data in the form of a timecode, referenced to the start time of the data acquisition (see chapter 3.2). With the exact start time, the DAQ frequency, and the timecode for each event the arrival time can be reconstructed.

In the OPTIMA raw files, all channels are written with increasing event times, irrespective of the channel number. Every event is saved with the corresponding channel number (see chapter 3) to the raw file. So, a replay server streaming the data into the ODASSE framework, must separate the events into the corresponding channels. This behaviour is very similar to the real-world case of event data coming from a live DAQ, where events occur randomly in different channels (see figure 4.9).

These events are then streamed to the corresponding channels in real-time as described in section 4.3.3. The time difference between two successive events is used to create a delay. This results in

69

real-time streaming of events like they were recorded in the raw file. The delay can be adjusted by a factor, allowing for slower or faster than real-time streaming of events.

The replay server also reads from the raw file header which channels were recorded in the file and sets the information in the *settings* accordingly. This provides clients with the same information they would encounter on a hardware-fed DAQ server.

4.3.5 DAQ Clients

Having access to the data through pointers received in *read requests*, clients can do their analysis on the streamed event data. This allows the creation of small, interchangeable applications performing specific tasks, without interferring with other running clients. A suite of reference implementations of clients will be described in the following.

Ratemeter

For inspection of event rates in the DAQ channels, a numerical ratemeter was created. The GUI was implemented using Trolltech's QT3.3 framework which allows rapid design of graphical user interfaces in C++. The application was statically linked against the ODASSE library, and uses a framework function to read the event rates of selected channels on regular intervals.

An internal timer implementation allows to adjust the update interval according to the user's preference with a slider. Also, there exists the option to read the descriptive names of available channels and use these instead of channel ID numbers. Because the channels of the channels present the raw count rate as output by the APDs, the ratemeter can read correction factors for all channels from an init file. This then allows to display the "flat-field" corrected, effective count rate of each detector (see chapter 5). Furthermore, since observers are usually interested in photon rates *above background* level, a drop-down list box permits to select one of the channels to be taken as background that is substracted from all other channels (see figure 4.10(a)).

Hard disk writing client

As the main task of any DAQ is storage of observational data, a simple hard disk recording client was implemented. This writer application uses *fwrite()* to directly write the event data off to hard disk in its raw format. This provides both the simplest implementation of a writing client (see diagram 4.11), and one of the quickest method of saving DAQ data.

The writing client saves the raw file in the new OPTIMA event raw format. Because data is provided already separated by channel through the shared memory, this implementation saves events for each channel in a separate file. The file contains an ASCII header followed by the 64-bit integers representing photon events in their absolute time format as described above.
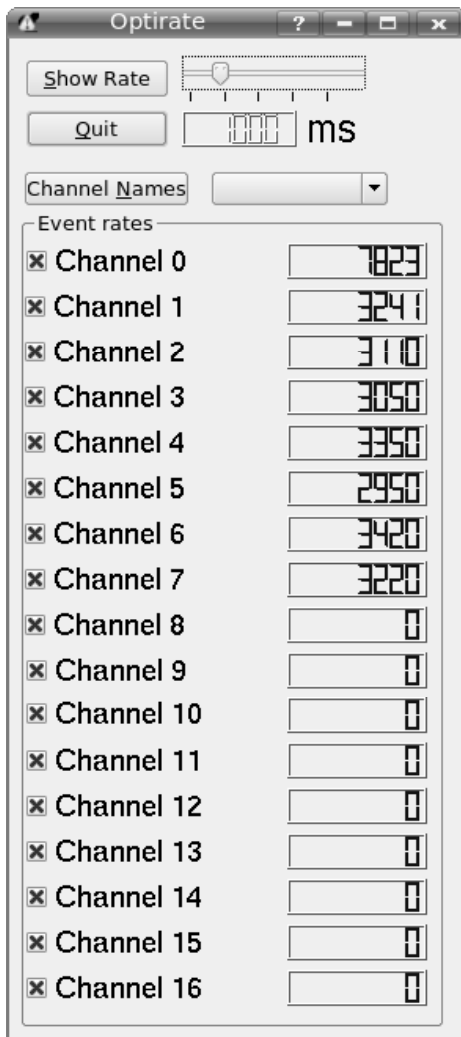
(a) Simple ratemeter (b) Hard disk writing client

Figure 4.10: Examples of simple data client GUIs
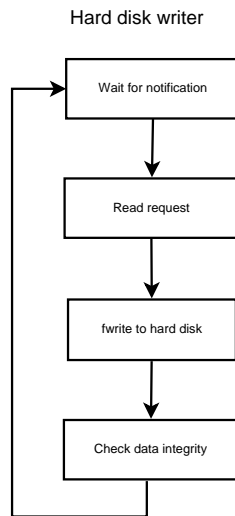
Hard disk writer

Figure 4.11: Simple hard disk writer implementation

An implementation of a *wait for notification* function provides an easy way for the client to react to *notifications* from the server, without using mechanisms such as call-back functions to perform asynchronous reception of messages. If using the *wait for notification* function provided by the library, a channel waiting for new events to arrive blocks and the execution of the event loop halts. This means that for a client accessing multiple channels, one low rate channel may block the reading of data from other channels. The design of the framework allows to launch a separate client for each channel to be accessed, so that the blocking of a channel is uncritical. The number of running clients is not limited in the ODASSE framework.

Another approach lies in using threads. A multithreaded client can spawn a thread for each channel with a loop executing the cadence of *read request*, reading of data, *wait for notification* (see section 4.3.3). Thus, a channel waiting for new events to arrive does not block the whole client application, but only its own thread.

Plotting client

A numerical ratemeter is helpful to determine dark counts of APDs (see chapter 2.3.3), but during observations of variable sources, it is difficult to have a feedback from numerical values alone. As a demonstration for a quick-look analysis client an application was created that plotes the data rates of selected channels on a graphical display. Similar to the numerical ratemeter, it offers the same options in terms of using descriptive names instead of IDs for the channels. Also, one channel can be selected as background channel which is then substracted from the other channels to display the rates above the background level (see figure 4.12).
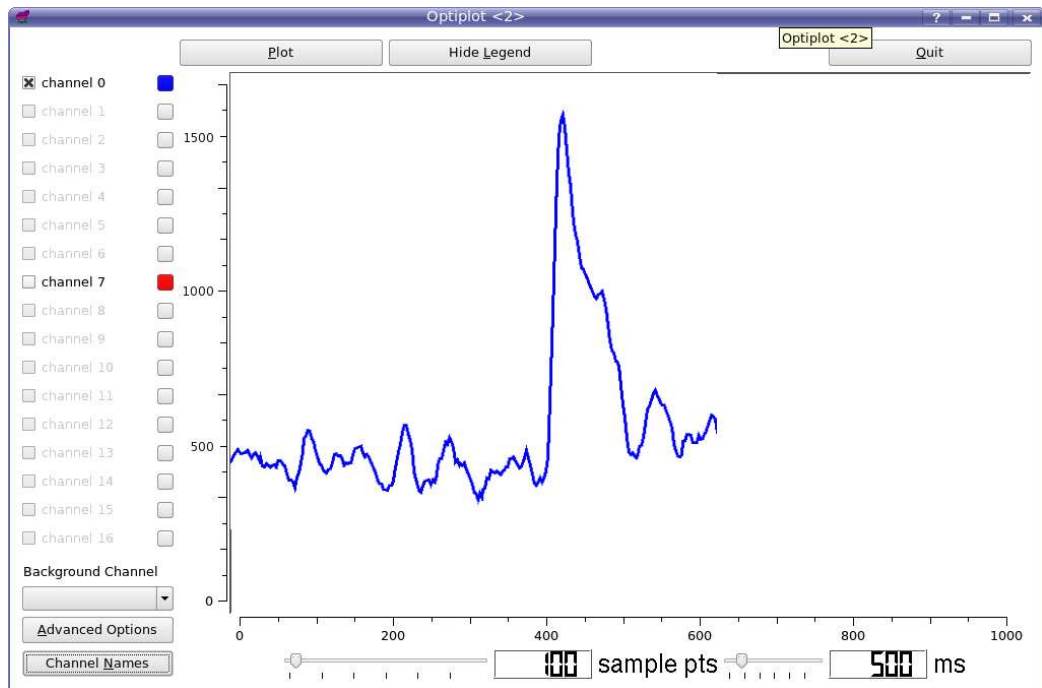
Figure 4.12: Plotting client

Remote control client

As mentioned in section 4.3.3 communication via sockets can be used to send commands to the DAQ server. An implementation of a remote control client that connects to the server and sends commands via the socket connection demonstrates how a running server can be controlled externally by another application. Events generated in the GUI, e.g. pressing buttons, are translated by the client into the ODASSE communication protocol and send through a *send message* library function over the socket. Changes in the configuration that the server performs upon these commands are in turn broadcast to the client and it changes its display of this information accordingly, e.g. available channels. The establishment of a connection via TCP/IP allows to run the client on another computer than the actual server is running on (see figure 4.13).

Figure 4.13: Replay server remote control client

Chapter 5

Scientific Results

This chapter covers a set of scientific observations performed with OPTIMA. Data reduction steps necessary to reduce OPTIMA raw data will be described in the first part, while the second part will give a selection of astronomical objects that were observed with the instrument during campaigns in 2006 and 2007. Light curves of AM Her type cataclysmic variable HU Aqr were chosen as an example of an interesting cataclysmic variable star (see section 5.2). The Low-Mass X-ray Binary Aql X-1 showed a flare during an OPTIMA observation on 1 August 2006 which is discussed in section 5.3. Crab pulsar light curves are presented in section 5.4 to compare OPTIMA observations with observations of Karpov et al. who report a deviation from the usual pulse shapes seen in the Crab light curve during 2005/2006.

5.1 Data Reduction

As with every instrument, the data recorded during observation constitutes only a raw form. Before any scientific analysis on the observations can be done, the data must be cleanly reduced. Instrumental and background effects can be to a great extend minimised by proper data reduction. The steps necessary for scientific data reduction of OPTIMA data are covered in the next sections of this chapter.

5.1.1 Analysis software

Since the DAQ software records the raw data in the form of photon event times in UTC, data reduction software for later analysis of the observation is necessary. For performance reasons the existing DAQ software writes in its own raw data format which takes only 5 Bytes per event. Most event based instruments today use a FITS-based file format. Existing analysis tools therefore could not easily be applied to OPTIMA data.

In [Str01] tools for data analysis of OPTIMA raw data were also developed and implemented in
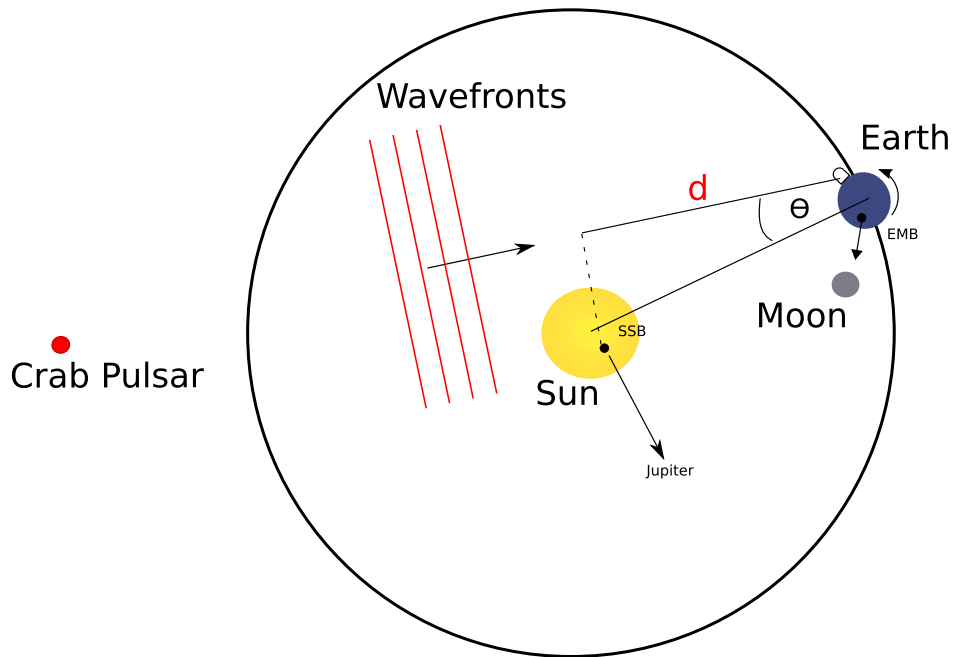
Figure 5.1: Barycentric correction of photon arrival times, where SSB: Solar System Barycenter, EMB: Earth-Moon Barycenter, Θ: angular separation of source from Sun's center of mass (for Shapiro delay)

an analysis software package for local use.

Barycentric correction of arrival times

OPTIMA records photon events with a GPS-based UTC time tag. UTC time references to the zero meridian in Greenwich. For high-precise timing of variable sources and correlation with space-based and ground-based observations, these must be transferred to a common inertial reference frame. Then coincidental analysis of single photon events can be performed.

In order to derive the barycentre-corrected arrival times of photon events, several effects must be taken into account.

- **Ephemeris of the solar system:** The position of all nine planets[1], Moon, and major aster-oids determines the position of the solar system barycentre (SSB). NASA's Jet Propulsion Laboratory publishes a numerical integration of the orbits with an accuracy of 200m, this corresponds to a time difference of less than $1\mu s$.

- **Geographical position of the observer:** Due to the rotation of the Earth, the longitude and the lattitude of the observer's location on Earth determines the arrival time of photons at his

---

[1]Jupiter as the planet with the greatest mass has by far the biggest contribution of all planets to the position of the solar system barycentre.

position.

- **Position of the source:** The position of the source must be known very precisely for measurements, since a small inaccuracy in its assumed position in the sky, can affect the barycentric timing.

- **Shapiro Delay:** The curvation of space-time caused by the Sun's mass, creates a time-dilation for photons travelling nearby the Sun. The dilation is given by

$$\Delta t = -\frac{2GM_\odot}{c^3} \cdot log\left(1 + cos\theta\right) \tag{5.1}$$

where

G:	gravitational constant
$M_\odot$:	mass of the Sun
θ:	angle between the source and the line connecting Earth and Sun

The Shapiro delay can be up to a few microseconds.

- **Gravitational blue shift:** Photons entering the Solar system experience a relativistic blueshift due to the Sun's gravitation. Due to the elliptic orbit of the Earth around the Sun this value differs over one revolution, because the Earth is at different positions of the Sun's gravitational potential.

- **Dispersion in the Interstellar Medium (ISM):** The ISM causes a dispersion of light of different wavelengths. For multiwavelength observations the arrival time of photons at different wavelengths must be taken into account.

OPTIMA's data reduction software uses the TEMPO code[2] library [ERE+82] to account for all of the above mentioned effects.

Binning of events

In order to get intensities and thus to create light curves, the event data must be binned. The data recorded in the OPTIMA raw files gives the individual arrival time of each photon detected. Intensity is defined as the number of photons per time interval, thus the individual photons must be binned into time bins.

Since the (barycentred[3]) arrival times of all photon events are known, they can be easily sorted into time bins with fixed interval sizes.

---

[2]http://www.atnf.csiro.au/research/pulsar/tempo/
[3]Depending on the scientific investigation the events may not needed to be barycentred.
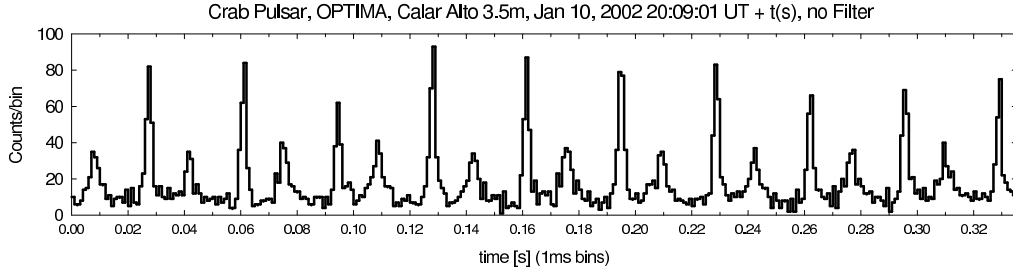
Figure 5.2: Light curve with 1ms resolution showing main pulse and inter pulse of the Crab pulsar

Light curves and Folding

The optical pulses of pulsars are very faint. Even at telescopes with large apertures, the achievable signal-to-noise ratio is rather low. In order to improve the signal-to-noise ratio several periods of the pulsar light curve can be added phase-coherently, through the mathematical method known as folding.

The Crab nebula has a period of $\sim$33 ms, thus, to detect individual pulses in its light curve a small bin size must be chosen. This means there is only a small number of events per bin and the signal to noise ratio is rather low. OPTIMA has shown that it can detect individual pulses in the Crab pulsar light curve during an observational campaign at the 3.5 m Calar Alto telescope in Spain (see figure 5.2).

Folding of strictly periodic objects is mathematically done by the modulo operator on the light curve with respect to a certain orbital phase, ϕ_0. Through equation 5.2 the corresponding phase ϕ is given by:

$$\phi_i = [t_0 - t_i] \,\% P + \phi_0 \tag{5.2}$$

where t_0 is the time taken as phase reference, ϕ_0 the corresponding phase, P the object's period, and t_i the barycentred time index of the bin.

In the case of objects with varying periodicity the change of their period must be taken into account, when being folded over several periods. The Jodrell Bank Radio Observatory[4] provides monthly ephemeris data for the Crab pulsar[5]. These provide correction values for the first period derivative due to pulsar braking. Using a Taylor expansion, the phase calculation formula then becomes:

$$\phi_i = mod \left[P + (t_i - t_0) \, \dot{P} + \phi_0 \right] \tag{5.3}$$

---

[4]The Jodrell Bank Observatory resides in Macclesfield, United Kingdom. Further information at http://www.jb.man.ac.uk/

[5]http://www.jb.man.ac.uk/research/pulsar/crab.html

where

ϕ_0:   reference phase

t_0:   reference time

t_i: barycentred time index of bin i

$P, \dot{P}$:   pulsar period and its first derivative

Light curves of the Crab pulsar obtained over several periods, give a much better signal-to-noise ratio and allow investigation of phase-resolved details in its light curve. Folded optical light curves of the Crab pulsar, showing the main pulse and the inter pulse, are presented in section 5.4.

5.1.2 Light curve reduction

Barycentering and binning provides light curve data for each channel recorded with OPTIMA. This constitutes only the first step of data reduction. For illustration purposes the steps in OPTIMA data reduction are compared to those encountered in CCD data reduction with which most readers should be familiar.

Just as CCD frames taken in astronomical observations taken with imaging detectors, OPTIMA light curve data still contains instrumental and sky contributed background that must be removed to obtain cleanly reduced data, with as few instrumental artefacts left as possible.

At first the dark count rate of the avalanche photodiodes is determined. During OPTIMA observations, the first three to five minutes the shutter of the OPTIMA instrument is kept closed to determine dark rates. In the analysis the average over this time is taken as a suitable measure of the dark rate of the APDs. As mentioned in chapter 2.3.3 the Perkin & Elmer APDs are cooled by Peltier elements and their dark rate is rather constant. The median value taken for each APD separately is then substracted from the corresponding channel. In the CCD data reduction example this corresponds to the substraction of a dark frame.

Also as mentioned in chapter 2.3.3, the count rate output of each APD partly depends on the individual combination of the input coupling factor into the fibre, the transmission efficiency of the fibre and the output coupling from fibre into the APD's silicon. Thus, exposed to the same light flux, the APDs do not output the same count rate. The differences are of the order of 10 to 30 percent and the channels must be calibrated against each other. This is done by placing the fibre apertures on dark sky regions, which appear free of sources in a deep CCD exposure. The sky background is assumed to be uniform over a radius of a few arc minutes across the fibre apertures. Then the average of the sky background measurement for each fibre is calculated and the value used to determine each fibre's calibration factor. It is customary to calibrate the other fibres against the target fibre. The sky background median values of these are set in relation to the median of the target fibre and the count rates in these channels multiplied by these factors respectively. This calibration is similar to flat fielding with a sky flat in CCD data reduction.

Finally, for background reduction, all channels not contaminated by any star's light, i.e. the single background fibre (see chapter 2.3.1) and the surrounding fibres of the hexagonal bundle are coadded. By coadding several background fibres the signal to noise level can be improved. The hexagonal fibre bundle also allows to substract the nebula components for embedded sources, e.g. in case of Crab pulsar observations. the resulting background level is then substracted from the target fibre to give a fully reduced light curve.

An additional advantage of the fibre bundle is that an increase in flux in some of the surrounding fibres can be considered as an indication that the target star accidently moved off the central fibre. So, in addition to monitoring via the field view unit (see section 2.3.5), this can be an indication of a wrongly positioned target star. In principle an even increase in all surrounding bundle fibres can be considered as a measure for very bad seeing.

5.1.3 Quality monitoring

OPTIMA's CCD camera (see chapter 2) is used to take 10 second exposures of the field of view during observations. Although the sources themselves which are positioned on the fibre apertures are not visible in the frames, this gives the possibility to use these frames for monitoring seeing conditions. Unexpected changes in flux in the light curves need not necessarily be caused by the target source. Increases in the background level can be determined by the background reduction with the other channels (see section 5.1.2), but changes in atmospheric conditions can not be deduced from the APD count rates alone.

Passing clouds cause light to be reflected and result in an increased flux in the whole field. On the other hand, atmospheric extinction, due to an increase in airmass for example, results in a decrease of flux in the whole field. The CCD quality monitoring is also helpful in determining the character of flares and spikes in light curves. These might be caused by passing airplanes or satellites that only shortly fly over the fibre aperture. In the CCD frames these appear as streaks across the image. The CCD frames contain UTC times in their mid exposure time tags. The time tags are not as accurate as the GPS time tags of the OPTIMA light curves, but the accuracy is sufficient to relate the frames to features in the OPTIMA light curves.

5.2 Cataclysmic variable star HU Aqr

HU Aqr is an AM Her type Cataclysmic Variable (see chapter 2.5.2) with a WD primary and a M4V type secondary. In this type of CV the white dwarf (WD) has a strong magnetic field[6] [Cro90], reaching out far into the system. The material flowing from the secondary mainly consists of charged

---

[6]Typically 10-80 MG. AR UMa has the strongest magnetic field known in a white dwarf with a strength of 230 MG [Sch99].

particles and these are forced to move along the magnetic field lines in a spiral motion. In non-magnetic CVs the circulation radius is the radius at which a particle falling in on a ballistic trajectory towards the white dwarf has sufficiently lost so much of its angular momentum that it takes on a circular orbit; this constitutes the outer rim of the accretion disk around the WD. Thus, if the radius of the magnetosphere reaches beyond the circulation radius, no accretion disk is formed. The magnetic field lines emanate from the poles of the WD and particles are forced out of the equatorial plane of the binary system [Hel01]. The region outside the magnetoshphere is still dominated by the ballistic trajectories of the particles in the stream [SMH97], while closer to the WD the magnetosphere dominates particle movement [WKJM89]. The modelling of the geometry of the accretion stream in strong magnetic CVs is still a debated topic of theoretical models [HHS99], [FW99].

Charged particles are forced to move along the field lines, they are "frozen" into the extended magnetosphere and corotate with the white dwarf. This leads to spin-locking, where the spin period of the WD adjusts to the Keplerian orbital period of material just outside the magnetosphere. In this equilibrium situation there is no discontinuity in velocity for material flowing from outside into the magnetosphere [Hel01]. The strong magnetic field causes also the WD to get locked into synchronous rotation with its secondary star, so that the same side of the white dwarf is facing its secondary, the late-type main-sequence star, at all times.

The material flow from the secondary to the primary is a compact stream along the magnetic field lines, and is called the *accretion stream*. Due to the concentration of material into the thin stream, its density and hence its luminosity is high and can contribute up to half of the overall luminosity of the binary system in the optical. The exact geometry of the accretion stream is hard to determine, since it depends on the orbital phase and magnetic field configuration of the binary system, and the initial ballistic trajectory of the material stream. Collisions of particles with each other form shocks and lead to blobs of material of higher density within the stream. In CVs with a high inclination angle, i, as it is the case for HU Aqr, deep eclipses of the different components contributing to the observed light curve allow a good determination of the stream geometry (see section 5.2).

The material flows towards one of the magnetic poles of the WD. Hence, this type of CVs is also known as a "polar". Since it requires less energy to get not so far outside the plane, the material usually flows towards the weaker one of the magnetic poles, though some of the material might still accrete onto the other pole [Hel01].

The ionised particles circling around the magnetic field lines in a spiral motion, emit cyclotron radiation at the typical cyclotron frequency ω_c. The frequency of the emitted radiation is then given by

$$\nu_c = \frac{eB}{2\pi m_e} \qquad (5.4)$$

where B is the magnetic field, e is the electron unit charge , and m_e the rest mass of the electron.

At the small accretion region on the WD, the so-called "hot spot", almost half of the observed luminosity of the binary system is created, the other half is largely contributed by the accretion stream as mentioned above, and only a small fraction originates from the WD itself and the companion star. The nature of the radiation created in the impact depends on the density of matter that crashes onto the WD. If a diffuse stream of material hits, it is converted to thermal energy and the material extends into an accretion column. Incoming material from the stream hits the column and a shock forms where the collision of electrons and ions create X-rays through bremsstrahlung. The material slows down, cools, and accretes onto the WD's surface. Dense blobs on the other hand have a higher kinetic energy and do not experience an accretion shock. They fall directly onto the WD where their energy is absorbed by the WD's atmosphere which creates blackbody radiation of a temperature of ca. 200000 K [Hel01].

Depending on the amount of material flowing in the accretion stream and accreting onto the WD, HU Aqr can be seen in a high or a low accretion state. In high state its average brightness over one period is up to about $V \sim 14.7$.

5.2.1 Observations

Observations of HU Aqr were done during several nights as part of the secondary science program of the "OPTIMA Burst" campagin. Observations were carried out with the 1.3 m telescope at the Skinakas observatory during the nights listed in table 5.1.

Date	Telescope	Duration	Spectral range	Figure
Jul 1, 2006	SKO, Crete	7900 s	$400 - 950$ nm	5.3
Jul 8, 2006	SKO, Crete	7750 s	$400 - 950$ nm	5.4
Jul 15, 2006	SKO, Crete	7900 s	$400 - 950$ nm	5.5
Aug 6, 2007	SKO, Crete	13500 s	$400 - 950$ nm	5.6
Aug 7, 2007	SKO, Crete	9400 s	$400 - 950$ nm	5.7

Table 5.1: Log of observations

OPTIMA operated in photometer mode, using the fibre bundle. HU Aqr was positioned on the central fibre, while the surrounding six bundle fibres and the dedicated background fibre recorded sky background. In figures 5.3 to 5.7 the light curves recorded in the above mentioned nights are shown. The data shown was binned with one second bin size.
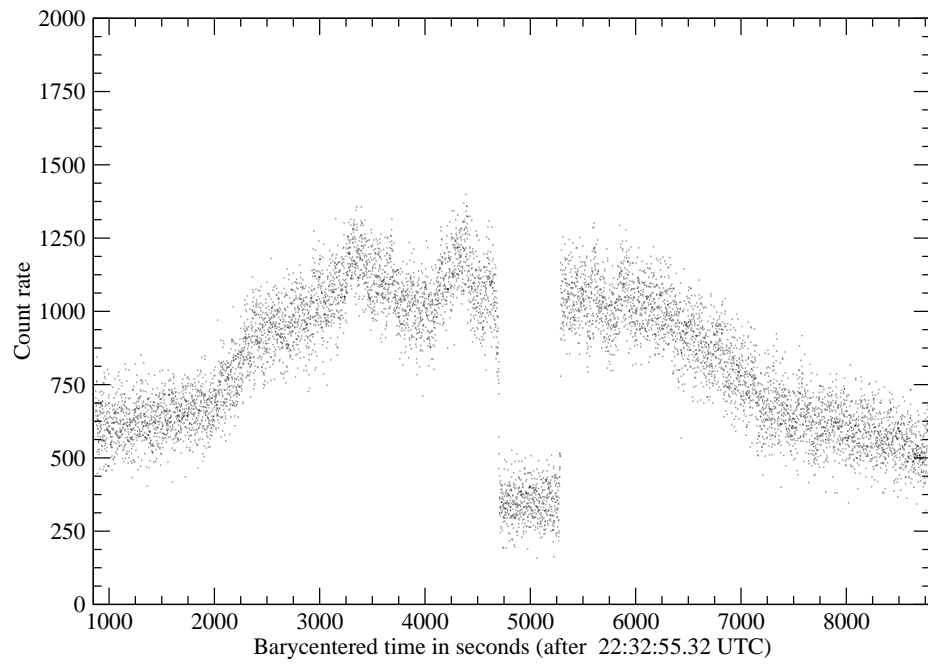
Figure 5.3: July 1, 2006: HU Aqr, 1 second binning
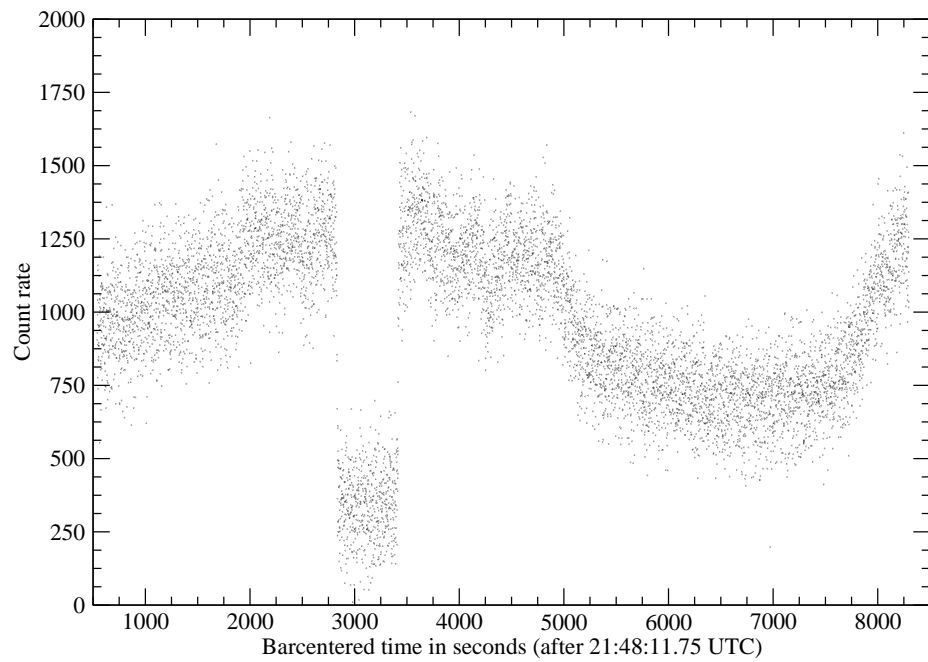
Figure 5.4: July 15, 2006: HU Aqr, 1 second binning

83
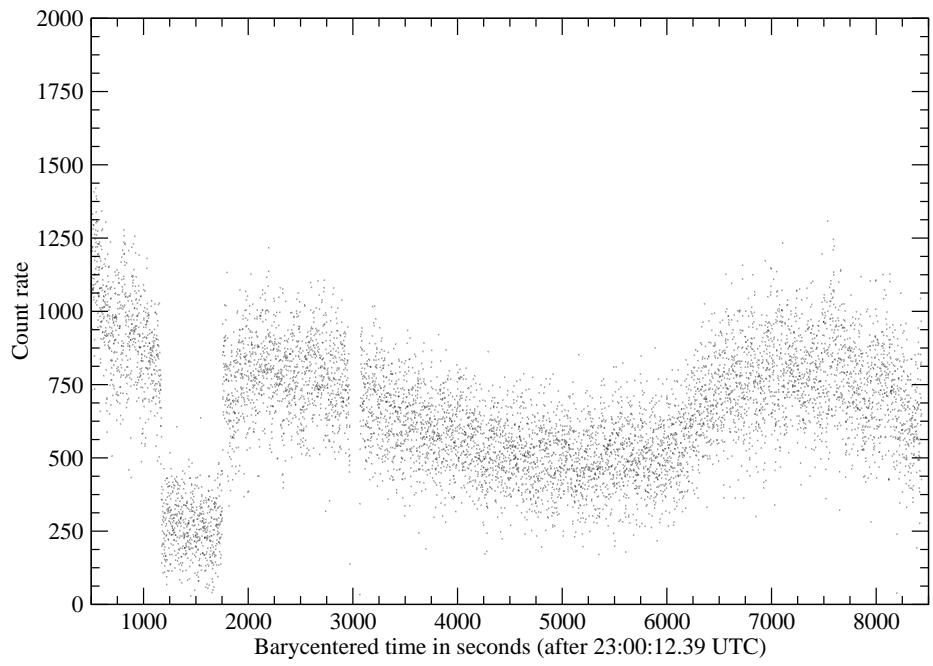
Figure 5.5: July 15, 2006: HU Aqr, 1 second binning
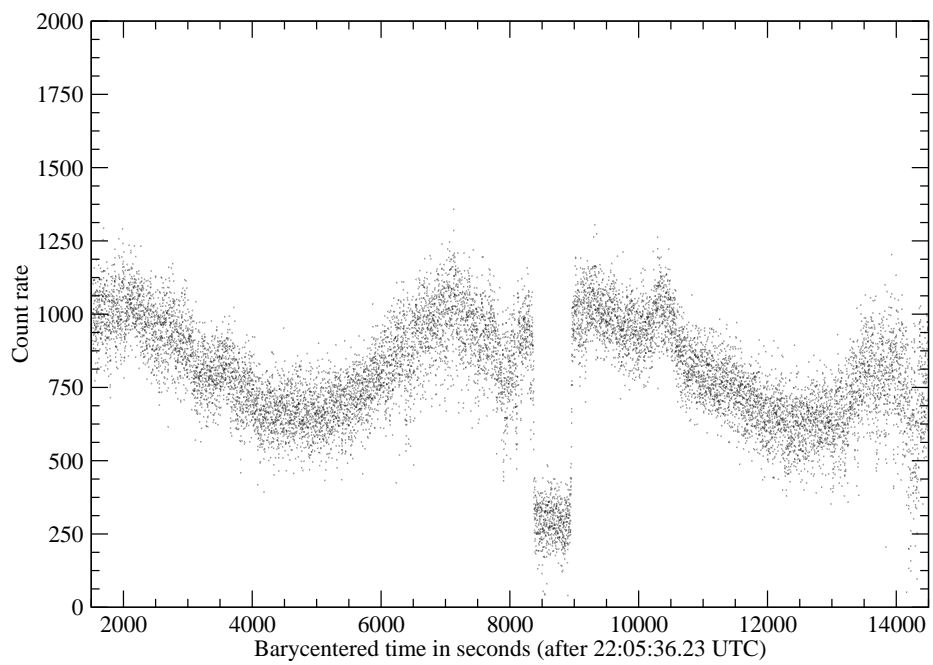
Figure 5.6: August 6, 2007: HU Aqr, 1 second binning

5.2.2 Analysis

Features in the light curve

The most prominent feature in the light curve of HU Aqr is the deep eclipse phase. HU Aqr is an eclipsing binary system that is seen nearly edge-on, where the secondary star entirely eclipses the WD. Due to the fact that the contribution of the luminosity of the WD to the overall brightness of the system is negligible, the greatest change in brightness can be seen when the hot spot near the magnetic pole of the WD is eclipsed by the main sequence star. Therefore the ingress phase is very steep, having a duration of only ca. 16 seconds (see table 5.2). Similarly the egress time is of roughly the same duration and very sharp. During the eclipse only the blackbody radiation of the secondary star is seen, when it passes in front of the WD and also eclipses the accretion stream. Its magnitude is $V \sim 19.1$, corresponding to the observed 250-300 counts in the OPTIMA observations[7].

In previous observations of HU Aqr, [HCH+99], [SMH97] and [BCR+02], the accretion stream was seen at a different phase, so that at egress and ingress of the system the brightness contribution of the accretion stream could be clearly distinguished. When the hot spot was already partially, and then fully, eclipsed, the accretion stream threading along the magnetic field lines leading to the WD's magnetic pole was further and further eclipsed by the secondary. Thus a linear decline in brightness could be observed in the light curve, until the entire accretion stream was hidden behind the secondary. The linear decrease in brightness suggests that the luninosity of the accretion stream is relatively even, with a slightly steeper decline towards the end. The same light curve shape was seen in OPTIMA observations in 2000 (see figure 5.8).

Just before the onset of the eclipse, a "pre-eclipse" dip can be seen in the light curve. In the observation on the 8th of July 2006, only a very faint dip can be identified, while it is prominent in the observations on the 1st of July 2006, 15th of July 2006 and on the 7th of August 2007. The observation of the night of the 6th of August 2007 started just before the eclipse of the system, so that the phase of the pre-eclipse dip is not visible in the light curve. The dip occurs, when the hot spot on the WD is partially eclipsed by the accretion stream. Therefore, the phase of the centre of the dip is related to the azimuth of the coupling region [BCR+02].

In all observations in 2006 and 2007 the light curve shows a wide dip to a about less than half of the maximum brightness, where both the accretion stream and the hot spot are visible. That feature can not be seen in the light curve observed by Straubmeier et al. in 2000 [Str01], though the data in Bridge et al. [BCR+02] does show a similar feature.

It is also notable that the overall brightness level (about 1250 cps) after egress is the same as before ingress, while the OPTIMA light curve in 2000 shows a higher level count rate before ingress

---

[7]At the 1.3 m telescope of the Skinakas observatory a 19th magnitude standard star yields about 250 counts per second above background level.
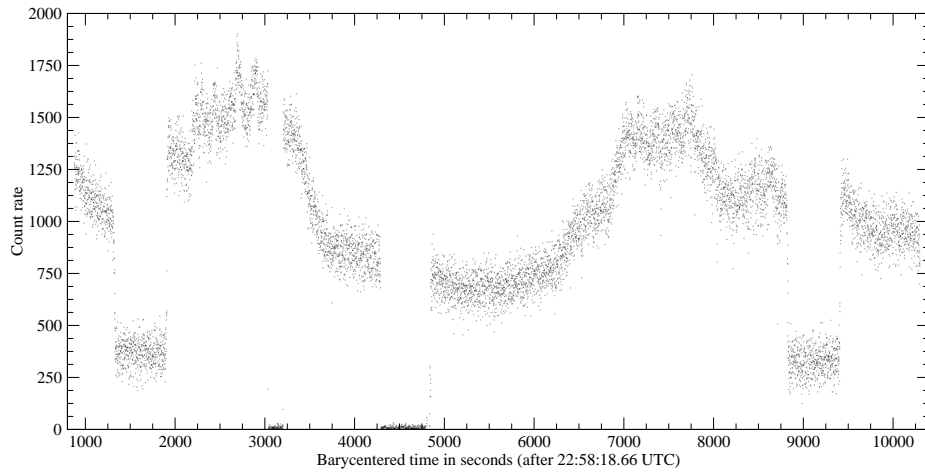
Figure 5.7: August 7, 2007: HU Aqr, 1 second binning, showing two successive eclipses
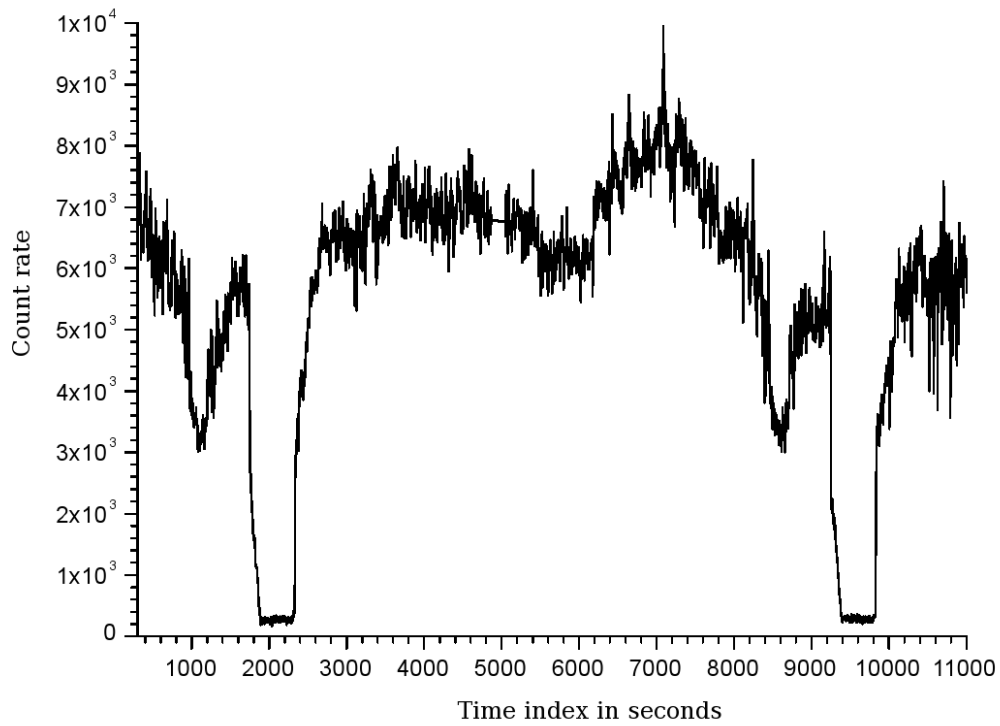
Figure 5.8: HU Aqr light curve recorded on 8th of July 2000 at the Skinakas 1.3 m telescope [Str01].

than after egress, about 7000 cps to 6000 cps. Another distinction between the observations is that the light curve in 2000 showed short time scale spikes of 1-2 seconds duration. Resolved at high time resolution these showed a Gaussian shape and their peak value was about two and a half the value at their baseline [Str01].

The light curves of the years 2006 and 2007 observations were recorded at the same telescope as that curve presented in [Str01] during the year 2000. Therefore the count rates of the two graphs can be compared with each other. It can be clearly seen that HU Aqr was in low accretion state during in 2006 and 2007, showing a peak count level of 1750 cps, while the curve of 2000 shows rates up 7500 cps. That is a four times higher intensity. In magnitude scale HU Aqr was in the visual 3.5 magnitudes brighter during the high accretion state in 2000 than its low accretion state in 2006/2007.

Ingress and egress time scales

As mentioned in the introductory paragraph of HU Aqr, the steep edges of the light curve hint at a very small, localized emission region on the white dwarf. This is known as the hot spot, and determining the ingress time, that is the time from the level of uneclipsed brightness to full eclipse, gives an estimate for its size.

In [Str01] a linear fit with four piece-wise defined segments was chosen due to the contribution of the accretion stream in the eclipse phases. As mentioned previously, the accretion stream is now in a different configuration, and not visible during ingress and egress phases of the eclipse. The shape of the light curve allows to use a three segments piece-wise linear fit for the ingress and egress phases.

The fit assumes a constant level before egress, falls off monotonously, and reaches a constant level at full eclipse. Similarly for egress, the fit starts at the constant level in full eclipse, increases monotonously, until it reaches the maximal brightness level. The two gradients for ingress and egress may differ from each other. Due to the synchronous rotation of the system and the orbital movement of the secondary star, the egress time is slightly longer than the ingress time. This effect was also observed by Bridge et al. [BCR+02].

Applying this fit to the ingress and egress phase of a particular eclipse, gives the parameters determining the size of the hot spot on the WD's surface. Due to the high noise level in the light curve, the fits have large errors. HU Aqr in low accretion state has only a low luminosity which leads to a bad S/N level in connection with the rather small aperture 1.3 m telescope of the Skinakas observatory. The resulting ingress and egress durations are given in table 5.2.

With knowledge of the separation of the WD and the main sequence star in the HU Aqr system, their Keplerian orbital velocities can be determined. This relates the duration of eclipsing the hot spot on the WD to the orbital velocity of the secondary star and hence gives a limit for the
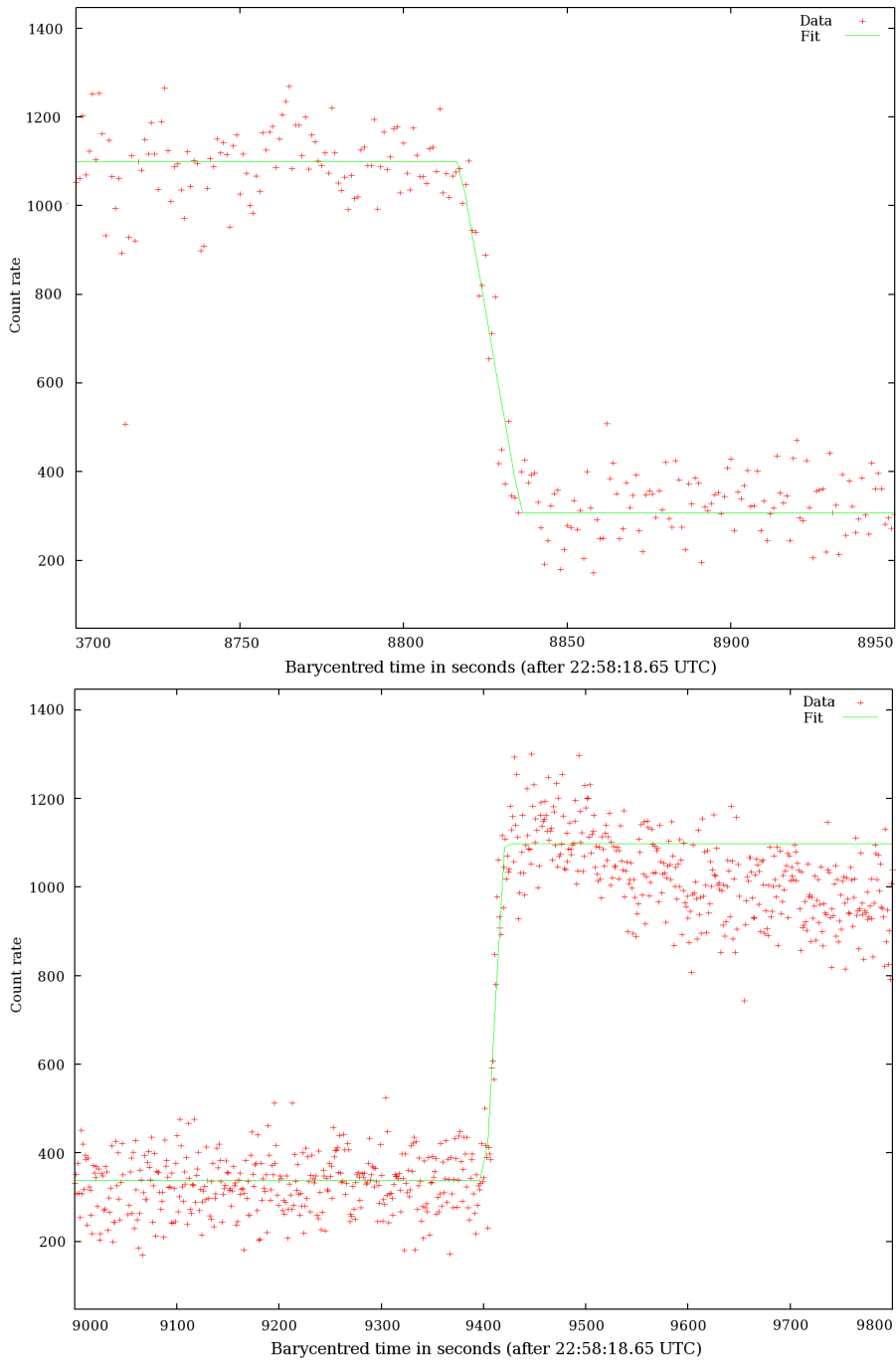
Figure 5.9: Three segment piece-wise linear fits to the ingress and egress phase of the second eclipse observed in the light curve of 7 August 2007.

Eclipse	Ingress duration	Egress duration
1 July 2006	5.5 s ± 17.5 s	6.7 s ± 3.6 s
8 July 2006	8.3 s ± 1.4 s	7.5 s ± 1.7 s
15 July 2006	8.3 s ± 2.2 s	5.2 s ± 2.3 s
6 August 2007	19.6 s ± 2.6 s	18.2 s ± 3.0 s
7 August 2007 (first)	16.8 s ± 1.6 s	12.0 s ± 1.1 s
7 August 2007 (second)	18.1 s ± 1.7 s	19.1 s ± 2.0 s

Table 5.2: Ingress and egress times for all observed eclipses in 2006 – 2007

dimensions of the hot spot on the WD's surface. The main sequence star's orbital velocity is ca. $200 \, \mathrm{kms^{-1}}$. Thus the above given time durations correspond to a spot size of about 1600 km in 2006 and $3600 - 4000$ km in the observations in 2007. The hot spot was in 2007 almost two and a half times larger in diameter than compared to 2006. Whether this is due to a change in material flow or in a change of the configuration in the magnetic field which changes the threading of the material confined to the field lines, cannot be determined from OPTIMA data alone. Accretion stream mapping, as described by Harrop-Allin et al. in [HCH+99] and [HPC01] and by Vrielmann et al. in [VS01] might provide a method to determine a change in configuration of the magnetic field threading in this years observations compared to the previous year.

Determination of the ephemeris for 2006 – 2007

Determination of mid-eclipse times allows the calculation of an accurate ephemeris for the cataclysimic variable star. HU Aqr has a period of about 124 minutes. By observing several eclipses and determining the their mid-eclipse times the period of the CV can be determined. From the period and absolute time tags of particular eclipses the ephemeris that allows to calculate past and future eclipses can be calculated to a high accuracy.

Although here only a smaller number of observations of the eclipse phase of HU Aqr is available the priciple of calculating an accurate ephemeris from a number of eclipse observations for which absolute time tags are available, can be demonstrated, using the above light curves as samples. Due to the steep ingress and egress edges in the light curve, determination of the mid-eclipse time is easily done. The error in the accuracy for that time is mainly given by the error of those edges and starting with the observation on 7th of August 2007, where two successive eclipses were observed, the period can be determined.

The mid-eclipse time can be determined from the fit values of the above used three segment piece-wise linear fits used to calculate ingress and egress times. The mid-eclipse time is then the difference between the two times, where ingress and egress reach the base level value over two:

$$t_{mid-eclipse} = \frac{t_{base-egress} - t_{base-ingress}}{2}$$

From two mid-eclipse times a first estimate for the period can be calculated. Using the two successive eclipses, observed in the night from the 7th to the 8th of August 2007, gives a period of 7498.3 s $\pm$ 2.6 s, where the error stated is due to the inaccuracy of the ingress and egress point measurements, which determine the start and end points of the fully eclipsed phase. Using the eclipse recorded on the previous night provides a suitable step in determining a more accurate value. The time difference between the two eclipses is, given in Julian Date:

$$\Delta t = \left(2454320.47590 \pm 2 \times 10^{-5}\right) - \left(2454320.47590 \pm 1 \times 10^{-5}\right) = 0.087 \pm 2 \times 10^{-4}$$

Dividing this difference by the orbital period derived from the two eclipses before, gives the number of orbits to be $10.97 \pm 3 \times 10^{-4}$. It is clear that the number of orbits between two eclipse must be an integer number, therefore the number of orbits must be 11. With this knowledge the error gets smaller through

$$\frac{period_{old} \cdot 10.97}{11} = period_{new} \Rightarrow period_{new} = \frac{0.087 \cdot 10.97}{11} \pm \frac{2}{11} \times 10^{-5} = 0.08676 \pm 2 \times 10^{-5}$$

This gives a more accurate estimate for the period of HU Aqr to be $JD(0.08676 \pm 2 \times 10^{-5})$, 7496.1 s$\pm$1.72 s , which now allows an extrapolation to time scales of more than a year. Therefore, the mid-eclipse times of the observations done in 2006 can also be used to calculate a better estimate for the period. By continuing this argument and using the mid-eclipse times of all five observational runs, covering six eclipses, the period and hence the linear ephemeris of HU Aqr can be determined to be:

$$T_{ecl} = JD\,(2453925.4429734438 \pm 0.00002) + E \times (0.0867618 \pm 0.000002)$$

where the eclipse time, T_{ecl}, can be calculated from the start time on the left plus the number of eclipses, E, times the period.

Schwope et al. determined the ephemeris with a high accuracy, using a far greater number of eclipse observations, than available with these OPTIMA observations [SMH97], which led to a value of, given in Julian Date format:

$$T_{ecl} = HJD2448896.543707(27) + E \times 0.086820446(9)$$

5.2.3 Results

Observations of the Cataclysmic Variable star HU Aqr in 2006 and 2007 reveal that the system shows different characteristics in its light curve. The most apparant fact is that the system was

now observed in a low accretion state, where the peak brightness in its light curve is almost 3.5 magnitudes less than during 2000 where it was observed in a high accretion state.

The observed brightness difference between the phase before the eclipse and after eclipse in the light curve of 2000 was explained through the fact that the hot spot is seen at different angles. The region above hot spot is the origin of high energy cyclotron radiation. The cyclotron radiation does not reach its maximum at observation along the magnetic field lines, but at greater angles subtended between the line of observation and the magnetic field line that emits the radiation. That angular dependency is also the reason why the eclipse-free region of the light curve does not show a constant brightness level.

The table of ingress and egress times (see 5.2) shows that both ingress and egress times are of comparable lengths for the year 2006, within the given error. The same applies for the times of the year 2007, if they are considered by themselves. The data shows, though, that ingress times in the observations recorded in 2007 are more than a factor two longer than those in the year 2006, while egress times are about two to two and a half times longer than those measured in 2006. This seems to be an indication for a change in the spot size of the accretion spot on the WD, due to an increase in material flow. Although this argument is in to contradiction to the fact that HU Aqr was in a low accretion state at both times of observation in 2006 and 2007. Another contributing factor could be the azithumal movement of the accretion spot on the WD's surface which leads to different angles it is observed on and thus longer ingress/egress times. The egress time of the first eclipse observed on 7th of August 2007 appears to be an odd value, being a third shorter than the one on the night before and the second eclipse observed in the next orbit. The reason for this is unclear, though, a possible explanation could be a less dense region in the accretion stream, where at that time the material flow accreting onto the WD was significantly lower.

The linear eclipse calculated from the 2006 and 2007 allows prediction of HU Aqr eclipses up to five years. The accuracy given for the ephemeris determined by Schwope et al. is far higher than the one calculated with the OPTIMA 2006 and 2007 data only. HU Aqr is believed to have non-linear components in the development of its ephemeris which is currently investigated by Schwope et al. in more detail using a greater set of eclipse data.

5.3   Low Mass X-ray Binary Aql X-1

Aql X-1 is a highly active LMXB [KDG+73], showing recurrent X-ray outbursts roughly on a yearly basis [PT84]. Its primary object is thought to be a neutron star [KIM+81] of an estimated mass of more than $1.6M_\odot$ [CCS+07], while the secondary star only has a mass of less than $1M_\odot$ and is thought to be of type K6-M0 [CILP99]. In contrast to LMXBs with a persistant accretion flow from the Roche lobe of its companion star, Aql X-1 is a soft X-ray transient (SXT) that occasionally shows short outbursts of a few weeks to months duration and then returns to a quiescent state. That

means the system can be observed in two different states, the so-called High Intensity State (HIS) or the Low Intensity State (LIS). The optical counterpart of Aql X-1, V1333 Aql, was identified in 1978 [TCB78] at a position with right ascension $19^h11^m16.0^s$ and a declination of $0°35'6''$ (for epoch 2000).[8]

The Aql X-1 system is dominated by processes in its accretion disk. While being in HIS the luminosity of the accretion disk by far outshines that of the companion star, both in the optical and the X-ray regime. For LMXBs the greatest part of the energy is emitted in X-rays. In HIS a great amount of material accretes onto the disk and the accretion disk rim is closer to the neutron star. This causes an increase in brightness in the visual magnitude from V∼ 19.26 [CILP99] during LIS to ∼ 17 during HIS.

5.3.1 Observation

Monitoring observations of Aql X-1 in the optical band showed an increase in brightness for the time from 28th to 31st of July 2006 [BNM06] and [IC06]. On 1 August 2006 it was observed by the Swift satellite [WMBL06a] and [WMBL06b], but no X-ray outburst was reported for the Swift observation. Triggered by notices in the Astronomer's Telegram, OPTIMA performed an observation of Aql X-1 on 1 August 2006 at the Skinakas 1.3 m telescope on Crete, Greece.

OPTIMA observed Aql X-1 for about one and a half hours on target. The field of the Aquila region is very crowded which led to stars being on two of the surrounding background fibres of the central fibre bundle (see figure 2.6). These stars show high count rates in those recorded channels[9] and their positions could be verified in the CCD exposures that were taken before Aql X-1 had been positioned on the fibre.

Aql X-1 shows a long flare in the light curve at 21:32:51 UTC (barycentred time), where the observed flux is about five times higher at the peak value than at the baseline. The observation was recorded with only four of the bundle fibres connected to the DAQ, the others were in ready mode for the polarimeter. Thus, only the dedicated background fibre ((1) in figure 2.2), could be used to determine the background intensity in the data reduction. This fibre showed a clean background rate and did not show any flaring activity that can be seen at 21:32:51 UTC (barycentred time). Thus, it can be ruled out that any overall increase in the whole field of view is the cause for the observed feature in the target fibre.

Another effect that can cause a sudden increase of light flux in one of the channels are passing satellites or meteorites. Their characteristic is a sudden sharp increase in the flux, when they fly over the fibre. As described in chapter 2 the optical fibres cover a circe of 6 arc seconds diameter on the sky, when OPTIMA is used at the Skinakas 1.3 m telescope. The flare's duration is about 80 seconds. This duration rules satellites and meteorites out, because their high angular velocity lets

---

[8]The most up to date position is for the radio counterpart [RMD04].

[9]These were channel 1 and channel 2 of the fibre bundle.
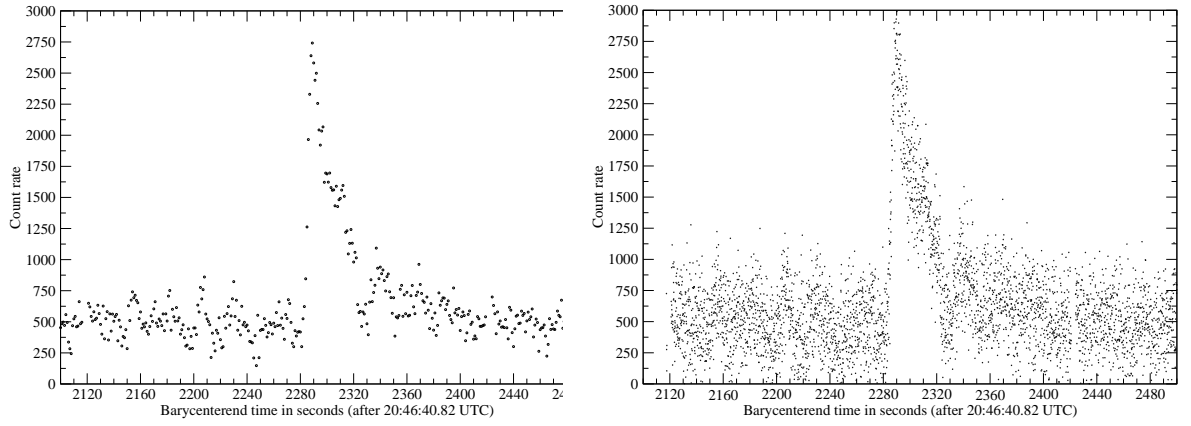
Figure 5.10: Aql X-1 light curve observed on 1 August 2006. The left graph shows the observed flare with 1 second binning. The figure on the right shows the flare in detail with 0.1 second binning.

them pass on the order of seconds. Even a meteorite coming in head on to the fibre would not last 80 seconds. Also, no traces as they would be caused by passing satellites or meteorites, were seen in the 10 second CCD exposures.

5.3.2 Analysis

The shape of the flare suggested fitting a fast rise and early decay (FRED) function to it. A FRED function is a piecewise defined function with an exponentially fast rising part, with time constant τ_{rise}, reaching a peak value at time t_{break}, after which a slower exponential decay starts with a slower time constant τ_{decay} until it falls off again to its constant value at base level c_{base}. The function definition is as follows:

$$f(t) = \begin{cases} f_{normalizaton} \cdot e^{\frac{t-t_{break}}{\tau_{rise}}} + c_{base} & if \quad t < t_{break} \\ f_{normalizaton} \cdot e^{\frac{t_{break}-t}{\tau_{decay}}} + c_{base} & if \quad t \geq t_{break} \end{cases} \tag{5.5}$$

The resulting fit, using an exponentially rising edge together with an exponentially falling edge after the maximum yields the following fit parameters, given in table 5.3.

Fit parameter	Value		Uncertainty	Unit
t_{break}	2286.8	$\pm$	0.29	s
τ_{rise}	1.6	$\pm$	0.26	s
τ_{decay}	24.4	$\pm$	0.85	s
$f_{normalization}$	2240	$\pm$	59	cps
c_{base}	475	$\pm$	4.2	cps

Table 5.3: FRED fitting parameters for the flare in the Aql X-1 light curve

93
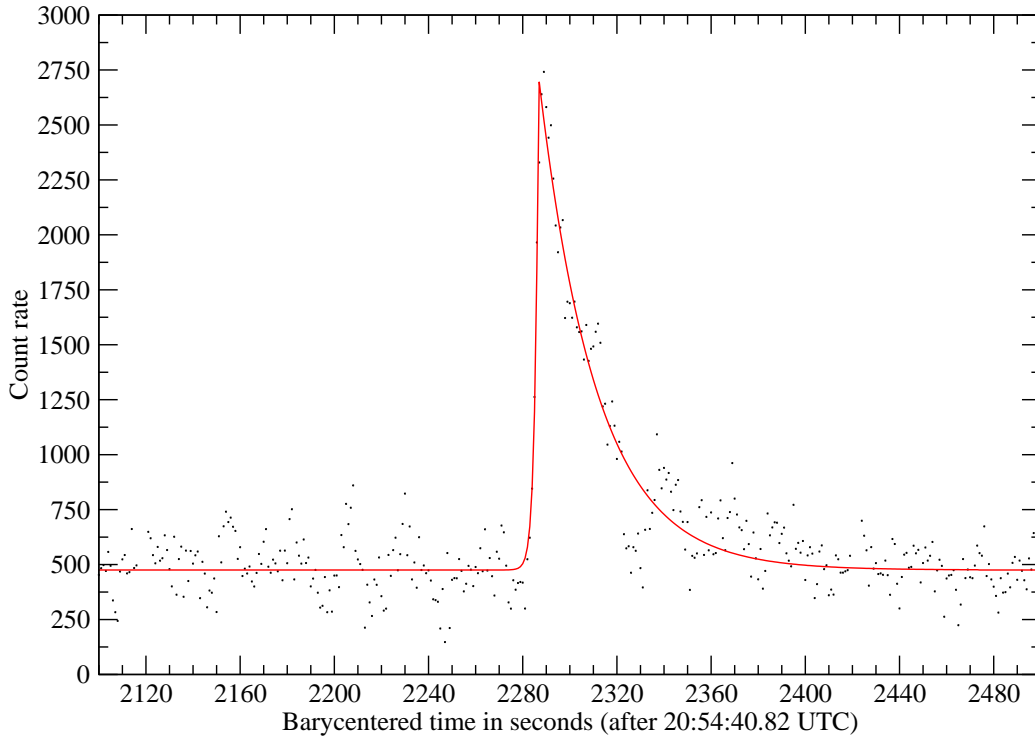
Figure 5.11: FRED fitted to the flare in the Aql X-1 light curve

The FRED fit is overplotted with the observational data in figure 5.11. The flare shows a steeply rising edge with time constant $\tau = (1.6 \pm 0.26)$ s. The flare reaches its peak value of 2715 ± 59 cps at 21:32:51 (barycentred UTC time). This constitutes more than a five-fold[10] increase in flux compared to the base value of 475.0 ± 4.2 cps. The falling edge falls off with a time constant of $\tau = (24.4 \pm 0.85)$ s. Integrating over the fit function gives an estimate of the t_{90} time, which is the time between 5 percent and 95 percent of the overall flux has been received. This value for the fitted curve is $t_{90} = 86$ seconds.

Checking for X-ray observations of Aql X-1 that were conducted around the time of the optical outburst, revealed that there is a 22 day long X-ray outburst that was observed with the All Sky Monitor (ASM) instrument on the Rossi X-ray Timing Explorer (RXTE) (see figure 5.12). The ASM on the RXTE X-ray satellite uses three so-called "Scanning Shadow Cameras" to provide observations in the $2 - 10$ keV X-ray band. The counts given in the graph are nominal rates of "one-day-averages" that are computed from the one-day average of the fitted source fluxes from usually 5–10 individual ASM dwells [asm07].

Figure 5.12 shows that the observations of increased optical activity of Aql X-1 mentioned in section 5.3 coincide with the onset of a X-ray outburst observed by the ASM over a period of 22 days from 28 July 2006 to 19 August 2006. The OPTIMA observations on the first of August 2006

---

[10]The flux ratio of the peak value to the baseline level is $\frac{2696 \text{ cps}}{475 \text{ cps}} \approx 5.7$.
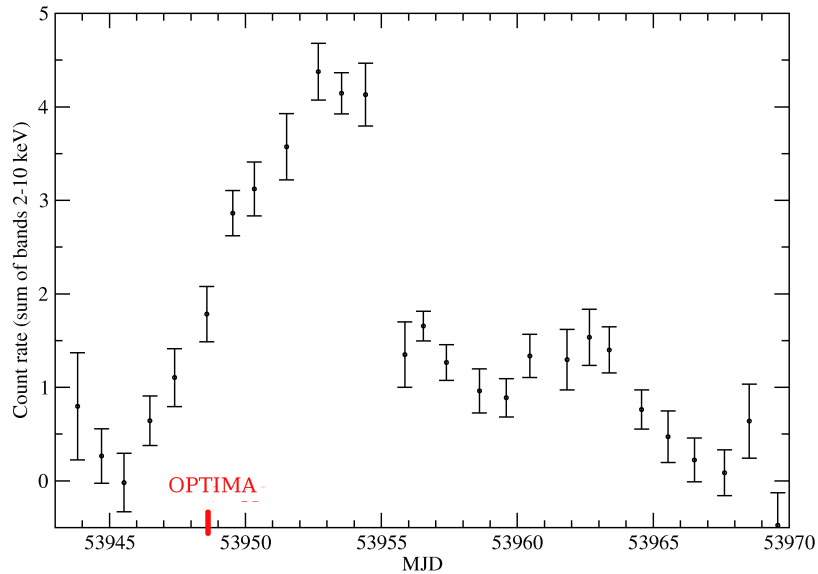
Figure 5.12: RXTE All Sky Monitor observations of Aql X-1 from July 27 2006 to 31 August 2006. The graphed data is the one day average rates over the summed bands from $2 - 10$ keV. The time of the observation with OPTIMA is marked in red on the timeline.

fall into the slowly rising slope at MJD53948, where the X-ray flux is about 1.75 counts per second in the $2 - 10$ keV band of the ASM. This value is significantly, above a $3\,\sigma$ limit, over the base line flux of ~ 0.5 counts.

5.3.3 Results

Comparison measurements with standard stars show that about 500 counts per second at the 1.3 m telescope of the Skinakas observatory correspond to a visual magnitude of $V \sim 18.5$. Thus, Aql X-1 was still in the LIS at the time of the observation with OPTIMA.

As mentioned at the beginning of this section section, Aql X-1 shows almost yearly outbursts. These outbursts in HIS usually last of the order of days to weeks. The increase in optical flux that has been observed to preceed the X-ray states are also of a similar duration, on the order of days to weeks [MB05]. Most of the outbursts observed in X-rays do not show a FRED shape. Thus, the nature of the short duration flare in the optical lightcurve from 1 August 2006 is different from those outbursts.

The so-called "Type I" X-ray outbursts in LMXB with a neutron star primary are caused by sudden explosive thermonuclear burning of accreted material on the neutron star's surface. This creates an increase in X-ray flux of one magnitude or more over a time of a few seconds. Subsequent reprocessing of X-rays in the accretion disk causes a sudden increase of a few factors in the optical light curve, too. Outbursts like this have been observed by Hynes et al. [Hyn05]. They report outbursts of EXO 0748-676 with a similar duration of 50–100 seconds. Simultaneous observations

with RXTE allowed to resolve the structure of individual X-ray outbursts and the shapes of optical/UV flares. These show a steep rise and a slower decay, following the FRED pattern, though the shape of the X-ray outbursts differs from those in the optical/UV regime. Cross-correlation between the simultaneous bands revealed a lag of the optical/UV flares of about $3\,\mathrm{to}\,5$ s with respect to the X-ray outburst peak. The dwell-by-dwell light curve of the ASM shows an X-ray outburst of 2 counts per second at MJD 53948.371996 close to the time of the peak of the optical outburst observed by OPTIMA at MJD 53948.371305. Due to insufficient time resolution of 90 s of the ASM, the flare observed with OPTIMA on 1 August 2006 cannot be verified to show a similar lag with respect to the X-ray region outburst.

The flare seen in the optical light curve is thought to originate from a small X-ray outburst, part of the long-duration 22 days X-ray activity observed in the ASM, that got reprocessed in the accretion disk. The absorption mechanism is dominated by photo-absorption below energies of 7 keV, and above ca. 10 keV Compton scattering takes over. At high energies Compton reflection takes place, significantly reducing the reprocessing efficiency [Hyn05]. Absorption and re-emission can also occur in the atmosphere of the secondary.

The decay of the optical light curve with a time constant of $\tau_{decay} = 24$ s might be an indication for reprocessing in the disk and the atmosphere of the secondary, though the latter depends on the phase of the system was in during time of observation. Different light travel times to different reprocessing sites might be a cause for the smeared out shape [OHH^{+}02].

This serendipituous observation of an optical flare in Aql X-1 during high X-ray activity provides further evidence for the reprocessing mechanisms in the interaction of LMXB accretion disks with Type I X-ray outbursts of the neutron star in the system.

5.4 Crab Pulsar

The Crab Pulsar as the brightest optical pulsar is an often used target for the test of high-time resolution optical instruments (see chapter 2.5.1). The 33 ms period light curve has been very well covered by observations in the past decades.

5.4.1 Features in the optical light curve of the Crab pulsar

Despite of the typical slow-down of the rotation period due to pulsar braking (see chapter 2.5.1), the shape of the Crab pulsar optical light curve has been observed to remain stable in terms of its pulse shape [Pac71].

The optical light curve of the Crab pulsar shows two distinct features. There is a sharp main pulse that preceeds the main pulse in the radio emission. The delayed emission is thought to be due to different regions the optical and radio emission originate from (see chapter 2.5.1). The second

feature is the so-called inter pulse at a phase delay of ~ 0.4 after the main pulse. It has about one quarter of the peak height of the main pulse (see figure 2.18). Referenced to the Jodrell Bank radio ephemeris, the main pulse of the optical light curve appears at a phase of about 0.99, and the inter pulse at a phase of ~ 0.4. The main pulse and the inter pulse are thought to originate from two distinct beams from the two poles of the pulsar (see chapter 2.5.1).

5.4.2 Crab pulsar observations by Karpov et al.

Karpov et al. conducted extensive observations of the Crab pulsar with optical detectors over the years 1994 to 2006 (see table 5.4). The group of Karpov et al. used a set of different instruments over the period of twelve years. All of these instruments provide a time resolution of up to 1μs, and data reduction was performed with the same software packages[11] to avoid inconsistencies by systematic differences due to data analysis [KBB$^+$07].

Date	Telescope	Instrument	Duration	Spectral range
Dec 7, 1994	BTA, Russia	Four-color photometer with photomultiplier	2400	U+B+V+R
Dec 2, 1999	WHT, Canary Islands	Avalanche photodiode	6600	R
Nov 15, 2003	BTA, Russia	Avalanche photodiode	1800	R
Dec 29, 2005- Jan 3, 2006	BTA, Russia	Panoramic spectro-polarimeter with position-sensitiv detector	48000	4000-7000 Å

Table 5.4: Log of observations [KBB$^+$07]

The photon events were binned into 5000 phase bins which gives a $6.6\ \mu$s resolution for the light curve. The light curves were then folded with Karpov et al.'s fast-folding based method of timing model fitting [KBB$^+$07]. The resulting light curves for all observations in 1994, 1999, 2003 and 2005/2006 are plotted in figure 5.14.

In contrast to the usual plots of the Crab light curves which show the main peak at the above mentioned phase of 0.99, the light curves shown in the Karpov et al. publication have been shifted in phase by about 0.65, so that the main pulse lies at a phase of ~ 0.34 and the inter pulse at a phase of ~ 0.75.

Pulse stability

After applying their second-order timing model, the data of Karpov et al. of 2005/2006 shows a quasi-periodic variation with $\sim 2.5 \cdot 10^{-3}$P rms amplitude with an estimated time scale of about 0.7

---

[11]Barycentering was performed by *axBary* code by Arnold Rots and Karpov et al.'s data reduction software

days [KBB+07]. The data from 1999 does not show these and behaves normal with a $4.1\mu s$ rms (see figure 5.13).
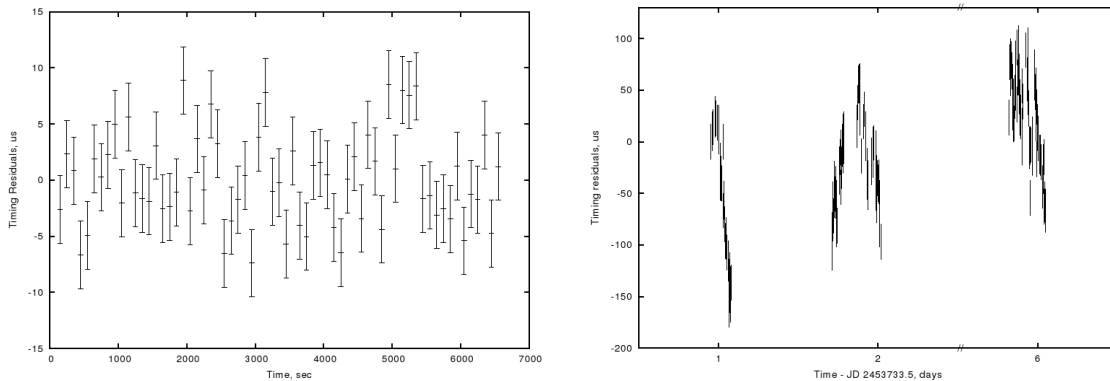
Figure 5.13: left: Timing residuals for data of 1999, corresponding to $4.1\mu s$ rms, right: Timing residuals for 2005-2006 data with a quasi-periodic characteristic timescale of 0.7 days [KBB+07]

The light curves recorded in the observational campaign in 2005/2006 deviate significantly from the usual shape of the Crab's optical light curve. While all the light curves of observations taken in 1994 to 2003 are in perfect agreement with each other, the profile of the one recorded in the years 2005 and 2006 differs significantly. The FWHM of the pulse stays the same, but its shape is much more symmetric and the skewness seen in the Crab pulses is much smaller in that data set. Along with the smaller skewness follows a shift in phase for the main peak. In contrast to the light curves in 1994 to 2003 the pulse shape is observed to be nearly symmetric [KBB+07].

Furthermore, the inter pulse appears also more symmetric. Its peak is smoothed out, resulting in a lower peak level and a slight movement of its phase to the right.

5.4.3   Crab pulsar observations with OPTIMA

OPTIMA was used to observe the Crab pulsar's optical light curve in short campaigns in 2005 and 2006 (see table 5.5). No observation was conducted at the same time as those done by Karpov et al. The closest observations were only two months before and nine months after (see figure 5.15) those where Karpov et al. recorded light curves showing unusual pulse shapes (see figure 5.14).

5.4.4   Analysis

The OPTIMA data was barycentered using the TEMPO-based barycentering software developed in [Str01] (see section 5.1.1) and binned to 1000 bins which corresponds to 33 μs bin size. The base level of the emission was substracted from the curve to give the peak emission only. OPTIMA light
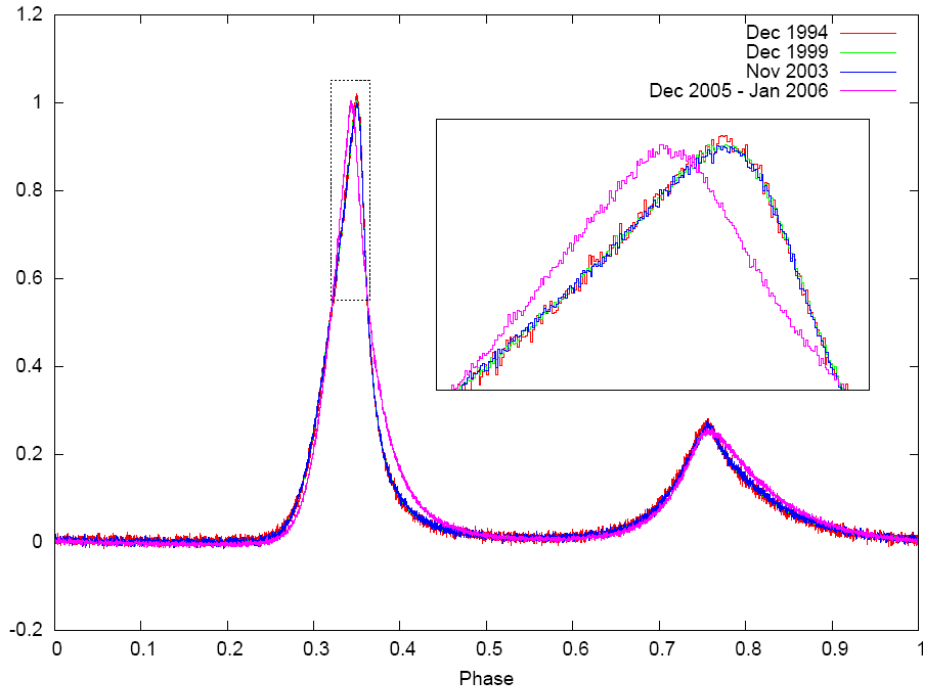
Figure 5.14: Peculiar pulse shape of the main pulse and the inter pulse in the Crab light curve in 2005/2006 [KBB$^+$07]

Date	Telescope	Instrument	Duration, sec	Spectral range
Nov 13, 2005	Skinakas Observatory, Crete	OPTIMA APDs	7200	$400 - 950$ nm
Sep 24, 2006	Skinakas Observatory, Crete	OPTIMA APDs	8400	$400 - 950$ nm

Table 5.5: Log of observations with OPTIMA

Figure 5.15: Timeline of OPTIMA and Karpov et al. Crab pulsar observations

99

Date	MJD	t_{JPL}	t_{acc}	ν	σ_ν	$\dot{\nu}$	$\sigma_{\dot{\nu}}$
	s	μs	Hz		$10^{-15}s^{-2}$		
15 SEP 05	53628	0.031767	140	29.7788534525	1	-372972.07	0.25
15 OCT 05	53658	0.022656	90	29.7778867428	1	-372940.45	0.30
15 NOV 05	53689	0.016803	90	29.7768878849	1	-372924.54	0.22
15 DEC 05	53719	0.026788	100	29.7759213143	1	-372886.52	0.25

Table 5.6: Radio ephemeris for the Crab pulsar published by the Jodrell Bank radio observatory, ftp://ftp.jb.man.ac.uk/pub/psr/crab/crab2.txt

curves are referenced to the Jodrell Bank radio ephemeris, so that the phase had to be shifted to the same phase shown in Karpov et al.'s graphs (see figure 5.14).

The observation in 2005 was performed with OPTIMA's parallel Wollaston polarimeter. The count rates in two channels[12], corresponding to the two polarization angles of one Wollaston, were added up to give the relative intensity, I. This arbitrary count rate was then baseline substracted and normalized to 1 to compare it to the graphs in [KBB+07]. Due to intrinsic light losses of the OPTIMA parallel Wollaston polarimeter, and the fact that only two channels could be used to calculate I, the noise level of the light curve shown for the year 2005 is higher than the one recorded with OPTIMA in photometer mode in 2006.

The OPTIMA light curves were then overplotted with those of [KBB+07] (see figure 5.16) to see if the peculiar pulse shape was present at the times the observations with OPTIMA had been recorded.

For comparison the photometer light curve of 2006 was overplotted with the peculiar light curve recorded by Karpov et al. in 2005/2006 (see figure 5.17). The graph shows that the OPTIMA light curve recorded nine months later, on the 24 September 2006, does not show the peculiar pulse shapes observed by Karpov et al. between December 29, 2005 and January 3,2006.

The Jodrell Bank radio ephemeris of the time around December 2005 and January 2006 does not show any pecularities for the Crab pulsar (see table 5.6):

The monthly ephemeris publication [LP07] for the Crab pulsar reports a significant glitch on 6 September 2004 (MJD 53254.2) and a small glitch for 22 November 2004 (MJD 53331.1). These fall into the time after the first Karpov et al. observations, but before the observation with the different pulse shape. The significant glitch was before the first OPTIMA observation, thus, can not be considered to be a cause for the observed properties in December 2005 and January 2006, but the second glitch on 22 November 2005 could be considered to be a cause for it. It must be noted though that glitches are taken into account for the computation of the Crab pulsar ephemeris, after

---

[12]At the time one fibre of one Wollaston side was broken. Hence not all channels could be used to calculate an intensity I.
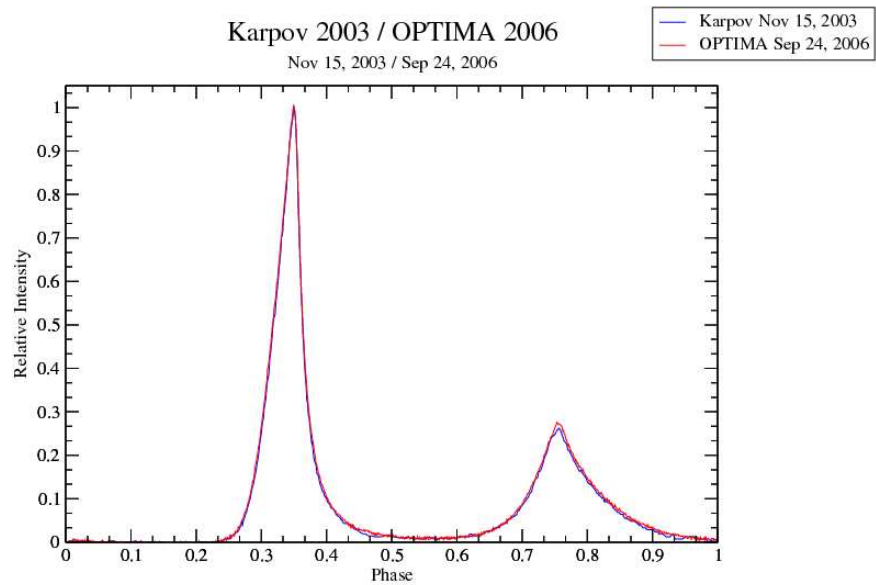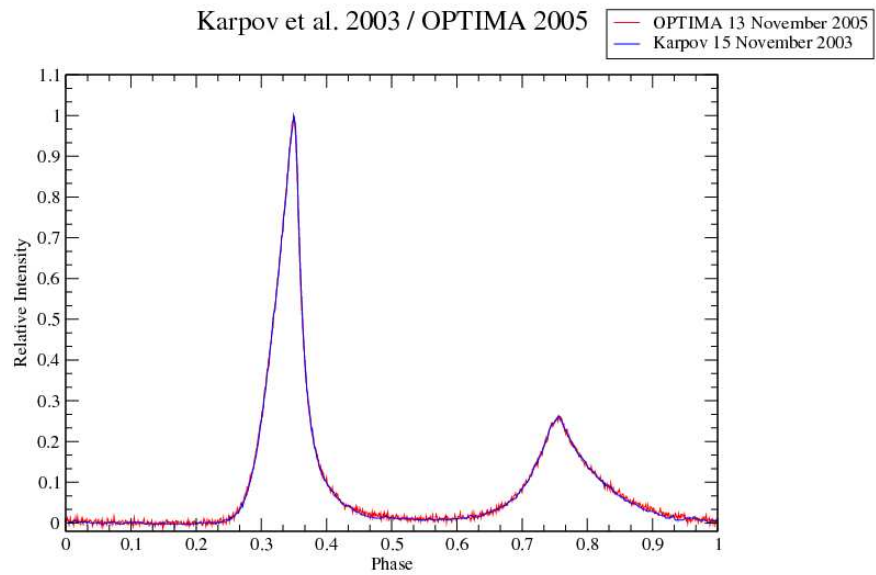
Figure 5.16: OPTIMA observations taken in 2005 and 2006 coincide with the Crab pulsar light curve recorded by Karpov et al. in 2003. Thus, the OPTIMA results show that the light curves at the two epochs are identical.
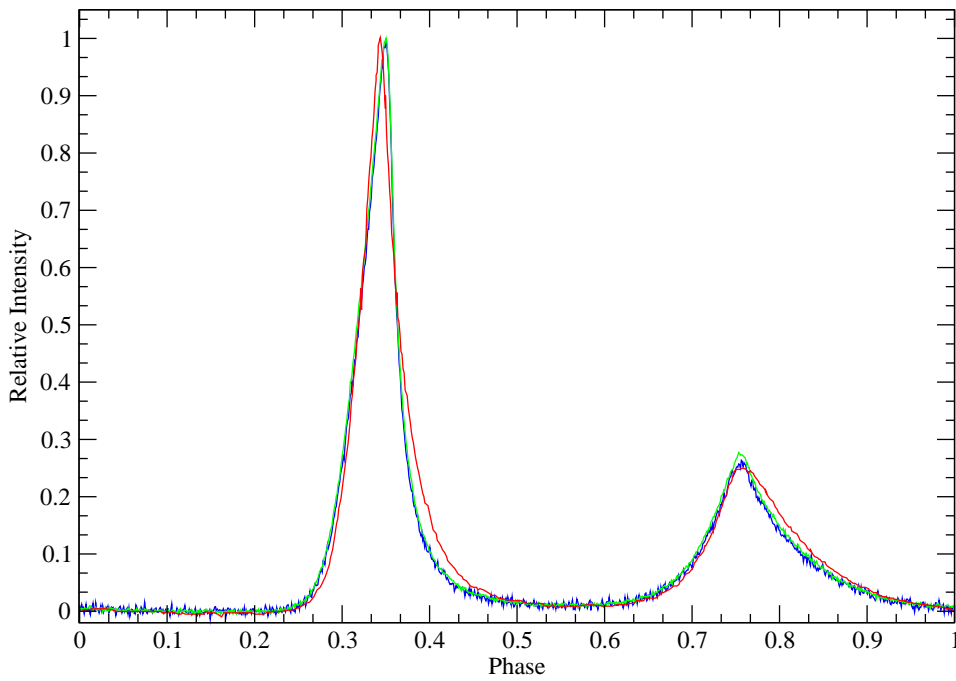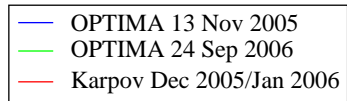
Figure 5.17: Crab light curve observed with OPTIMA on 13 November 2005 and 24 September 2006 overplotted with the Karpov et al. light curve of 2005/2006

sufficient data has been recorded to compensate it. So, the glitch should be already considered in the corresponding ephemeris.

5.4.5 Results

The skewed pulse shapes and phase shifts observed by Karpov et al. during their campaign from 29 December 2005 to 3 January 2006, do not show up in the light curve with OPTIMA nine months later. The OPTIMA observation on the 13 November 2005, which is only two months before, also does not show the peculiar pulse shapes. This further narrows the time for glitches of the pulsar ephemeris that could be considered to be the cause for these features. Comparison with the Jodrell Bank radio ephemeris notices shows that the significant glitch that happened on 6 September 2004 can therefore not be responsible, but the minor glitch observed on 22 November 2005, nine days after the OPTIMA observation could still be considered as a possible cause for the unusual Crab light curve 2005/2006. There was a significant glitch on 23 August 2006 [LP07] which preceeded the second OPTIMA observation on 24 September, which in principle could be a cause for the fact that any change in the pulse shape did not show up anymore in the OPTIMA observation.

Chapter 6

Conclusion

OPTIMA is a high speed photo-polarimeter, developed at the Max Planck Institute for Extraterrestrial Physics, for the observation of optical pulsars, cataclysmic variable stars, black hole transients and other compact, highly variable astronomical targets. Both the requirement to have a reliable system to record the amount of event data generated by the APD detectors, and the necessity to provide high accuracy absolute timing of the photon events put high demands on the data acquisition system that is used to record astronomical data.

The existing DAQ was developed along with the initial version of the OPTIMA detector system. With the extension of OPTIMA and its use for a wider range of astronomical observations the original design of the DAQ did not provide the desired potential anymore. The monolithic design of the existing DAQ software made an extension of its functionality difficult, and along with progress in operating systems and hardware an entirely redesigned software was desired.

6.1 Aims

The major aim of this project was to implement an improved data acquisition software for the OPTIMA high-speed photo-polarimeter. The design of the software should avoid the problems encountered during the use of the existing DAQ, and provide a modern approach to allow further development to meet OPTIMA's needs in the future.

This was achieved through a thoroughly modular design of the new DAQ software. It allows an entirely new approach of data handling within the DAQ system. The major obstacle that prevented extension of the existing DAQ was its monolithic design. The concept of the new DAQ separates hardware access from the rest of the system and transparent data handling allows easy access to the DAQ stream at any point. Therefore any further processing of the event data can be easily implemented without affecting any of the other DAQ processes.

By separating data access from data analysis, tasks to be performed on the online streamed data can be executed by small dedicated applications. This offers the advantage in terms of software

development that extensions of the DAQ application do not lead to one single program that becomes more and more difficult to maintain. Therefore, maintenance of the software gets easier, as specific tasks are performed by distinct applications whose operation is fully independent of the rest of the software package. The necessity of interaction and data exchange through shared memory is implemented into the library framework. Thus as long as the event data format stays the same, the framework does not need to be altered to implement new data analysis functions.

Furthermore clients providing single functionality need only to be run, when their task is required during the observation, no single huge application takes up unnecessary resources, even though only a small set of its functionality is needed at a time.

The difficulties that arise from concurrent data access within a multiprocessing/multithreading system were laid out in chapter 4. These prevent easy implementation of applications constantly accessing shared ressources, especially where high data rates must be achieved. This problem is not unique and became known in computer science as the producer-consumer-problem. The conventional solution lies in using locking mechanisms, assuring exclusive access to shared ressources on small timescales. In chapter 4 it was shown that by utilizing the managed access to shared ressources, the first readers-writers problem and the second readers-writers problem can be solved.

An access management through shared state variables locks only those sections in the ringbuffer of the DAQ the server is writing to at the moment. This allows efficient access to the streamed event data. The DAQ server only reserves those segments that are currently written, while clients have read access to those parts of the ringbuffer that are safe to read. Clients do not block each other, because they do not reserve exclusive access through acquiring of locks. The problems with data integrity that arise from the limited ringbuffer size in the DAQ streaming are handled by providing data integrity checks. The introduction of map values, giving the clients a clear indication about the integrity of the data they read from the shared ringbuffer, makes detection of data corruption possible. Both reading and writing access, combined with data integrity checks are implemented into framework functions that hide the afore-mentioned complexity from the application programmer.

Thus, through provding fully encapsulated writing and reading access for the server and its clients, access to the shared DAQ ringbuffer becomes as easy as access to local data of the applications. As long as data access is performed by using the dedicated framework functions, expansion of the system to new uses is reduced to merely connect to the server, use data access functions, read from the ringbuffer and then to implement the actual data analysis functionality. Implementations of demanding analysis tools that perform online analysis on streamed data do not require any knowledge of the DAQ process and such an application accessing the DAQ stream via the framework does not compromise the safe operation of the DAQ server.

Thus, by using the framework functionality, application programmers can utilize the concept of modularization without any difficulties regarding data safety. Separating the data stream from the data analysis makes the extension of the DAQ system non-critical in terms of its stability. All clients

are independently running processes and do not affect the DAQ server or other clients. This way the system provides memory integrity for the DAQ server and other clients, because one erroneous client does not lead to a crash of the whole DAQ system. The DAQ system becomes more reliable, because even after major changes, and extension with newer client software the systems integrity is not affected.

The interfacing via read access functions to shared memory also makes clients independent of the currently running DAQ hardware. That means that in principle any analysis client can run with any DAQ hardware[1], offering the same functionality for event data recorded on different hardware. All effort and engineering put into quick-look analysis tools is not lost if a future version of OPTIMA uses a different hardware to read photon events, if data access is done through the DAQ framework.

A selection of different classes of compact astrophysical objects was chosen to investigate OPTIMA's application in high time resolution astronomy. HU Aqr is a cataclysmic variable star that shows deep eclipses, and the high inclination of the system allows the study of the processes in a polar CV. In the light curves recorded during observations in 2006 and 2007 the three components contributing to the overall shape of the light curve could be clearly distinguished. Limits for the size of the hot spot on the white dwarf were derived, and an accurate determination of the ephemeris was calculated from a series of eclipses observed between 2006 and 2007.

The observation on August 1st 2006 of Aql X-1 showed a significant flare in the optical light curve. This is similar to observations of other LMXBs and provides an insight into the reprocessed emission in that system during the transition from LIS to HIS.

Observations of the Crab nebula performed during the "OPTIMA Burst" campaign were compared to observations of Karpov et al. They report optical light curves with a peculiar pulse shape between 2005 and 2006 [KBB$^+$07]. Neither in the OPTIMA observations three months before that time, nor nine months later any deviation from the normal Crab light curve could be noted.

6.2   Future Work

The work in this thesis showed that the implementation of a thoroughly designed DAQ framework is the basis for a modern, modular approach of online data handling. The external hardware to perform real-time event tagging in a FPGA did not get finished due to project restrictions. Hence, the reliability and performance of the software framework was demonstrated in a raw file server that streams archived OPTIMA data into the DAQ stream. Due to the design of the software (see section 6.1) the lack of hardware-access does not affect the back end of the framework. All clients can work together with an archive server, just as well as with a hardware-fed DAQ server. In order

---

[1]An exception are clients that are used to control specific DAQ servers.

to demonstrate the performance of the system a set of reference implementations of clients was presented (see chapter 4).

6.2.1 Implementation for new USB-based data acquisition hardware

As soon as the new FPGA-based hardware for OPTIMA is finished and a prototype is available, an USB-based server that reads the event stream from the external hardware could be developed. Because the event time tagging will be done by the FPGA, the task of this server is dedicated to the decoding of the data stream from the USB port. This task is far less time critical as the tagging of events that are read from an internal PCI card. The server must demultiplex the raw data stream into event data, status reports from the external hardware and system status messages from the GPS receiver. These must be separated in the DAQ event loop. While the event data is streamed through write request functions to the ringbuffers in shared memory, the status information is displayed to the user in the form of a log or a graphical control client.

6.2.2 Adaption to existing data acquistion hardware

Although the use of the existing hardware does not solve the time critical problem of reading the DMA buffer of the DAQ card on regular intervals (see chapter 3), the DAQ framework can be adapted to be used with the existing hardware. Due to the fact that the exsiting DAQ was developed for Windows operating systems, the hardware-polling part and access to the GPS receiver must be re-implemented on a Linux system. The National Instruments' DAQ used in the old DAQ system is listed to be supported by the open source "Comedi" driver library. This is a library providing drivers and a high-level framework to access analogue and digital I/O cards in Linux. Using the Comedi library an adaption of the DAQ framework could be written to use the principle of hardware-triggered timecode generation described in chapter 3 to create a DAQ server running with the old hardware.

6.2.3 Further DAQ clients and Outlook

The full potential of the framework library lies in the fact that creation of new clients becomes easy, once the principle of data access is understood. By hiding all data integrity management from the application programmer, implementation of a generic client is easily done by using the framework's API ([Dus07]). The actual task of the client is not limited by the access to the DAQ anymore, only by performance requirements of the actual implementation of the analysis algorithm. A series of common tasks that could be done by further client software interfacing with the DAQ framework is presented in this section.

Instead of writing to a compact OPTIMA specific raw file format, a client can read event data from the memory and utilize the FITS library for writing to that common format. A **FITS writer**

client can be implemented by converting the library's internal event format to a FITS table and write that to permanent storage. This process is not as fast as writing the event data directly to hard disk, but using the FITS library also provides the option to use highly efficient compression algorithms. There exists also the option to define FITS headers that allow to write the data in an own format, as long as it can be converted by using the appropriate table entries. The format is widely used in the astronomical community, which allows easier use of common software packages for later (off-line) data analysis. So writing directly into FITS format makes data exchange easier than using a proprietary OPTIMA raw format.

The plotting client provides a quick-look online investigation of the properties of targets observed in photometer mode (see chapter 4 section 4.3.5). For observations performed with the parallel Wollaston polarimeter a dedicated **polarimeter client** can read the count rates in the four Wollaston channels, corresponding to polarization angles of $0°$, $45°$, $90°$ and $135°$ in case of OPTIMA's Wollaston prism, and use the simplified Stoke's formulae [SA99] to display the polarization angle and degree of polarization of the target. Sudden changes in polarization that would indicate unusual physical processes going on in the target source could then be easily identified while an observation is running and a decision about further investigation could be taken. Deduction of the degree of polarization from the rates in the four Wollaston channels on the ratemeter alone is possible for a skilled observer, but any varying features, especially on fast time scales, can not be identified.

For searches for (quasi-)periodic signals, Fast Fourier analysis provides a good tool to identify periodicities in the target's light curve. Especially in light curves with bad signal to noise ratios, periodicities are not visible by eye, or the frequencies are too high to see them on an online plotter. A client executing a **Fast Fourier Transform** on a channel, could output maxima it finds at specific frequencies in the FFT spectrum of a signal. Since FFT works only on data sets with an 2^n number of entries, the read request function has an option to provide the client only with sized segment of a preferred size that the client desires.

As mentioned in chapter 2 the central fibre bundle of OPTIMA provides a hexagonal close-packaged arrangement of seven optical fibres of $300 \ \mu m$ diameter. It is possible to write a small client application that montors changes in the surrounding background channels. An even change in all six fibres would be contributed to a change in background level, while a change in only one or two fibres could be considered to be an indication of the target source having moved off the central fibre. Although the accuracy of the OPTIMA control computer (see chapter 2 section 2.3.5) is at sub arc second level, such a **target position client** could be used to support correct positioning of the source of interest.

All event data exchange in the current implementation is handled via shared memory, and TCP/IP connections are only used to control the server application. The idea of an **ethernet streaming client** that reads event data from shared memory, puts the events into ethernet frames that are

sent via ethernet to a remote computer. On the remote machine a second ethernet-reading client would take over the data it receives via the network and streams it into the shared memory of the remote computer. This would provide the possibility of distributed clients accessing the same DAQ data. The main task of the DAQ framework lies in providing functions for developing DAQ applications; during normal observational runs online analysis is restricted to practical considerations, and no in-depth analysis is taking place. Nontheless one could think of a scenario where another operator wants to monitor OPTIMA event data on a remote computer, where such an ethernet streaming client seems a practical solution. It has to be kept in mind that the library provides only easy access to the event data in shared memory. Furthermore, even Gigabit ethernet[2] quickly reaches its limits, at high event rates of OPTIMA data being streamed from the DAQ.

The Semiconductor Lab of the Max Planck Institute for Extraterrestrial Physics is currently developing a **pn-camera with avalanche amplification**. A pn-CCD camera with conventional amplification has already been successfully tested at Skinakas Observatory in August 2007. The avalanche amplified version will provide single photon sensitivity and is intended as a successor for the current fibre-fed version of OPTIMA. In principle the framework developed in this thesis could be used to handle the event data from the pn-CCD camera, provided a server back end for accessing the CCD read-out hardware will be implemented. The fundamental difference in this lies in the fact that the pn-CCD camera provides a far greater number of data channels, since every pixel would be considered as an individual channel[3]. Preprocessing of events in the server and grouping photon events coming from an identified source region and treating this as a "channel" might be a solution to reduce the number of individual channels handled within the framework. Thus the DAQ framework itself and the corresponding clients provide a basis even for OPTIMA's long term future improvements.

In order to give an astronomical outlook the new DAQ system will provide OPTIMA with modern and suitable data recording capabilities for HTRA. In particular for the aim to observe GRB afterglows in the optical with OPTIMA, providing insight into the early phases GRB observations that are still highly debated by theorists. The serendipituous observation of the flare in Aql X-1 showed similarities with observations of those seen in other LMXBs. Further observation of Aql X-1 with OPTIMA, preferably in the scope of a multiwavelength campaign that could provide simultaneous high time resolution X-ray data, could yield more outbursts in the system. With a greater number of flares their characteristics could be more clearly determined and cross-correlation with X-ray data could give insight into the regions of reprocessed emission and the orbital parameters of the Aql X-1 binary.

---

[2]Gigabit ethernet is currently the fastest specification of the ethernet standard, providing a net rate of 1000 Mbit/s, which is about 100 MB/s in practical applications.

[3]The current design of the pn-CCD camera has a 264×264 array of a size of $51~\mu m \times 51~\mu m$.

Bibliography

[asm07]   Asm light curves. `http://xte.mit.edu/ASM_lc.html`, September 2007.

[atn07]   Australia telescope national facility pulsar catalogue. `http://www.atnf.csiro.au/research/pulsar/psrcat/`, September 2007. 25-09-2007.

[BCR+02]   C. M. Bridge, M. Cropper, G. Ramsay, M. A. C. Perryman, J. H. J. de Bruijne, F. Favata, A. Peacock, N. Rando, and A. P. Reynolds. STJ observations of the eclipsing polar HU Aqr. MNRAS, 336:1129–1138, November 2002.

[BNM06]   C. Bailyn, E. Neil, and D. Maitra. Atel no. 869: New outburst of Aql X-1. Astronomer's Telegram, Jul 2006.

[BR01]   V. Burwitz and K. Reinsch. ROSAT discovered soft x-ray intermediate polars: UU Col and RX J0806.3+1527. *X-ray Astronomy: Stellar Endpoints, AGN, and the Diffuse X-ray Background*, 599:522–525, December 2001.

[BSM+01]   P. Boumis, A. Steiakaki, F. Mavromatakis, G. Paterakis, and I. Papamastorakis. Seeing Measurments at Skinakas Observatory using the DIMM method. In *5th Hellenic Astronomical Conference, held 20-22 September, 2001 in Crete, Greece. Online at http://www.astro.auth.gr/elaset/helasmtg/2001/proceedings.htm, p.134.1*, September 2001.

[BZ34]   W. Baade and F. Zwicky. On Super-novae. *Proceedings of the National Academy of Science*, 20:254–+, 1934.

[CCS+07]   R. Cornelisse, J. Casares, D. Steeghs, A. D. Barnes, P. A. Charles, R. I. Hynes, and K. O'Brien. A detection of the donor star of Aquila X-1 during its 2004 outburst? MNRAS, 375:1463–1470, March 2007.

[CDT69]   W. J. Cocke, M. J. Disney, and D. J. Taylor. Discovery of Optical Signals from Pulsar NP 0532. Nature, 221:525–+, 1969.

[CILP99]   C. Chevalier, S. A. Ilovaisky, P. Leisy, and F. Patat. Magnitude, color and spectral type of AQL X-1 in quiescence. A&A, 347:L51–L54, July 1999.

[Cro90]   M. Cropper. The Polars. *Space Science Reviews*, 54:195–295, December 1990.

[DDD+93]   H. Dautet, P. Deschamps, B. Dion, A. D. MacGregor, D. MacSween, R. J. McIntyre, C. Trottier, and P. P. Webb. Photon-counting techniques with silicon avalanche photodiodes. In J. R. Lakowicz and R. B. Thompson, editors, *Proc. SPIE Vol. 1885, p. 240-250, Advances in Fluorescence Sensing Technology, Joseph R. Lakowicz; Richard B. Thompson; Eds.*, volume 1885 of *Presented at the Society of Photo-Optical Instrumentation Engineers (SPIE) Conference*, pages 240–250, May 1993.

[DH82]   J. K. Daugherty and A. K. Harding. Electromagnetic cascades in pulsars. ApJ, 252:337–347, January 1982.

[DM01]   V. Dhillon and T. Marsh. ULTRACAM - studying astrophysics on the fastest timescales. *New Astronomy Review*, 45:91–95, January 2001.

[DR03]   J. Dyks and B. Rudak. Two-Pole Caustic Model for High-Energy Light Curves of Pulsars. ApJ, 598:1201–1206, December 2003.

[Dus07]   Sven Duscha. *ODASSE Framework API.* MPE, 2007.

[ERE+82]   T. M. Eubanks, M. G. Roth, P. B. Esposito, J. A. Steppe, and P. S. Callahan. An analysis of JPL TEMPO Earth orientation results. In W. E. Carter and A. Tusuchiya, editors, *Geodetic Applications of Radio Interferometry*, pages 81–+, 1982.

[FW99]   L. Ferrario and R. Wehrse. Accretion funnels in AM Herculis systems - I. Model characteristics. MNRAS, 310:189–202, November 1999.

[gcn07]   Gamma ray bursts coordinates network. `http://gcn.gsfc.nasa.gov/`, 06 2007. 13-07-2007.

[Gin60]   O. Gingerich. The Missing Messier Objects. S&T, 20:196–+, October 1960.

[GJ69]   P. Goldreich and W. H. Julian. Pulsar Electrodynamics. ApJ, 157:869–+, August 1969.

[Gol68]   T. Gold. Rotating Neutron Stars as the Origin of the Pulsating Radio Sources. Nature, 218:731–+, May 1968.

[HBP+68]   A. Hewish, S. J. Bell, J. D. Pilkington, P. F. Scott, and R. A. Collins. Observation of a Rapidly Pulsating Radio Source. Nature, 217:709–+, February 1968.

[HCH⁺99] M. K. Harrop-Allin, M. Cropper, P. J. Hakala, C. Hellier, and T. Ramseyer. Indirect imaging of the accretion stream in eclipsing polars - II. HU Aquarii. MNRAS, 308:807–817, September 1999.

[Hel01] Coel Hellier. *Cataclysmic variable stars: how and why they vary*. Springer, 2001.

[HHS99] C. Heerlein, K. Horne, and A. D. Schwope. Modelling of the magnetic accretion flow in HU Aquarii. MNRAS, 304:145–154, March 1999.

[HPC01] M. K. Harrop-Allin, S. B. Potter, and M. Cropper. Indirect imaging of the accretion stream in eclipsing polars - III. HU Aquarii low state. MNRAS, 326:788–798, September 2001.

[Hyn05] R. I. Hynes. Correlated X-ray and Optical Variability in X-ray Binaries. In J.-M. Hameury and J.-P. Lasota, editors, *The Astrophysics of Cataclysmic Variables and Related Objects*, volume 330 of *Astronomical Society of the Pacific Conference Series*, pages 237–+, August 2005.

[IC06] S.A. Ilovaisky and C. Chevalier. Atel no. 870: Aql x-1 is active again. Astronomer's Telegram, Aug 2006.

[IPC⁺99] G. L. Israel, M. R. Panzera, S. Campana, D. Lazzati, S. Covino, G. Tagliaferri, and L. Stella. The discovery of 321 S pulsations in the ROSAT HRI light curves of 1BMW J080622.8+152732 = RX J0806.3+1527. A&A, 349:L1–L4, September 1999.

[ira06] Image reduction and analysis facility. http://iraf.noao.edu/, 11 2006. 16-07-2007.

[JM03] W. A. Joye and E. Mandel. New Features of SAOImage DS9. In H. E. Payne, R. I. Jedrzejewski, and R. N. Hook, editors, *Astronomical Data Analysis Software and Systems XII*, volume 295 of *Astronomical Society of the Pacific Conference Series*, pages 489–+, 2003.

[KBB⁺07] S. Karpov, G. Beskin, A. Biryukov, V. Debur, V. Plokhotnichenko, M. Redfern, and A. Shearer. Short time scale pulse stability of the Crab pulsar in the optical band. Ap&SS, pages 104–+, March 2007.

[KDG⁺73] P. K. Kunte, N. Durgaprasad, G. S. Gokhale, V. Iyengar, R. K. Manchanda, and B. V. Sreekantan. X-ray astronomy-Hard radiation from AQL X-1. Nature, 245:37–+, September 1973.

[Kel02] Stephan Kellner. Einsatz und Weiterentwicklung von OPTIMA als hochzeitauflösendes Photo- und Polarimeter. Master's thesis, TU München, 2002.

[KIM+81]   K. Koyama, H. Inoue, K. Makishima, M. Matsuoka, T. Murakami, M. Oda, Y. Os-
            gawara, T. Ohashi, N. Shibazaki, Y. Tanaka, F. J. Marshall, I. S. Kondo, S. Hayakawa,
            H. Kunieda, F. Makino, K. Masai, F. Nagase, Y. Tawara, S. Miyamoto, H. Tsunemi,
            and K. Yamashita. Discovery of X-ray bursts from Aquila X-1. ApJ, 247:L27–L29,
            July 1981.

[KKS+03]   G. Kanbach, S. Kellner, F. Z. Schrey, H. Steinle, C. Straubmeier, and H. C. Spruit.
            Design and results of the fast timing photo-polarimeter optima. In M. Iye and
            A. F. M. Moorwood, editors, *Instrument Design and Performance for Optical/In-*
            frared Ground-based Telescopes. Edited by Iye, Masanori; Moorwood, Alan F. M.
            Proceedings of the SPIE, Volume 4841, pp. 82-93 (2003)., volume 4841 of *Presented*
            at the Society of Photo-Optical Instrumentation Engineers (SPIE) Conference, pages
            82–93, March 2003.

[Kra98]   M. Kramer. Determination of the Geometry of the PSR B1913+16 System by Geode-
            tic Precession. ApJ, 509:856–860, December 1998.

[Kro46]   G. E. Kron. Application of the Multiplier Phototube to Astronomical Photoelectric
            Photometry. ApJ, 103:326–+, May 1946.

[KSD+06]   G. Kanbach, A. Stefanescu, S. Duscha, M. Mühlegger, F. Schrey, H. Steinle,
            A. Slowikowsky, and H. Spruit. Optima: A high time resolution optical photo-
            polarimeter. The 1st Galway workshop on High Time Resolution Astrophysics, 2006.

[KSG02]   J. G. Kirk, O. Skjæraasen, and Y. A. Gallant. Pulsed radiation from neutron star
            winds. A&A, 388:L29–L32, June 2002.

[KSKS05]   G. Kanbach, A. Słowikowska, S. Kellner, and H. Steinle. New optical polarization
            measurements of the Crab pulsar. In T. Bulik, B. Rudak, and G. Madejski, editors,
            Astrophysical Sources of High Energy Particles and Radiation, volume 801 of *Amer-*
            ican Institute of Physics Conference Series, pages 306–311, November 2005.

[KSSB01]   G. Kanbach, C. Straubmeier, H. C. Spruit, and T. Belloni. Correlated fast X-ray and
            optical variability in the black-hole candidate XTE J1118+480. Nature, 414:180–182,
            November 2001.

[Las97]   Laser Components GmbH, Werner-von-Siemens-Str. 15, D-82140 Olching. *Single*
            Photon Counting Module, SPCM-AQ Series, January 1997.

[LG98]   Andre.G. Lyne and Francis Graham-Smith. *Pulsar Astronomy*. Cambridge University
            Press, 1998.

[LP07]   A.G. Lyne and R.S. Pritchard. Jodrell bank crab pulsar timing results, monthly ephemeris. University of Manchester, Nuffield Radio Astronomy Laboratories, Jodrell Bank, Macclesfield, Cheshire, UK, September 2007.

[Lub06]   B. K. Lubsandorzhiev. On the history of photomultiplier tube invention. *NUCL.INSTRUM.METH.A*, 567:236, 2006.

[MÖ6]   M. Mühlegger. Entwicklung und Einsatz eines Wollaston-Polarimeters für die Hochgeschwindigkeitsastronomie mit OPTIMA-Burst. Master's thesis, University of Technology Munich, 2006.

[m5107]   Astronomie.de - sketch of m97. http://www.astronomie.de/bibliothek/artikel/ 09 2007. 14-09-2007.

[m9707]   Seds - sketch of m51. http://seds.lpl.arizona.edu/messier/Pics/More/m97r 09 2007. 14-09-2007.

[MB05]   D. Maitra and C. D. Bailyn. Low-Intensity States in the Neutron Star X-ray Binary Aql X-1. *ArXiv Astrophysics e-prints*, October 2005.

[MBSK03]   J. Malzac, T. Belloni, H. C. Spruit, and G. Kanbach. The optical and X-ray flickering of XTE J1118+480. A&A, 407:335–345, August 2003.

[MHTH05]   R. N. Manchester, G. B. Hobbs, A. Teoh, and M. Hobbs. The Australia Telescope National Facility Pulsar Catalogue. AJ, 129:1993–2006, April 2005.

[mis07]   The missing messier objects. http://www.maa.agleia.de/Messier/missing.html, 09 2007. 14-09-2007.

[MP85]   J. Middleditch and C. R. Pennypacker. The optical pulsar in the Large Magellanic Cloud remnant 0540-693. In M. C. Kafatos and R. B. C. Henry, editors, *The Crab Nebula and Related Supernova Remnants*, pages 179–186, 1985.

[MVP04]   D.D.E. Martin, P. Verhoeve, and A. Peacock. A 1210 pixels superconducting tunnel junction array based spectro-photometer for optical astronomy. *NIM-A*, 520:512, 2004.

[OBS+02]   S. O'Tuairisg, R. Butler, A. Shearer, M. Redfern, and D. Butler. A new survey of variability in the core of M15 with TRIFFID-2. *ArXiv Astrophysics e-prints*, December 2002.

[OHH+02]   K. O'Brien, K. Horne, R. I. Hynes, W. Chen, C. A. Haswell, and M. D. Still. Echoes in X-ray binaries. MNRAS, 334:426–434, August 2002.

[Pac68]   F. Pacini.   Rotating Neutron Stars, Pulsars and Supernova Remnants.   Nature, 219:145–+, July 1968.

[Pac71]   F. Pacini. The Secular Decrease of Optical and X-Ray Luminosity of Pulsars. ApJ, 163:L17+, January 1971.

[Per07]   PerkinElmer   Optoelectronics,   44370   Christy   Street,   Fremont,   CA 94538-3180.   *SPCM-AQR,   Single   Photon   Counting   Module*, `http://optoelectronics.perkinelmer.com/content/Datasheets/DTS_SPCMAQR.pdf` edition, 28 June 2007.

[PT84]   W. C. Priedhorsky and J. Terrell. Long-term observations of X-ray sources - The Aquila-Serpens-Scutum region. ApJ, 280:661–670, May 1984.

[RC69]   D. W. Richards and J. M. Comella. The Period of Pulsar NP0532. Nature, 222:551–+, May 1969.

[Red91]   R.M. Redfern.   High-resolution imaging in la palma.   *Vistas in Astronomy*, 34(201):201–233, 1991.

[RMD04]   M. P. Rupen, A. J. Mioduszewski, and V. Dhawan. On-going radio flare in Aql X-1. *The Astronomer's Telegram*, 286:1–+, May 2004.

[RRS06]   O. Ryan, M. Redfern, and A. Shearer. An avalanche photodiode photon counting camera for high-resolution astronomy. *Experimental Astronomy*, 21:23–30, February 2006.

[RY95]   R. W. Romani and I.-A. Yadigaroglu. Gamma-ray pulsars: Emission zones and viewing geometries. ApJ, 438:314–321, January 1995.

[SA99]   W. B. Sparks and D. J. Axon.   Panoramic Polarimetry Data Analysis.   PASP, 111:1298–1315, October 1999.

[Sch99]   G. D. Schmidt. Accretion in High Magnetic Fields: The Stellar Interaction. In C. Hellier and K. Mukai, editors, *Annapolis Workshop on Magnetic Cataclysmic Variables*, volume 157 of *Astronomical Society of the Pacific Conference Series*, pages 207–+, 1999.

[SG02]   A. Shearer and A. Golden. Why study pulsars optically? In W. Becker, H. Lesch, and J. Trümper, editors, *Neutron Stars, Pulsars, and Supernova Remnants*, pages 44–+, 2002.

[SGH$^+$98]   A. Shearer, A. Golden, S. Harfst, R. Butler, R. M. Redfern, C. M. M. O'Sullivan, G. M. Beskin, S. I. Neizvestny, V. V. Neustroev, V. L. Plokhotnichenko, M. Cullum, and A. Danks. Possible pulsed optical emission from Geminga. A&A, 335:L21–L24, July 1998.

[SKS01]   C. Straubmeier, G. Kanbach, and F. Schrey. OPTIMA: A Photon Counting High-Speed Photometer. *Experimental Astronomy*, 11:157–170, 2001.

[SKS07]   A. Słowikowska, G. Kanbach, and A. Stefanescu. Fully Resolved Optical Polarization of the Crab Pulsar. In *American Institute of Physics Conference Series*, volume 921 of *American Institute of Physics Conference Series*, pages 419–420, July 2007.

[SMH97]   A. D. Schwope, K.-H. Mantel, and K. Horne. Phase-resolved high-resolution spectrophotometry of the eclipsing polar HU Aquarii. A&A, 319:894–908, March 1997.

[SRG$^+$97]   A. Shearer, R. M. Redfern, G. Gorman, R. Butler, A. Golden, P. O'Kane, G. M. Beskin, S. I. Neizvestny, V. V. Neustroev, V. L. Plokhotnichenko, and M. Cullum. Pulsed Optical Emission from PSR 0656+14. ApJ, 487:L181+, October 1997.

[SSK$^+$07]   A. Stefanescu, A. Slowikowska, G. Kanbach, S. Duscha, F. Schrey, H. Steinle, and Z. Ioannou. GRB 070610: OPTIMA-burst high-time-resolution optical observations. *GRB Coordinates Network*, 6492:1–+, 2007.

[Ste04]   A. Stefanescu. Anpassung und Einsatz des OPTIMA Photometers zur Messung von GRB-Afterglow-Kandidaten. Master's thesis, University of Technology Munich, 2004.

[Str01]   C. Straubmeier. *OPTIMA - Entwicklung und erste astronomische Messungen eines optischen Hochgeschwindigkeitsphotometers*. PhD thesis, University of Technology Munich, 2001.

[TCB78]   J. Thorstensen, P. Charles, and S. Bowyer. The optical counterpart of Aquila X-1 /3U 1908+00/. ApJ, 220:L131–L134, March 1978.

[TSHC06]   J. Takata, S. Shibata, K. Hirotani, and H.-K. Chang. A two-dimensional electrodynamical outer gap model for γ-ray pulsars: γ-ray spectrum. MNRAS, 366:1310–1328, March 2006.

[VS01]   S. Vrielmann and A. D. Schwope. Accretion stream mapping of HU Aquarii. MNRAS, 322:269–279, April 2001.

[WG79]   D. C. Wells and E. W. Greisen. FITS - a Flexible Image Transport System. In
            G. Sedmak, M. Capaccioli, and R. J. Allen, editors, *Image Processing in Astronomy*,
            pages 445–+, 1979. 1979ipia.coll..445W.

[WKJM89]   M. G. Watson, A. R. King, M. H. Jones, and C. Motch. Absorption dips and the
            properties of the accretion stream in polars. MNRAS, 237:299–310, March 1989.

[WMBL06a]   R. Wijnands, D. Maitra, C. Bailyn, and M. Linares. Atel no. 871: New Outburst of
            Aql X-1. Astronomer's Telegram, Aug 2006.

[WMBL06b]   R. Wijnands, D. Maitra, C. Bailyn, and M. Linares. Atel no. 872: Correction to
            atel 871: A swift/xrt observation of aql x-1 during its recent outburst. Astronomer's
            Telegram, Aug 2006.

[WPM$^+$77] P. T. Wallace, B. A. Peterson, P. G. Murdin, I. J. Danziger, R. N. Manchester, A. G.
            Lyne, W. M. Goss, F. G. Smith, M. J. Disney, K. F. Hartley, D. H. P. Jones, and G. W.
            Wellgate. Detection of optical pulses from the VELA pulsar. Nature, 266:692–694,
            April 1977.

[xep07]   Xephem 3.7.2. `http://www.clearskyinstitute.com/xephem/`, 07
            2007. 11-07-2007.